EFFECT OF ALLOYING AND NANOSTRUCTURING ON THERMOELECTRIC PROPERTIES

PRABHJOT KAUR
(PH15209)

A thesis submitted for the partial fulfillment of

the degree of Doctor of Philosophy

Institute of Nano Science and Technology

Phase 10, Sector-64, Mohali, Punjab-160062, India.

And

Indian Institute of Science Education and Research Mohali

Knowledge city, Sector 81, SAS Nagar, Manauli PO, Mohali 140306, Punjab, India.

May 2019

ii

Declaration

The work presented in this thesis has been carried out by me under the guidance of my supervisors DR CHANDAN BERA and DR SUVANKAR CHAKRAVERTY at the Institute of Nano Science and Technology, Mohali. This work has not been submitted in part or in full for a degree, a diploma, or a fellowship to any other university or institute. Whenever contributions of others are involved, every effort is made to indicate this clearly, with due acknowledgement of collaborative research and discussions. This thesis is a bona fide record of original work done by me and all sources listed within have been detailed in the bibliography.

PRABHJOT KAUR

In my capacity as the supervisor of the candidates thesis work, I certify that the above statements by the candidate are true to the best of my knowledge.

DR CHANDAN BERA

DR SUVANKAR CHAKRAVERTY

Acknowledgements

By God's grace, it is a time of great ecstasy for me to pay gratitude to my PhD supervisors Dr. Chandan Bera and Dr. Suvankar Chakraverty for their immense support and guidance. This thesis could not be possible without their constant hard working nature and help.

I owe my special thank to former INST director Prof. Ashok K. Ganguli and present INST director Prof. Hirendra N. Ghosh for their constant enthusiasm and help. I am thankful to all my mentors during course work specially Dr. Kiran Hazra, Dr. Ehesan Ali and Dr. Abhishek Chowdhari (IISER) for their valuable discussions.

I am thankful to the PETr group for discussions during presentations, tea break and meal times. I would like to acknowledge the support from my group members: Vishal Kumar, Ajit Singh, Arnab Das, Sonali, Maneesh, Dr. Lenin, Parrydeep Kaur, Raveena. I am also thankful to my friends from co-groups for numerous discussions : Prabhleen Kaur, Dr. Seema Gautam, Aashish, Dimple, Nitya, Neha, Ruchi. I specially thank Mr. Vikram and Mr. Boota Singh for providing us tea at all those high times.

I am thankful to my hostel friends Satnam Singh, Rashmika, Taru, Guratinder, Ritu for their constant support and companionship, without them the hostel would have never felt like home.

I would like to acknowledge the financial support from Department of Science and Technology (DST), India during my PhD. I extend my huge thanks to CDAC Pune for providing cluster facilities without any hassle.

I would not be able to just thank my father Late S. Malkit Singh who has brought me up to watch dreams and fulfill them. I am extremely grateful to my mother Dr. Gurmel Kaur who apart from all odds has helped me more like a friend. I am under debt to thank my husband Dr. Paramjit Singh for standing like a wall and helping me to complete my thesis. I am also thankful to my parents-in-law and whole family for their silent help and cooperation.

Finally, I thank my dearest friend Manpreet Kaur for always being there for me. I lovingly thank my younger cousin sister Jashanpuneet Kaur for her childish pleasure and all help. And last but not the least, I thank my brother Harinder Singh whole heartily.

Abstract

There has been a constant search for thermoelectric materials with higher power conversion efficiency to enhance waste heat recovery. Efficiency of a thermoelectric material is calculated as figure of merit ($ZT = S^2\sigma T/\kappa$ where $S^2\sigma$ is power factor and κ is thermal conductivity). The expedition for exploring better thermoelectric performance among a copious number of materials is based either on finding a new material or on modifying the thermoelectric properties of existing ones. To enhance the thermoelectric performance of already existing materials, different methods have been used like nanostructuring, doping, rattling atoms, alloying etc. These methods either target at modifying the electronic band structure to enhance the power factor, or on the other hand, steering the phonon scatterings to reduce the thermal conductivity. In result, it increases the overall performance based on the strategy of "Phonon glass electron crystal". Thermal conductivity is one of the dominant parameters for efficiency optimization. Besides the intrinsic properties, alloying and nanostructuring have been found to be very effective in controlling the thermal conductivity in large range of materials. Apart from promising low-cost binary thermoelectric materials (CdSe, PbTe etc), only a few ternary MZX (M=group IX, X; Z= Group V; X is chalcogenide) chalcogenides such as CoSbS, NiSbS, FeSbS have been studied for thermoelectric applications. Thermoelectric performance of ternary pnictide chalcogenide of d^8 transition metal materials PdPS, CoAsS have been investigated in this thesis work. A worth appraised values of ZT have been calculated for these materials. Thermoelectric figure of merit calculated for PdPS is very significant in the nano regime and due to its layered structure, it will be having many applications in the field of biology, space, computers etc. Another very important application of this research is in the thermoelectric modules in which the provision to use both legs of the module from CoAsS alloy can be possible. A significant reduction in the lattice thermal conductivity of type-I clathrate $Ba_8Cu_6Si_{40}$ by introducing alloy scattering and boundary scattering is observed which can be useful for many Si based technologies.

The contents of the thesis have been divided into five chapters whose brief account is outlined as below:

Chapter 1 introduces an overview of the concept of thermoelectricity. It includes the state-of-the-art of evolution and advancement of the performance of thermoelectric materials. We start by introducing the Boltzmann transport theory to quantify the thermoelectric effect. Best thermoelectrics are epitomes of "phonon glass electron crystal" concept, which tend to increase the transport ratio. Such naturally occurring thermoelectric materials hardly exist. The electronic transport can be enhanced by band structure engineering and doping of the pure semiconductor material. The thermal transport can be decreased by various methods such as nanostructuring, alloying, rattling, complex structuring etc. This chapter sheds light on all the ways to increase the figure of merit of thermoelectric materials. We discuss in this chapter the theoretical calculation details and the procedure for finding thermoelectric properties of different materials.

Chapter 2 presents the thermoelectric properties of layered ternary metal chalcogenide Palladium Phosphide Sulphide (PdPS). Unlike few other ternary metal chalcogenides, orthorhombic PdPS has anisotropic transport properties both for electron as well as phonon. Seebeck coefficient found by our calculations is as high as 300 μVK^{-1} at 300 K and reaches upto 400 μVK^{-1} at 800 K for both p-type and n-type PdPS. Strong in-plane anisotropy in power factor is highly promising for two different type of legs in a thermoelectric module. Sound speed is almost 20 times lower in z-direction of PdPS compared to bulk sound speed due to flat phonon dispersion in z-direction. Low phonon velocity in z-direction plays a crucial role in reducing thermal conductivity. In the z-direction, larger wavelength phonon carries most of the heat, which can be easily blocked by nanostructuring. So larger reduction in κ along z-direction is obtained compared to bulk or x- and y-direction. Along the z-direction, thermal conductivity is ultra-low and more than ten times lower than the bulk thermal conductivity. Nanostructured p-type PdPS shows a much superior value of ZT in the z-direction than n-type. The anisotropy in the in-plane electrical and thermal conductivity can also be related to the periodic fashion in which all the three atoms are aligned in PdPS. It can be seen that the position of Pd atoms is same in x- and y-directions but that of P and S is though periodic in y-direction but not in the x-direction. This unevenness in the arrangement of P and S atoms gives anisotropy in the in-plane conductivity. These high Seebeck coefficient values, large anisotropic power factor, and low thermal conductivity suggest that PdPS can be a utilitarian thermoelectric in the medium temperature range, 300 K - 800 K.

Chapter 3 shows the effect of alloying on the thermoelectric properties of cobaltite (CoAsS) and paracostibite (CoSbS), both having orthorhombic structure. From electronic band structure calculations, it is shown that flat regions in conduction band of CoAsS lead to higher Seebeck values ($\sim$ 193 μVK^{-1}), whereas valence band having lesser flat maxima gives smaller Seebeck coefficient value ($\sim$ 154 μVK^{-1}) at 300 K temperature. Due to substantially higher conductivity values $\sim$ 304 Ω^{-1}cm^{-1} of the p-type than n-type $\sim$ 98 Ω^{-1}cm^{-1}, the power factor values for the p-type CoAsS are more enhanced than n-type. Phonon calculations estimate the thermal conductivity of CoAsS quite higher $\sim$ 12 Wm^{-1}K^{-1} at temperature of 300 K than other thermoelectric materials like PbTe,

Bi$_2$Se$_3$ and even CoSbS. The effect of alloying has been calculated for the CoAs$_x$Sb$_{1-x}$S, CoAsS$_x$Se$_{1-x}$, and CoSbSe$_x$S$_{1-x}$ and it is seen that the reduction of thermal conductivity from 13 Wm^{-1}K^{-1} to 5.37 Wm^{-1}K^{-1} is maximum when the concentration of Sb in the CoAs$_x$Sb$_{1-x}$S alloy is 80%. A 44% reduction in thermal conductivity is also observed for 20% of Sb in CoAs$_x$Sb$_{1-x}$S alloy. The behavior of ZT is seen to be different for the two charge carriers. ZT values show up the maximum for n-type and p-type at different fractional values of alloying. The substantial superiority of charge carriers depend upon the alloy concentration and temperature leading to maximum value of n-type $ZT \sim 0.45$ and that of p-type ~ 0.41. Thus, alloyed cobaltite and paracostibite is seen to have enhanced thermoelectric properties which can be utilized as both n-type and p-type in different temperature ranges and concentration. This work provides insight into rational design of alloy for thermoelectric device, and the high ZT values of CoAs$_x$Sb$_{1-x}$S alloy is good enough to encourage further investigation of this alloy.

Chapter 4 studies the enhancement of thermoelectric figure of merit under the effect of alloying and nanostructuring on the type-I clathrate Ba$_8$Cu$_6$Si$_{40}$. We have also calculated the contribution of various atoms in reducing the lattice thermal conductivity in the clathrate structure. Atomistic Gr$\ddot{u}$neisen calculations show that the Ba atoms of one type are major cause of enhanced anharmonicity in the material. Alloy scattering has been shown to reduce the lattice thermal conductivity of pure Si-clathrate Ba$_8$Cu$_6$Si$_{40}$ from 1.64 Wm^{-1}K^{-1} to 0.80 Wm^{-1}K^{-1} in Ba$_8$Cu$_6$Si$_{17}$Ge$_{23}$ clathrate alloy at 400 K. Furthermore, the effect of boundary scattering is calculated and there has been seen a reduction of the clathrate lattice thermal conductivity to 0.15 Wm^{-1}K^{-1} in case of 30 nm sized Ba$_8$Cu$_6$Si$_{17}$Ge$_{23}$ clathrate alloy nanowire. Such reduced values of the nanostructured clathrate alloy can direct to make good performing Si based thermoelectric. A nanowire Ba$_8$Cu$_6$Si$_{17}$Ge$_{23}$ clathrate alloy with $ZT \sim 0.40$ around room temperature can be useful for micro refrigeration in Si-chips. It can also benefit the industry for heat barrier application in nanoelectronics.

Chapter 5 discusses the findings of present thesis work and future applications. In this chapter, we consider major outcomes of the work and discuss their relevance in the present status of energy conversion and power generation. We also discuss here the possible ways to steer this work for further enhancement in the thermoelectric performance.

List of Publications

1. **Prabhjot Kaur**, Suvankar Chakraverty, Ashok Kumar Ganguli and Chandan Bera. High anisotropic thermoelectric effect in palladium phosphide sulphide. *Physica Status Solidi B*, pages 1-5, 2017.

2. **Prabhjot Kaur** and Chandan Bera. Effect of alloying on thermal conductivity and thermoelectric properties of CoAsS and CoSbS. *Physical Chemistry Chemical Physics*, 19:24928-24933, 2017.

3. **Prabhjot Kaur**, Georg K. H. Madsen and Chandan Bera. Thermoelectric figure of merit and thermal conductivity of type-I clathrate alloy nanowires. *MRS Communications*, 9:370-374, 2019.

Conference Proceedings

1. **Prabhjot Kaur** and Chandan Bera. Layered Ternary Chalcogenide for Thermoelectric Application. *6th Interdisciplinary Symposium on Materials Chemistry*, Mumbai-400094, India, December 6-10, 2016.

Contents

List of Figures

Chapter 1

Introduction

The world's sustainable energy is going through a huge crisis since last many decades. Vehicles' exhaust, industrial processes, thermal power plants and space programs generate enormous amount of waste heat. This waste heat is toggling the global climate change on an alarming level. The only way to dump this waste is to scavenge it for useful purposes. The conversion of this waste heat into electricity is worth accomplish for. Thermoelectrics could be the solution for surviving this energy problem. Thermoelectricity is the process by which waste heat is converted into useful electrical energy. This thesis is a comprehensive introduction to the every aspect of the thermoelectric energy conversion. The efficiency of a thermoelectric material is measured by figure of merit ZT. The progress in the thermoelectric performance is achieved by increasing the efficiency of thermoelectric materials by reducing the thermal conductivity of crystal lattice and improving the power factor by alloying and nanostructuring.

1.1 Thermoelectric and related effects

1.1.1 Seebeck effect and Peltier effect

T. J. Seebeck in 1821 discovered that on heating the junction of two dissimilar electrical conductors, an electromotive force could be produced. These two dissimilar conductors are said to form a thermocouple (Fig.1.1). The amount of voltage produced is directly proportional to the difference in the temperature of two junctions. When a temperature difference ΔT is applied between the junctions of two conductors A and B, a potential difference V is appeared across them. The appeared voltage V is directly proportional to the temperature difference ΔT with constant of proportionality known as differential Seebeck coefficient S_{AB}, given by

$$S_{AB} = \frac{V}{\Delta T} \tag{1.1}$$

After a decade, J. Peltier found the reverse effect, in which the passage of an electric current through junction produces heating or cooling depending on the direction of current.

When an external potential is applied across the junction, current starts moving in the circuit and the junctions start heating up or cooling down. Peltier coefficient Π_{AB} in this case is equal to ratio of rate of heating or cooling Q at the junction to the amount of current I passing through the junction,

$$\Pi_{AB} = \frac{Q}{I} \tag{1.2}$$

The interdependency of these two effects was realized much later by W. Thomson (Lord Kelvin). He coined the third thermoelectric effect known as Thomson effect which happens in a homogeneous conductor. The effect states that when there are both electric current and temperature gradient in the conductor, reversible heating or cooling occurs. Seebeck coefficient and Peltier coefficient are related as $\Pi_{AB} = TS_{AB}$, where T is the absolute temperature. Thomson coefficient β is defined as,

$$\beta = T\frac{dS}{dT} \tag{1.3}$$

Thomson coefficient is seldom taken care of, however it is important for precise observations. Both Seebeck and Peltier effects depend on the bulk material properties despite of showing only the inter-facial phenomenon. Energy carried by electrons is different when current passes from one conductor to another. This difference in energy appears at the junction as heating or cooling making the Peltier effect. In Seebeck effect, electrons generate potential difference when they go from lower energy material to that in which their energy is higher under the application of heat.
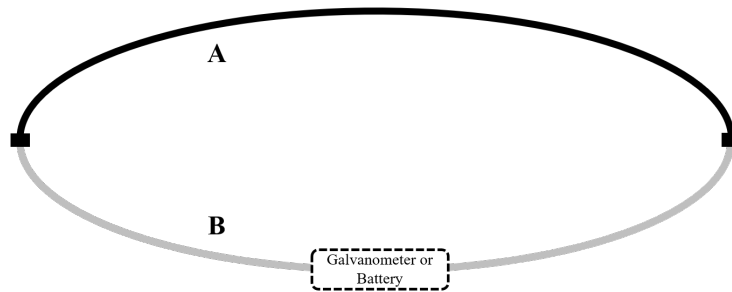
Figure 1.1: Thermoelectric couple made up of two conductors A and B.

In a thermocouple, heat flow and charge flow are linked to one another. Current flux due to electric charge and heat is given as [1],

$$J_e = L_{11}(-\frac{d\phi}{dx}) + L_{12}(-\frac{dT}{dx}) \tag{1.4}$$

$$J_q = L_{21}(-\frac{d\phi}{dx}) + L_{22}(-\frac{dT}{dx}) \tag{1.5}$$

where L_{ij} are transport coefficients, ϕ is the electric potential. For isothermal condition, $dT = 0$, heat current flux is given as,

$$J_q = \frac{L_{21}}{L_{11}}J_e = \Pi_{AB}J_e \tag{1.6}$$

2

When there is no current, $J_e = 0$, value of Seebeck coefficient is defined as,

$$S_{AB} = \frac{-d\phi}{dx} / \frac{dT}{dx} = \frac{-V}{\Delta T} = \frac{L_{12}}{L_{11}} \tag{1.7}$$

Both the coefficients S_{AB} and Π_{AB} are defined for a pair of two conductors. However, it would be much significant if these coefficients could be found for a single material. The absolute value of these coefficients can be found by regarding zero absolute value for the second material. In such case, absolute values will be equal to the differential values of these coefficients. In practice, most metals have very small values of absolute Seebeck coefficient as compared to semiconducting thermoelectric materials. One of these metals can be chosen as a reference to determine the absolute coefficients. Due to irreversible Joule heating and heat conduction effects, thermocouples were not used for significant conversion of heat to electricity and vice-versa before 1950's. After the introduction of semiconductor thermoelectric materials, the conversion of this energy became practical as Peltier refrigerators. Thermoelectric effects are always associated with irreversible processes like electrical resistance and thermal conduction. In addition to thermoelectric coefficients, these two also come under the category of transport properties of the solid. Electrical conductivity σ (reciprocal of electrical resistivity ρ) is defined for flow of charges through a material of area A and length L,

$$I = \frac{\sigma V A}{L} \tag{1.8}$$

where I is the electric current and V is the voltage applied to the material. Similarly, thermal conductivity (κ) is defined for rate of flow of heat (Q) through the same material when a temperature difference (ΔT) is applied across it,

$$Q = \frac{-\kappa A \Delta T}{L} \tag{1.9}$$

1.1.2 Efficiency and figure of merit of thermoelectric material

Assessment of thermoelectric performance is done by using one thermocouple, while practical modules are used made up of number of thermocouples. These thermocouples are connected electrically in series and thermally in parallel. Area of application of Peltier effect lies in the refrigeration and heat pumps. In this case, the source of electrical energy is provided by applying a potential difference across the two elements in series. The performance of refrigeration is calculated by quantity called coefficient of performance (COP) which is the ratio of amount of heat extracted from the source (at lower temperature T_1) to the amount of electrical energy consumed [2]. The rest of the energy is given to sink (at higher temperature T_2). The optimum or maximum value of COP is calculated as,

$$(COP)_{max} = \frac{T_1[(1 + Z_C T_m)^{1/2} - (T_2/T_1)]}{(T_2 - T_1)[(1 + Z_C T_m)^{1/2} + 1]} \tag{1.10}$$

where T_m is the average temperature, Z_C is the figure of merit of the thermocouple given as,

$$Z_C = \frac{(S_p - S_n)^2}{[(\kappa_p \rho_p)^{1/2}(\kappa_n \rho_n)^{1/2}]^2} \tag{1.11}$$

where S_p and S_n are Seebeck coefficients for p-type and n-type semiconductors respectively and κ_p and κ_n are thermal conductivities of p-type and n-type semiconductors respectively. While searching for good thermocouple, figure of merit $Z = S^2\sigma/\kappa$ of the single material is more convenient to find. Although, the value of Z cannot be used to assess the thermocouple performance. However, the value of Z_C tends to be the average of two Z_p and Z_n. Therefore, it is practical to search materials on the basis of single material figure of merit Z.
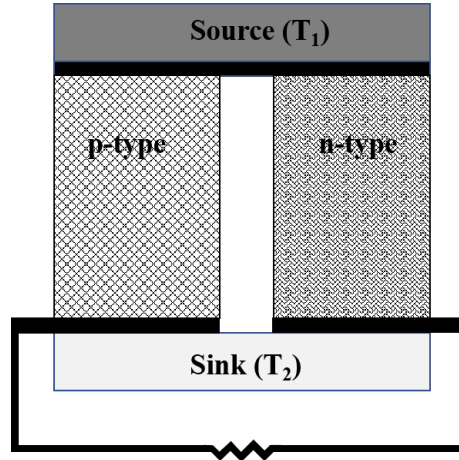
Figure 1.2: Thermoelectric generator using one thermoelectric element with p-type and n-type semiconductor. Temperature T_1 is source temperature and T_2 is sink temperature ($T_1 > T_2$).

On the other hand, Seebeck effect finds its area of application in thermoelectric generators. The arrangement for thermocouple is same as in Peltier effect, with only difference that temperature difference is applied across its end and potential difference is calculated (Fig.1.2). The quantity of importance is efficiency, η of the generator, defined as the ratio of generated output voltage to the heat extracted from the source [3].

$$\eta = \frac{(T_1 - T_2)((1 + Z_C T_m)^{1/2} - 1)}{T_1((1 + Z_C T_m)^{1/2} + T_2/T_1)} \tag{1.12}$$

If $Z_C T_m$ would be very large, the efficiency $\eta = (T_1 - T_2)/T_1$ becomes equal to carnot's efficiency. Present day efficiency of thermoelectrics is not competing with the conventional converters such as steam engines [4]. On the other hand, the cooling is also not up to the mark to compete with conventional refrigerator. Thermoelectrics are interesting due to solid state operation, noise proof working, reliability and compact size.

1.1.3 State-of-the-art of thermoelectric materials

Thermoelectric material Bi_2Te_3 opened a window of thermoelectric applications in long back 1950's. Till then, there has been a constant search for thermoelectric materials as shown in Fig.1.3 [5]. The performance of thermoelectric materials was enhanced as suggested by Ioffe using alloying of Bi_2Te_3 with Bi_2Se_3 and Sb_2Te_3. Similarly, the alloy of PbTe was made with PbSe and SnTe [3, 6, 7, 8]. These compounds contain heavy elements which reduce the phonon velocity [9], thus affecting the thermal conductivity. Bi_2Te_3 alloys with Bi_2Se_3 and Sb_2Te_3 have shown ZT values of ~ 1.0 in temperature range of 300 K-500 K for both n-type and p-type [10]. PbTe alloys having $ZT \sim 1.0$ at room temperature is stretched up to ~ 2.2 for p-type [11]. TAGS $((AgSbTe_2)_{1-x}(GeTe)_x)$ has also shown $ZT \sim 1.2$ for p-type [9, 12]. On the other hand, SiGe alloys are operated at high temperature [13, 14, 15].

Slack had proposed the idea of enhancing the ZT by reducing lattice thermal conductivity [16]. This was done by introducing rattler atoms in open and large cage structures of crystals like skutterudites, clathrates etc [10]. Skutterudites have shown thermoelectric coverage in large temperature region for power generation [17]. General formula for skutterudites is MX_3, where M is Co, Rh, Ir and X is P, As, Sb. These crystal structures occupy large empty space [18]. Huge reduction in thermal conductivity is seen by introducing rare earth atoms in the empty space [19]. For e.g., n-type $Ba_xYb_yCo_4Sb_{12}$ has an order of magnitude reduction in thermal conductivity at 300 K in comparison to $CoSb_3$ and ZT values reached 1.7 at room temperature [18, 19, 20, 21].

Clathrates have large unit cells containing huge number of atoms. Their open structures host loosely bound atoms. They have usually very low lattice thermal conductivity (1 $Wm^{-1}K^{-1}$) at room temperature. There are many types of clathrate structures, among which type-I is the most explored [5, 10]. General formula for type-I clathrates is $X_2Y_6E_{46}$, where X and Y are guest atoms which fill the two types of voids in the clathrate structure, E represents Si, Ge, Sn. The ZT of ~ 1.4 is obtained for n-type $Ba_8Ga_{16}Ge_{30}$ [22, 23]. These structures have been shown with their ZT values in Fig.1.4. Complex crystal structures are prone to have extra low thermal conductivity due to large optical branches having low velocity phonons. Examples of compounds with extra low values of thermal conductivity are β- Zn_4Sb_3 with 0.65 $Wm^{-1}K^{-1}$ and Zintl $Yb_{14}MnSb_{11}$ with 0.4 $Wm^{-1}K^{-1}$ [24, 25].

Half heusler compounds made of transition metal atoms, usually have cubic structure. Uher et al. have studied pure and alloyed half heusler compounds. Figure of merit ZT of half heusler alloy $Zr_{1-x}Ti_xCoSb_{0.8}Sn_{0.2}$ is obtained around 1.0 for p-type and n-type [26].

Oxides show stable behavior for high temperature applications. Despite of low mobility of carriers, $NaCo_2O_4$ and $Ca_4Co_3O_9$ have shown $ZT \sim 1.0$ at high temperature around 800 K [27, 28]. The n-type perovskites $SrTiO_3$ and $CaMnO_3$ are good thermoelectric oxides [29, 30].

In addition to bulk engineering of ZT, PGEC (phonon glass electron crystal) can be found in low dimension materials too. The interest in thermoelectric was rejuvenated after multiple decades with the theoretical prediction of high efficiency nanostructure materials contingent to experimental observations. According to Hicks and Dresselhaus, phonons
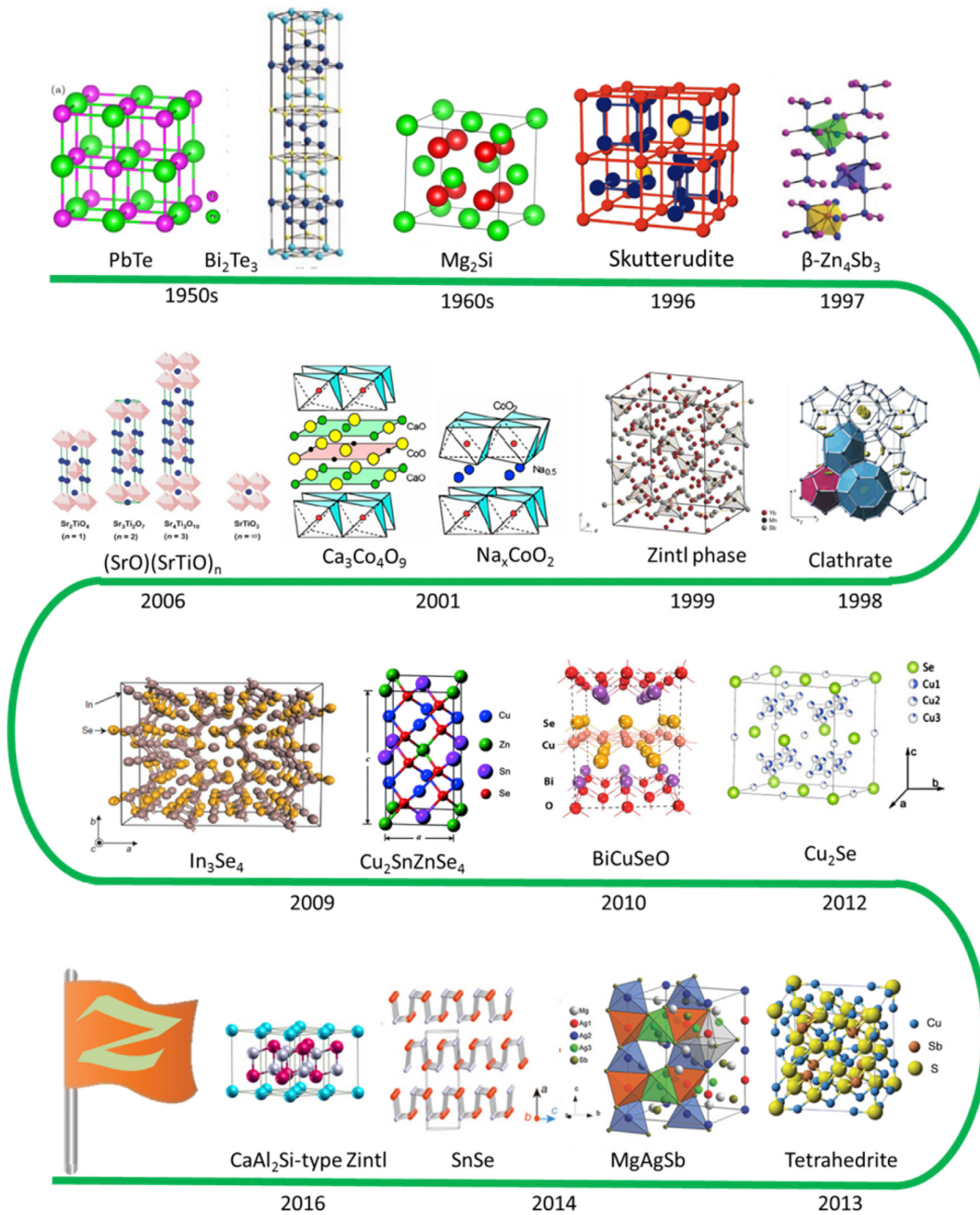
Figure 1.3: Time-line of thermoelectric materials (Ref.[5]).

having classical effects and electrons with quantum effects in nano-dimensions can tend to high ZT values [31, 32, 33]. Both power factor and thermal conductivity are modified as required to give high ZT values. There are two branches comprising single nanostructures such as nanowires, super-lattices and bulk nanostructures [31]. Superlattice Bi_2Te_3/Sb_2Te_3 have shown $ZT \sim 2.4$ at room temperature with lattice thermal conductivity of 0.2 $Wm^{-1}K^{-1}$ [34]. This value of thermal conductivity is 2.5 times smaller than
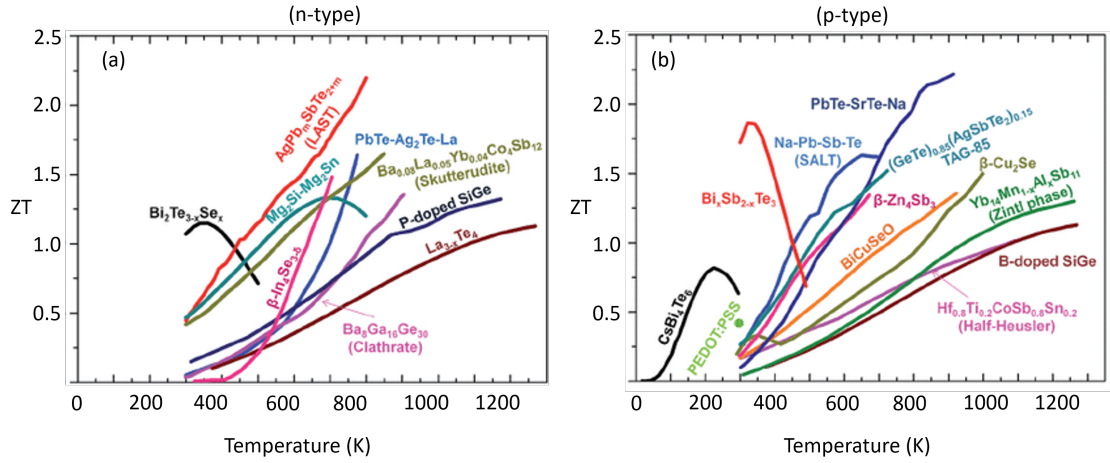
Figure 1.4: Summary of some of the best ZT for bulk thermoelectric materials to date as a function of temperature (a) n-type (b) p-type (Ref.[17]).

alloy $Bi_{0.5}Sb_{1.5}Te_3$ values of 0.5 $Wm^{-1}K^{-1}$. Hence, superlattices have lower thermal conductivity than their alloy counterparts.

Nanostructured thin films and wires have been predicted to have superior ZT values which was afterwards proved experimentally [31]. Films of Bi_2Te_3-Sb_2Te_3 and PbTe-PbSe have shown extremely low value of thermal conductivity (~ 0.3 $Wm^{-1}K^{-1}$) [35, 36, 37]. Nanowires of GaN, Bi_2Te_3, InSb and InAs have reduced thermal conductivity due to phonon-boundary scattering. Si-nanowires have two orders of lattice thermal conductivity reduction without disturbing electronic transport. Si-nanowires have $ZT \sim 1.0$ at 200 K [38]. WSe_2 crystals in layered form have thermal conductivity below the minimum predicted value [39]. Polycrystalline Si-Ge alloy nanostructure are studied with enhanced ZT values [13, 40].

Nanotubes also claim even reduced values of lattice thermal conductivity. Nanocomposites have geometry in which nanoinclusions such as nanowires or nanoparticles are embedded in host structure. Similar lattice thermal conductivity reduction is shown by nanograined materials.

1.2 Boltzmann transport equation

The phenomenon of transport of charge carriers is linked with the average macroscopic quantities like thermal conductivity, electrical conductivity etc. Microscopic behavior of charge particles gives rise to macroscopic behaviour of a material. Due to difficulty in tracking the microscopic motion of particles (such as electrons, holes, phonons etc) in the system, the statistical approach is considered for the evaluation of transport coefficients. Such a statistical approach is hired using Boltzmann transport equation which gives the position and velocity of particles as its solution. The equation balances the various processes in the steady state and extract out macroscopic physical properties of carriers in

metals or semiconductors [41, 42].

The motion of carriers in a metal or semiconductor are affected by external fields, temperature gradients, concentration gradients, impurities and lattice waves etc. We consider the scenario where the electron gains energy under the effect of a field or a temperature gradient and loses its energy and momentum by scattering. The particular state of carriers in the material is defined by distribution function $f(\boldsymbol{k}, \boldsymbol{r}, t)$ which is a function of phase-space and time. Distribution function $f(\boldsymbol{k}, \boldsymbol{r}, t)$ is the local concentration of carriers in the state $\boldsymbol{k}$ (momentum space) in the neighborhood of $\boldsymbol{r}$ in space. The probability of finding a particle (electron or phonon) in the phase space region $[\boldsymbol{r}, \boldsymbol{r} + \mathrm{d}\boldsymbol{r}]$ and $[\boldsymbol{k}, \boldsymbol{k} + \mathrm{d}\boldsymbol{k}]$ at time t is given by $f(\boldsymbol{k}, \boldsymbol{r}, t)\mathrm{d}\boldsymbol{r}\mathrm{d}\boldsymbol{k}$. Electron wave vector or momentum vector is represented by $\boldsymbol{k}$ and phonon wave vector will be represented by $\boldsymbol{q}$.

Carriers move in and out of the region $\boldsymbol{r}$ as a result of various forces acting on it. Boltzmann transport equation accounts for all possible mechanisms by which f changes.

$$\frac{df}{dt} = \frac{\partial f}{\partial \boldsymbol{r}}\frac{d\boldsymbol{r}}{dt} + \frac{\partial f}{\partial \boldsymbol{k}}\frac{d\boldsymbol{k}}{dt} + \frac{\partial f}{\partial t}\frac{dt}{dt} \qquad (1.13)$$

where the first term on right hand side represents the change in f due to various processes based on the position like temperature gradient, concentration gradient etc, second term represents the effect of external fields which will change the momentum of the particle and third term contains the various scattering (collision) processes which use to be random. Rate of change of distribution f due to temperature or concentration gradient is given as:

$$\frac{\partial f}{\partial t}\Big|_{diffusion} = -\boldsymbol{v_k}\cdot\frac{\partial f}{\partial \boldsymbol{r}} = -\boldsymbol{v_k}\cdot\nabla f \qquad (1.14)$$

where $\boldsymbol{v_k}$ is velocity of the particle in state $\boldsymbol{k}$. Distribution changes due to the fields (electric field $\boldsymbol{E}$) at the rate:

$$\frac{\partial f}{\partial t}\Big|_{fields} = -\frac{e}{\hbar}\boldsymbol{E}\cdot\frac{\partial f}{\partial \boldsymbol{k}} \qquad (1.15)$$

where e is the electronic charge and $\hbar$ is the reduced Planck's constant.

Regarding the collision term, there are numerous processes which would affect the electron's motion. Electron may collide with other electrons, however this can be neglected in non-degenerate semiconductors. The effect of electron-electron collision is more in degenerate semiconductors. Apart from this, electron may collide with defects, impurities in the crystal and exchange its energy. While calculating the effect of collision term, it is assumed that the collision time is extremely small. Due to collisions, electrons get transferred from one point in k-space to another. The probability of transition from a point around $\boldsymbol{k}$ to a point $\boldsymbol{k}'$ is given by $Q(\boldsymbol{k}, \boldsymbol{k}')$. Q will have various expressions based on different scattering mechanisms (e-e scattering, e-phonon scattering, e-impurity scattering etc). Effect of scattering is more complicated. This gives rise to rate of change of f as,

$$\frac{\partial f}{\partial t}\Big|_{scatt.} = \int [f'(1-f) - f(1-f')]Q(\boldsymbol{k}, \boldsymbol{k}')d\boldsymbol{k}' \qquad (1.16)$$

where $f^{'}$ is the distribution corresponding to point $\boldsymbol{k}^{'}$. Our theory is based upon the Boltzmann equation for the motion of carriers in the material. Boltzmann equation combines the effects of externally applied fields and the scattering of carriers by different mechanisms. Due to the different physical processes, the function f would change and we suppose that this change is relatively smaller and the Boltzmann equation is written in steady state ($df/dt = 0$) as,

$$-\boldsymbol{v}_{\boldsymbol{k}} \cdot \frac{\partial f}{\partial \boldsymbol{r}} - \frac{e}{\hbar} \boldsymbol{E} \cdot \frac{\partial f}{\partial \boldsymbol{k}} = -\frac{\partial f}{\partial t}|_{scatt.} \tag{1.17}$$

The two terms on left hand side are related with temperature gradient or concentration gradient and electric field respectively. The left hand side of the equation is deterministic, however the right hand side is non-deterministic. The scattering or collision term is comprising of non-linear integrals which are difficult to solve analytically. Therefore, Boltzmann transport equation is solved for distribution function by various methods like numerical methods (Monte Carlo method, finite element method etc.) and approximation methods (variational method and relaxation time approximation method etc). Among numerous methods of solving Boltzmann transport equation, some of the methods have been explained below briefly.

1.2.1 Variational method

Boltzmann transport equation is an integral equation over many variables. Its solution is found by various approximations. As this is an integral equation, mathematics of integral equations can be used to link this theorem with variational problem. By interpreting Boltzmann equation as variational problem, its approximate solution will be found by variational theorem.

Physical interpretation of Variational theorem: Variational function or the integral expression is directly proportional to rate of entropy production by collisions or scatterings [43]. Moreover, entropy plays an important role in macroscopic theory of thermodynamics of irreversible processes, therefore connection between microscopic statistical theory which originates from Boltzmann equation and macroscopic thermodynamic theory is by transport coefficients like electrical conductivity (σ) and thermal conductivity (κ). Now, both of the approaches have the same scalar quantity. Entropy signifies a connection between equilibrium statistical mechanics and thermodynamics. In case of non-equilibrium statistical mechanics, variational theorem corresponds to steady state thermodynamics.

Boltzmann equation represents the state originating from balancing the rates at which electrons transfer from one quasi-stationary state to another. The solution of this equation can be obtained by applying variational theorem to a general function. In the steady state, total rate of change should be zero and Boltzmann transport equation is given by Eq.(1.17), assuming the change in the distribution function from equilibrium distribution function (f_0) to be very small ($f \approx f_0$) and the electron is under the effect of electric field only,

$$-\boldsymbol{v}_{\boldsymbol{k}} . e\boldsymbol{E} \frac{\partial f_0}{\partial E_{\boldsymbol{k}}} = \int [f^{'}(1-f) - f(1-f^{'})]Q(\boldsymbol{k}, \boldsymbol{k}^{'}) d\boldsymbol{k}^{'} \tag{1.18}$$

where $E_{\boldsymbol{k}}$ is the energy in state $\boldsymbol{k}$. Introduce a new function ϕ such that f can be expanded by using Taylor's theorem,

$$f = f_0 - \phi \frac{\partial f_0}{\partial E_{\boldsymbol{k}}} \tag{1.19}$$

$$f = f_0 + \phi \frac{f_0(1 - f_0)}{k_B T} \tag{1.20}$$

Boltzmann equation becomes:

$$-\boldsymbol{v}_{\boldsymbol{k}}.e\boldsymbol{E} \frac{\partial f_0}{\partial E_{\boldsymbol{k}}} = \int [f'(1-f) - f(1-f')]Q(\boldsymbol{k},\boldsymbol{k}')d\boldsymbol{k}' \tag{1.21}$$

$$-\boldsymbol{v}_{\boldsymbol{k}}.e\boldsymbol{E} \frac{\partial f_0}{\partial E_k} = \frac{1}{k_B T} \int (\phi - \phi')P(\boldsymbol{k},\boldsymbol{k}')d\boldsymbol{k}' \tag{1.22}$$

where $P(\boldsymbol{k},\boldsymbol{k}')$ is the equilibrium transition probability rate between $\boldsymbol{k}$ and $\boldsymbol{k}'$. This equation can be written in general form where this is solved for unknown distribution function ϕ:

$$X(k) = \int (\phi(k) - \phi(k'))P(k,k')dk' \tag{1.23}$$

where $X(k)$ is a known function of k and depends upon the external fields. And $P(k,k')$ is also known, $\phi(k)$ has to be found. This equation can be written in the other form as,

$$X = L\phi \tag{1.24}$$

Scattering operator L transforms ϕ into another function of k by integration. Notations:

$$< \phi, \psi > = \int \phi(k)\psi(k)dk \tag{1.25}$$

$$< \phi, L\psi > = < \psi, L\phi > \tag{1.26}$$

Variational Principle: "If ϕ is the solution of the Boltzmann integral equation and ψ is any function which satisfies the condition $< \psi, L\psi > = < \psi, X >$: then the variational theorem states that of all the functions which satisfy this condition, ϕ makes $< \psi, L\psi >$ a maximum." In another way the principle is written as,
"If ϕ is the solution of the Boltzmann equation then

$$\frac{< \phi, L\phi >}{(< \phi, X >)^2} \tag{1.27}$$

has its minimum value and we are left with the inverse of the one side ($< \phi, L\phi >$ say) or the other which by principle is maximized."

For constructing the variational function ($< \phi, L\phi >$), it is needed to multiply the Boltzmann equation by $\phi(k)$ and integrate over $\boldsymbol{k}$. The scattering part :

$$\frac{\partial f}{\partial t}\Big|_{scatt.} = -\frac{1}{k_B T} \int (\phi - \phi')P(\boldsymbol{k},\boldsymbol{k}')d\boldsymbol{k}' \tag{1.28}$$

$$- \int \phi \frac{\partial f}{\partial t}|_{scatt.} d\mathbf{k} = \frac{1}{k_B T} \int \phi \int (\phi - \phi^{'}) P(\mathbf{k}, \mathbf{k}^{'}) d\mathbf{k}^{'} d\mathbf{k} \tag{1.29}$$

Statistical definition of entropy is given by:

$$S = -k_B \int [f ln f + (1 - f) ln(1 - f)] d\mathbf{k} \tag{1.30}$$

Differentiating with respect to 't' ($f=f_0$):

$$\frac{\partial S}{\partial t} = -\frac{1}{T} \int (\phi \frac{\partial f}{\partial t}) d\mathbf{k} \tag{1.31}$$

In the steady state, $\partial S/\partial t$ is zero, but separately they have values using the Boltzmann equation. Using Eq. 1.29, the scattering part of above equation becomes,

$$\frac{\partial S}{\partial t}]_{scatt.} = -\frac{1}{T} \int \phi \frac{\partial f}{\partial t}]_{scatt.} d\mathbf{k} = \frac{1}{k_B T^2} \int \phi \int (\phi - \phi^{'}) P(\mathbf{k}, \mathbf{k}^{'}) d\mathbf{k}^{'} d\mathbf{k} \tag{1.32}$$

By using Eq. 1.26, above equation becomes,

$$\frac{\partial S}{\partial t}]_{scatt.} = \frac{1}{k_B T^2} \int \int (\phi - \phi^{'})^2 P(\mathbf{k}, \mathbf{k}^{'}) d\mathbf{k}^{'} d\mathbf{k} \tag{1.33}$$

The field part can be written by using Eq 1.20 and Eq 1.22,

$$-\frac{\partial S}{\partial t}]_{field} = \frac{1}{T} \int \phi \frac{\partial f}{\partial t}]_{field} d\mathbf{k} = -\frac{1}{T} \int \phi e \mathbf{E}.\mathbf{v_k} \frac{\partial f_0}{\partial E_{\mathbf{k}}} d\mathbf{k} \tag{1.34}$$

$$-\frac{\partial S}{\partial t}]_{field} = \frac{1}{T} \mathbf{E}. \int e \mathbf{v_k} (f - f_0) d\mathbf{k} = \frac{1}{T} \mathbf{E}.\mathbf{J} \tag{1.35}$$

where $\mathbf{J}$ is the electric current density in steady state. In the thermodynamics of irreversible processes, entropy production (by Onsager relations) is given by:

$$\frac{\partial S}{\partial t} = \sum_k X_k J_k \quad (k = 1, 2, 3.....) \tag{1.36}$$

From above equation we can see that the analogue of current is ϕ and generalized force corresponding to this is,

$$X_{\mathbf{k}} = -\frac{1}{T} e \mathbf{E}.\mathbf{v_k} \frac{\partial f_0}{\partial E_{\mathbf{k}}} = \int L(\mathbf{k}, \mathbf{k}^{'}) \phi^{'} d\mathbf{k}^{'} \tag{1.37}$$

We can write in general,

$$X_k = \sum_k L_{k,k'} J_{k'} \tag{1.38}$$

And Onsager relations from this comes out as: $L_{k,k'} = L_{k',k}$. It can be written in this form as:

$$\frac{\partial S}{\partial t}]_{scatt.} = \sum_{k,k'} L_{k,k'} J_k J_k^{'} = <\phi, L\phi> \tag{1.39}$$

11

$$-\frac{\partial S}{\partial t}]_{drift} = \sum_k X_k J_k = <\phi, X> \tag{1.40}$$

For all current distributions (for which $\frac{\partial S}{\partial t}]_{scatt.} = -\frac{\partial S}{\partial t}]_{field}$), steady state distribution makes the $\frac{\partial S}{\partial t}]_{scatt.}$ a maximum. In other words, currents be such that

$$\sum_{k,k'} L_{k,k'} J_k J_{k'} - 2 \sum_k J_k X_k \tag{1.41}$$

is a minimum. It is just the negative of the actual entropy production in dissipative processes.

1.2.2 Monte Carlo method

This method is used to solve Boltzmann transport equation for small scale transport processes. As this is one of the numerical methods, it has many applications in high energy physics, device designing, radiative transfer, nuclear reactor designing etc. This is a semi-classical approach to study the transport of charge carriers in the semiconductors. Trajectories of charge particles are simulated under the effect of external fields. The free paths and the scattering events are assumed on the basis of random numbers [44, 45].

The numerical solution of transport equation is done on the basis of stochastic approach in Monte Carlo method. This statistical method gives the solution of Boltzmann transport equation using band structure and scattering mechanisms. Fermi-Golden rule is used to extract scattering mechanism, which is quantum mechanical in nature. In this method, the particle's free flight and scattering mechanism is chosen stochastically, by giving quantum mechanical treatment to various scattering mechanisms.

There are various types of Monte Carlo simulations among which a few are one particle simulation, ensemble simulation and self consistent simulation. One particle simulation is suitable for studying bulk properties such as drift velocity. The motion of single particle is tracked at one time and the same process is repeated for another particle and the ensemble of trajectories is collected. On contrary to it, in ensemble simulation, a large number of particles are tracked at a same time. Third type known as self consistent, clubs the ensemble simulation with the Poisson equation and is useful for device simulation.

Time of free path flight is determined from the scattering rate. Scattering events can be characterized in two ways as elastic in which energy is not changed, and other is inelastic in which energy is transferred during the scattering. Electron impurity and surface scattering are examples of elastic scattering. Inelastic scattering includes electron phonon scattering. At the end of the flight, scattering rates determined by Born approximation are randomly selected. In Born approximation, transition between two states is calculated in the scattering event. Fermi-Golden rule gives the first order transition probability per time for scattering from a $\boldsymbol{k}$-state to $\boldsymbol{k}'$-state,

$$Q(k,k') = \frac{2\pi}{V} | <k|H'|k'> |^2 \delta(E - E') \tag{1.42}$$

where H' is the collision Hamiltonian and E and E' are initial and final energies respectively. After scattering probability, scattering rate is calculated for a given scattering process.

1.2.3 Relaxation time approximation

To understand the transport of electrons and holes in semiconductors, the concept of relaxation time $\tau_{\boldsymbol{k}}$ is used. This time is assumed to be the interval during which a disturbed distribution function f relaxes back to its equilibrium value f_0. The concept of relaxation time for the carriers will be used and the disturbance of distribution function from its equilibrium state is supposed to be linear. The total relaxation time builds itself from various scattering processes as scattering by acoustic lattice vibrations, ionized impurities etc. The Boltzmann equation after incorporating above suppositions is given as,

$$-\boldsymbol{v_k}\cdot\frac{\partial f}{\partial T}\nabla T - \boldsymbol{v_k}\cdot e\frac{\partial f}{\partial E_{\boldsymbol{k}}}\boldsymbol{E} = \frac{f_0 - f}{\tau_{\boldsymbol{k}}} \tag{1.43}$$

Thermoelectric behavior of a material depends upon its transport properties, which usually come from charge carriers. Therefore, transport coefficients are related to electronic band structure of a material. Transport of electric charge is executed by quasi-free electrons in metals. While in semiconductors, charge transport is done by holes in addition to free electrons. The process of conduction of electrons was successfully explained by quantum theory [46]. According to this theory, an electron can acquire energy levels in a crystal depending upon its interaction with the crystal's periodic potential. This interaction gives rise to energy bands for electrons separated by forbidden energy gaps. The difference in the forbidden gap sheds light on the superior transport of electric charge in metals than insulators. The probability that an energy state having energy E will be occupied by an electron is given by Fermi distribution function as,

$$f_0(E) = [exp(\frac{E - E_F}{k_B T}) + 1]^{-1} \tag{1.44}$$

where E_F is the Fermi energy level and k_B is the Boltzmann constant. The probability of finding the electron goes from one to zero as $E - E_F$ goes from less than $k_B T$ to more than $k_B T$ respectively. Every electron state is dependent upon the momentum (i.e. wave vector $\boldsymbol{k}$) in addition to energy. Energy bands which are only near the Fermi level contribute in the transport process. For conduction of electrons, they must go from one filled energy state to empty state. In case of metals, Fermi level exists well inside the conduction band, which gives great number of electrons to jump into the empty states. This makes a metal highly conducting in nature. On the other hand, when the Fermi level lies in between the energy gap, there will be no electrons to fill the states in conduction band which leads to insulating behavior. When the Fermi level lies close to conduction band, a small amount of conductivity is present due to few number of electrons present near the conduction band empty states. In case when the Fermi level is close to valence band, there will be a conduction of charge due to empty states in valence band. The conduction is still due to

13

negative electrons but the process is defined by motion of positive holes. Both these cases make the material semiconducting with moderate amount of conductivity.

The transport of charge carriers is understood with the help of Boltzmann equation. The transport coefficients are obtained by using boundary conditions. Electrical conductivity σ is defined at zero temperature gradient and electronic thermal conductivity κ_e is defined for zero electric current. The current density is given as the integral of group velocity times the probability of occupation integrated over all the possible states,

$$\boldsymbol{J} = -\frac{2e}{8\pi^3} \int \boldsymbol{v}(\boldsymbol{k}) f d\boldsymbol{k} \tag{1.45}$$

For defining transport coefficients, assuming no concentration or temperature gradient, and assume system to be in steady state, $df/dt = 0$, the Boltzmann equation (Eq 1.17) becomes,

$$\frac{F}{\hbar} \cdot \nabla_{\boldsymbol{k}} f = \frac{\partial f}{\partial t}]_{scatt.} \tag{1.46}$$

Assuming the change in the distribution to be very small, we can expand the f to first order in $\delta\boldsymbol{k}$ using Taylor expansion,

$$f(\boldsymbol{k}) = f_0(\boldsymbol{k} - \delta\boldsymbol{k}) = f_0(E) - \nabla_{\boldsymbol{k}} f_0(E)\delta\boldsymbol{k} \tag{1.47}$$

$$f(\boldsymbol{k}) = f_0(E) - \hbar \frac{df_0(E)}{dE} v(\boldsymbol{k}).\delta\boldsymbol{k} \tag{1.48}$$

$$f(\boldsymbol{k}) = f_0(E) + e\tau(E)\frac{df_0(E)}{dE} v(\boldsymbol{k}).\boldsymbol{E} \tag{1.49}$$

where $\delta\boldsymbol{k} = -(e\boldsymbol{E}\tau(E))/\hbar$. Putting the above equation in the formula for current density $\boldsymbol{J}$ in Eq. 1.45,

$$\boldsymbol{J} = -\frac{2e}{8\pi^3} \int \boldsymbol{v}(\boldsymbol{k})(e\tau(E)\frac{df_0}{dE}\boldsymbol{v}(\boldsymbol{k}).\boldsymbol{E})d\boldsymbol{k} \tag{1.50}$$

As $\boldsymbol{J} = \sigma\boldsymbol{E}$, thus the formula for electrical conductivity can be obtained as,

$$\sigma = -\frac{2e^2}{3(8\pi^3)} \int v^2(E_{\boldsymbol{k}})\tau(E_{\boldsymbol{k}})\frac{df_0}{dE}d\boldsymbol{k} \tag{1.51}$$

The value of σ can be written in a more generalized manner as,

$$\sigma = e^2 \int dE(-\frac{\partial f_0}{\partial E})\Sigma(E) \tag{1.52}$$

where Σ is known as transport distribution function and is given as,

$$\Sigma = \sum_{\boldsymbol{k}} v_x^2(\boldsymbol{k})\tau(\boldsymbol{k})\delta(E - E(\boldsymbol{k})) \tag{1.53}$$

The electrical conductivity is seemed to depend on the relaxation time. On the other hand, the Seebeck coefficient comes out to be independent of the relaxation time and is given as,

$$S = \frac{e}{\sigma T} \int dE(-\frac{\partial f_0}{\partial E})\Sigma(E)(E - E_F) \tag{1.54}$$

The electronic thermal conductivity is given as,

$$\kappa_e = \frac{1}{T} \int dE(-\frac{\partial f_0}{\partial E})\Sigma(E)(E - E_F)^2 - \sigma S^2 T \tag{1.55}$$

We approximate the values of these parameters by considering low and high extremes of E_F compared to $k_B T$. When $E_F >> k_B T$, we deal with conductor under degenerate case. The electrical conductivity is given as,

$$\sigma = \frac{8\pi}{3}(\frac{2}{h^2})^{3/2}e^2(m^*)^{1/2}\tau_0 E_F^{r+3/2} \tag{1.56}$$

where r denotes the scattering mechanism for the electrons and τ_0 also depends upon the scattering process. Electronic thermal conductivity in case of metal is related to electrical conductivity by Wiedemann-Franz law. According to this law, the ratio of κ_e/σ is equal $L = (\pi^2 k^2)/3e^2$ for all metals at a particular temperature. The expression for Seebeck coefficient for metals is,

$$S = \mp\frac{\pi^2}{3}\frac{k}{e}\frac{r + 3/2}{E_F/k_B T} \tag{1.57}$$

As $(E_F/k_B T) >> 1$, so Seebeck coefficient is smaller for metals. On the other hand, when $E_F << k_B T$, we consider the case of intrinsic semiconductor under the non-degenerate approximation. The values of electrical conductivity and Seebeck coefficient are,

$$\sigma = \frac{8\pi}{3}(\frac{2}{h^3})^{3/2}e^2(m^*)^{1/2}T\tau_e(k_B T)^{r+3/2}\Gamma(r + 5/2)exp(E_F/k_B T) \tag{1.58}$$

$$S = \mp\frac{k}{e}[\frac{E_F}{k_B T} - (r + 5/2)] \tag{1.59}$$

In case of extrinsic semiconductor, $E_F/k_B T >> 1$, so S may be much smaller. Value of S in case of semiconductor is much different from metals, however the ratio of κ_e/σ differ by factor less than two. Electronic thermal conductivity is linked to electrical conductivity by Lorentz factor L. This factor varies with carrier concentration [47]. For low value of concentration, the Lorentz factor is reduced from its free electron value. The calculated electronic thermal conductivity is thus, overestimated in this case of lower concentration. S for n-type semiconductor is negative because E_F is calculated upwards from conduction band edge. Whereas S acquires positive value for p-type semiconductor because E_F is measured downwards from valence band edge.

Value of E_F depends on amount of doping and it is measured from the edge of conduction band E_C in case of n-type. Seebeck coefficient is seen as average value of electron energy in the range of Fermi level E_F. Looking at σ closely, we observe that $\partial f_0/\partial E$ is having non-zero value only near the Fermi level. Seebeck coefficient expression reveals that, as for a metal E_F is well inside the band so electron distribution above and below E_F cancel each other, therefore metals have smaller S values. Deeper E_F gives rise to higher

electrical conductivity because of higher density of states (DOS) inside the band. G. D. Mahan had proposed ideal DOS to be equivalent to Dirac delta function [48]. After this idea, materials with such electronic DOS were searched for. Materials having d-electrons and f-electrons give rise to such DOS values.

1.3 Factors affecting charge transport

1.3.1 Bipolar effects

At ordinary temperature, narrow band gap semiconductor has both electrons and holes available for conduction. For wide band gap material, such condition occurs at high temperature. In such a material, electrical conductivity is linear sum of conductivities of individual carriers.

$$\sigma = \sigma_n + \sigma_p \tag{1.60}$$

whereas S is weighted average of Seebeck values of both types,

$$S = \frac{S_n \sigma_n + S_p \sigma_p}{\sigma_n + \sigma_p} \tag{1.61}$$

As Seebeck values for n-type and p-type are opposite in sign so overall S will be lower. Therefore, bipolar term decreases the Seebeck coefficient, because both types of carriers move from hot end to cold end and neutralize the appeared voltage. The expression for electronic thermal conductivity is,

$$\kappa_e = \kappa_n + \kappa_p + \frac{\sigma_n \sigma_p}{\sigma_n + \sigma_p}(S_n - S_p)^2 T \tag{1.62}$$

The additional term is due to bipolar flow of charges [49]. The bipolar term is although not included in W-F law, therefore this contribution goes into lattice thermal conductivity part erroneously. Bipolar contribution rises at high temperature and usually coincides with peak value temperature of S and σ. The κ_e/σ ratio also increases much in case of bipolar conduction. This can be reduced by selectively removing the minority carriers.

1.3.2 Importance of energy gap

The value of Seebeck coefficient is maximum when carrier concentration of minority carriers is small. The maximum value of Seebeck coefficient S_{max} depends on the energy gap of the semiconductor [50]. Estimate of the energy gap E_g is done by measuring the Seebeck coefficient, according to Goldsmid-sharp rule [51],

$$E_g = 2k_B T S_{max} \tag{1.63}$$

The maximum value of Seebeck coefficient is obtained when Fermi level lies somewhere between the middle and edges of the conduction or valence bands. Seebeck coefficient for a bipolar semiconductor can be written as,

16

$$S = \frac{S_n \frac{\sigma_n}{\sigma_p} + S_p}{\frac{\sigma_n}{\sigma_p} + 1} \tag{1.64}$$

$$\frac{\sigma_n}{\sigma_p} = C exp(\frac{(E_F)_n}{k_B T} - \frac{(E_F)_p}{k_B T}), \quad C = \frac{\mu_n}{\mu_p}(\frac{m_n^*}{m_p^*})^{3/2} \tag{1.65}$$

where $(E_F)_n$ and $(E_F)_p$ are Fermi levels corresponding to conduction band and valence band, μ_n and μ_p are carrier mobilities and m_n^* and m_p^* are effective masses of electrons and holes in n-type and p-type respectively. The maximum Seebeck coefficient for a small gap semiconductor need not lie for Fermi level far from either band. When both type of carriers have equal product value of mobility and effective mass, maximum Seebeck coefficient remains close to $E_g/2k_B T$. Even if one of the carriers dominates, the value of S remains close to above given value. For an optimum value of Seebeck coefficient, energy gap should be larger than $6k_B T$, however the practical materials having high mobility and mass product have smaller energy gaps.

1.3.3 Mobility and effective mass

The condition of high effective mass contradicts with high value of mobility simultaneously to make maximum ZT. Larger effective mass increases Seebeck coefficient, though decreases the electrical conductivity. Density of states effective mass m^* becomes larger for less sharper and high density of narrow bands near the Fermi level. Larger effective mass reduces the carrier mobility. However, the precise relationship between the two depends on many perspectives such as electronic band structure, scattering of carriers and anisotropy in the crystal [52]. For a semiconductor material having multi-valley valence and conduction bands, the effective mass is given by product of effective mass of single band and $N_v^{2/3}$ where N_v is the number of valleys. Effective mass is given as,

$$m^* = N_v^{2/3}(m_1 m_2 m_3)^{1/3} \tag{1.66}$$

where m_1, m_2 and m_3 are effective masses along symmetry axes. Variation of mobility with m^* depends on scattering mode. For acoustic mode scattering, inertial mass for single valley M_I is given as,

$$\mu(m^*)^{3/2} \propto \frac{N_v}{M_I}, \quad M_I = \frac{3}{\frac{1}{m_1} + \frac{1}{m_2} + \frac{1}{m_3}} \tag{1.67}$$

Therefore to achieve optimum ZT, we should choose a semiconductor having more number of valleys and low inertial mass for carriers. Covalent compounds usually have high mobility and ionic compounds have low mobility with narrow bands. However, both types show good thermoelectric properties [53, 54].

1.3.4   Power factor

The numerator of figure of merit Z at a given temperature is known as power factor $(S^2\sigma)$. Its value depends upon the carrier concentration. A large value of power factor corresponds to high voltage and current. In case of metals or degenerate semiconductor, the value of S and σ is given as,

$$S = \frac{8\pi^2 k_B^2}{3eh^2} m^* T (\frac{\pi}{3n})^{2/3} \tag{1.68}$$

$$\sigma = ne\mu \tag{1.69}$$

where n is carrier concentration, μ is carrier mobility. As carrier concentration increases, Seebeck coefficient decreases and electrical conductivity increases. In case of non-degenerate semiconductor, the expression for carrier concentration and carrier mobility is given by,

$$n = 2(\frac{2\pi m^* k_B T}{h^2})^{3/2} exp(\frac{E_F}{k_B T}) \tag{1.70}$$

$$\mu = \frac{4}{3\pi^{1/2}}\Gamma(r + \frac{5}{2})\frac{e\tau_0(k_B T)^r}{m^*} \tag{1.71}$$

where Γ is gamma function. The electrical conductivity varies as exponential function of $E_F/k_B T$ whereas S varies linearly with $E_F/k_B T$. There will be a particular value of Fermi level which will correspond to maximum power factor. The peak of ZT is obtained at carrier concentration of 10^{19} to 10^{21} cm^{-3}, which is found in heavily doped semiconductors. Figure of merit depends on carrier mobility and effective mass,

$$ZT = \frac{[\frac{E_F}{k_B T} - (r + 5/2)]^2}{(\beta exp(\frac{E_F}{k_B T}))^{-1} + (r + 5/2)} \tag{1.72}$$

where $\beta = (k/e)^2\sigma_0 T/\kappa$ and $\sigma_0 = 2e\mu(\frac{2\pi m^* k_B T}{h^2})^{3/2}$. For particular type of material and scattering, $ZT \sim \mu\,(m^*)^{3/2}$. For high value of ZT, we require materials having high value of mobility and high effective mass of carriers. There is a particular value of E_F or carrier concentration which makes $S^2\sigma$ maximum. Therefore, such value of carrier concentration can be achieved by doping.

1.4   Phonon conduction

In addition to heat conduction by electrons, lattice atoms also contribute in transporting heat across the solid. The phenomenon of heat conduction in solids was understood with the help of quantum theory of lattice dynamics. Solid is composed of regular array of atoms connected with one another by means of hypothetical springs (almost harmonic potential). When one of the atoms in the solid is given a displacement, the resultant disturbance is travelled in whole of the lattice passing through all the atoms. This disturbance constitutes lattice vibrational spectrum which is characteristic of every solid. Vibrational

spectrum consists of acoustic and optical branches in case of more than one atom in the unit cell of solid. If unit cell contains n atoms, there will be three acoustic modes and rest of 3n modes will be optical. Debye proposed that only a definite number of wavelengths can pass in a solid [55]. Lower limit for the wavelength is set by the lattice constant of the solid. The amount of energy associated with each vibrational mode is,

$$W = \hbar\omega[exp(\frac{\hbar\omega}{k_B T}) - 1]^{-1} \tag{1.73}$$

where ω is the angular frequency of the phonons. The trend of specific heat with temperature was solved by Einstein's model and Debye's model. Specific heat at constant volume is given by,

$$C_v = 9nk_B(\frac{T}{\theta_D})^3 \int_0^{\theta_D/T} \frac{x^4 exp(x)}{(exp(x) - 1)^2} dx, \quad x = \frac{\hbar\omega}{k_B T} \tag{1.74}$$

where θ_D is the Debye temperature. The results of Debye model comes out to be almost close to real solids for their general behavior. Einstein treated the ideal solid as harmonic oscillator. In real solids though, harmonic oscillator approximation is not valid. However, the model was unable to explain the behavior of lattice thermal conductivity. Peierls introduced the idea of phonons and their interaction to explain the thermal conductivity trend in real solids taking anharmonicity into picture [56]. According to him, phonons interact with one another based on the anharmonic interatomic potential. The interactions among phonons consist of Normal or N-processes and Umklapp or U-processes. N-processes conserve momentum and implicitly affect the thermal conductivity by redistributing the energy among phonons. On the other hand, U-processes do not conserve momentum and lead to thermal resistivity in the solid. The representation of the two processes is as under,

(a)   (b)
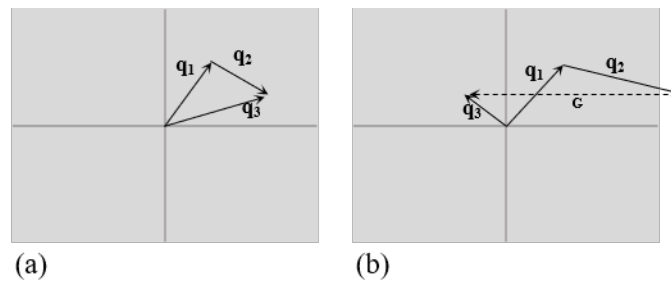
Figure 1.5: Representation of three phonon scattering processes (a) Normal process (b) Umklapp process. The shaded part shows the first Brillouin zone.

$$\boldsymbol{q_3} = \boldsymbol{q_1} + \boldsymbol{q_2} \quad (N - process) \tag{1.75}$$

$$\boldsymbol{q_3} = \boldsymbol{q_1} + \boldsymbol{q_2} + \boldsymbol{G} \quad (U - process) \tag{1.76}$$

where $\mathbf{G}$ is the reciprocal lattice vector (Fig.1.5). The number of U-process increases with temperature. Peierls had taken into account only the U-processes. This is due to the fact that as temperature rises, number of phonons with large wave-vectors also increases.

1.4.1 Relaxation time approximation for lattice thermal conductivity

Heat current is determined by distribution of phonons, which is obtained by the solution of Boltzmann transport equation. Like electrons, let the distribution function for phonons is given as N, and the Boltzmann transport equation for phonons is written as,

$$-v_G.\nabla T\frac{\partial N}{\partial T} = \frac{\partial N}{\partial t}|_{scatt.} \tag{1.77}$$

where v_G is the group velocity of phonons. The left hand side is due to convection and right hand side is due to discontinuous processes.

$$\frac{\partial N}{\partial t}|_{scatt.} = \sum_{(\alpha)} \frac{\partial N}{\partial t}]_{(\alpha)} \tag{1.78}$$

where (α) are constituting various processes: (1) N-proceess, (2) U-process, (3) Defect Scattering etc. Processes (1),(2) arise from anharmonicities of inter-atomic forces. Perturbation results in a transition where one phonon is destroyed and two are created and vice-versa.

$$\frac{\partial N_i}{\partial t}] = \sum_j \sum_k N_i N_j (N_k + 1) - (N_i + 1)(N_j + 1)N_k \tag{1.79}$$

For (1)-proceeses : $\omega_i + \omega_j = \omega_k$ and $\boldsymbol{q}_i + \boldsymbol{q}_j = \boldsymbol{q}_k$.
For (2)-processes : $\omega_i + \omega_j = \omega_k$ and $\boldsymbol{q}_i + \boldsymbol{q}_j = \boldsymbol{q}_k + \boldsymbol{G}$.
The equilibrium distribution function N_0 is assumed to be changed by a small amount n. Due to small change, we can take its first order in new distribution function only, as higher order terms would be negligibly effective.

$$N = N_0 + n \tag{1.80}$$

As $n << N_0$, therefore $dn/dT << dN_0/dT$. The term $\partial N/\partial t$ will have only first order of n.

For the calculation of formula for thermal conductivity, the equation of heat current is given by,

$$Q = \sum_j \int \int \int N_j(\boldsymbol{q})\hbar\omega \frac{\boldsymbol{q}.\nabla T}{|\boldsymbol{q}||\nabla T|} \boldsymbol{v}_{Gj}(\boldsymbol{q}) p(\boldsymbol{q}) d\boldsymbol{q} \tag{1.81}$$

where $\hbar\omega$ is the energy of one phonon, N_i is the number of phonons in one normal mode, $d\boldsymbol{q}$ is the interval. $p(\boldsymbol{q})d\boldsymbol{q}$ is the number of modes in the interval $d\boldsymbol{q}$. $N_i p(\boldsymbol{q})d\boldsymbol{q}$ is the total number of phonons in the interval $d\boldsymbol{q}$. $\hbar\omega N_i p(\boldsymbol{q})d\boldsymbol{q}$ is the total energy in the interval $d\boldsymbol{q}$. Heat current is energy flux which is given by (energy $\times$ velocity). Mode is represented as wave-vector $\boldsymbol{q}$ and polarization j.

$$Q = \sum_j \int \int \int n_j(\boldsymbol{q})\hbar\omega\mu\boldsymbol{v}_{Gj}(\boldsymbol{q})p(\boldsymbol{q})d\boldsymbol{q} \tag{1.82}$$

μ is cosine of angle between $\boldsymbol{q}$ and ∇T. First order approximation is valid if n and ∇T are small. For isotropic systems:

$$Q = \sum_j \int \frac{4\pi}{3} n_j \hbar\omega \boldsymbol{v}_{Gj}(\boldsymbol{q}) p(\boldsymbol{q}) d\boldsymbol{q} \tag{1.83}$$

Under relaxation time approximation, defining relaxation time $\tau_{(\alpha)}$ for each scattering process separately such that the rate of change of distribution function due to one type of scattering process is given as,

$$\frac{\partial N}{\partial t}\big]_{(\alpha)} = -\frac{n}{\tau_{(\alpha)}} \tag{1.84}$$

Here we assume that discontinuous processes tend to cut exponentially any deviation from equilibrium. Assuming all the scattering proceesses, the Boltzmann equation (Eq. 1.77) can be written as,

$$\boldsymbol{v}_G \mu \frac{dT}{dz} \frac{dN_0}{dT} = \frac{n}{\tau} \tag{1.85}$$

where τ is the total relaxation time due to all the processes. Various processes scattering rates get added according to the Matthiessen's rule. According to this rule, the total resistivity of a crystalline material is the sum of the resistivity due to various processes like thermal agitation and resistivity due to the presence of defects and impurities in the crystal.

$$\frac{1}{\tau} = \sum_{(\alpha)} \frac{1}{\tau_{(\alpha)}} \tag{1.86}$$

Eq 1.85 can be written to obtain the expression of n,

$$n = \tau \boldsymbol{v}_G \mu \frac{dT}{dz} \frac{dN_0}{dT} \tag{1.87}$$

$$n = \tau \boldsymbol{v}_G \mu \frac{dT}{dz} \frac{\hbar\omega}{k_B T^2} \frac{e^{\frac{\hbar\omega}{k_B T}}}{(e^{\frac{\hbar\omega}{k_B T}} - 1)^2} \tag{1.88}$$

Putting this value of n in Eq 1.83, the heat current is written as,

$$Q = \sum_j \int \frac{4\pi}{3} \tau \boldsymbol{v}_G \mu \frac{dT}{dz} \hbar\omega k_B T^2 \frac{e^{\frac{\hbar\omega}{k_B T}}}{(e^{\frac{\hbar\omega}{k_B T}} - 1)^2} \hbar\omega \boldsymbol{v}_{Gj}(\boldsymbol{q}) p(\boldsymbol{q}) d\boldsymbol{q} \tag{1.89}$$

From above equation, the formula of thermal conductivity can be obtained as,

$$\kappa = \frac{4\pi}{3} \sum_j \int \tau(\boldsymbol{q}) \frac{\hbar^2 \omega^2}{k_B T^2} \boldsymbol{v}_G^2(\boldsymbol{q}) \frac{e^{\frac{\hbar\omega}{k_B T}}}{(e^{\frac{\hbar\omega}{k_B T}} - 1)^2} p(\boldsymbol{q}) d\boldsymbol{q} \tag{1.90}$$

Energy per unit volume from normal modes between $\boldsymbol{q}$ and $d\boldsymbol{q}$ is given as:

$$E(\boldsymbol{q}, T) = \frac{\hbar\omega}{(e^{\frac{\hbar\omega}{k_B T}} - 1)} p(\boldsymbol{q}) 4\pi \tag{1.91}$$

Relaxation length $= l(\boldsymbol{q}) = \boldsymbol{v}_G(\boldsymbol{q})\tau(\boldsymbol{q})$. The formula for thermal conductivity is,

$$\kappa = \frac{1}{3}\sum_j \int \frac{\partial E(\boldsymbol{q}, T)}{\partial t} l(\boldsymbol{q})\boldsymbol{v}_G(\boldsymbol{q})d\boldsymbol{q} \tag{1.92}$$

Lattice thermal conductivity can be expressed under relaxation time approximation (RTA) by solving BTE as,

$$\kappa_l = \frac{1}{3}\int_0^{\omega_{max}} C(\omega)v^2(\omega)\tau(\omega)d\omega \tag{1.93}$$

Callaway had claimed to include both the processes into thermal conductivity expression as N-processes indirectly do affect the thermal transport [57].

Specific heat and velocity are directly calculated from vibrational spectrum. Klemens found expression for different phonon scattering mechanisms and different scatterings rates were added according to Matthiessen's rule. The trend of lattice thermal conductivity with temperature is having a particular shape for almost all the crystalline semiconductors. Different temperature regions contain different dominating scattering mechanisms for phonons. At high temperature, thermal conductivity behaves as T^{-n}, with $n\sim 1$. The value of specific heat at elevated temperature is constant. As temperature increases, number of phonons also increases linearly. As scattering rate is directly proportional to number of phonons, thermal conductivity reduces as temperature rises in high temperature range. The specific heat goes as T^3 at low temperature. Due to less number of phonons at lower temperature, scattering of phonons is also smaller. Due to this, phonon wavelengths are larger than sample sizes. Therefore, phonons will get scattered from the boundaries of the sample. This was discovered by De Haas and studied by casimir [58, 59]. Phonon mean free path becomes equal to the size of the sample and thus becomes independent of the frequency of phonons. Thermal conductivity in this region is $\propto T^3$. In the intermediate temperature range, the flatter part and peak is dependent on impurity scattering. The variation of lattice thermal conductivity with crystal density and atomic mass is given by Keyes expression,

$$\kappa_l T \propto \frac{T_m^{3/2}\rho^{2/3}}{\gamma^2 A^{7/6}} \tag{1.94}$$

where T_m is the melting temperature, ρ is density of unit cell and A is atomic weight of unit cell. Low melting point corresponds to low thermal conductivity. Thermal conductivity will be less for crystals having large inter-atomic distances between its atoms. The transport of charge carriers and phonons remain independent in most of the solids. In some of the cases, a new effect introduces based on the interlinking of the two transports, known as phonon drag. This effect is significant when carrier concentration and temperature both have lower value. Electrons scatter by phonons of much lower energy and transfer their momentum to phonons. But according to saturation effect at high concentration, momentum is transferred back to electrons from phonons. Due to this effect, phonon drag is not significant in enhancing the thermoelectric parameters.

Apart from formula for thermal conductivity given by Klemens, in 1980's, thermal conductivity calculations were carried out using molecular dynamics simulations. However, results of MD simulations based on empirical potentials can have entirely different

results than experiments. Quite satisfying agreement between calculations and measurements is obtained using first principle calculations also known as ab-initio. Density functional theory provides electronic charge density which then is used to find the inter-atomic potential. These calculations are free from any fitting parameters and are highly reliable though expensive too. There are rare experimental methods to explore phonon dispersion. These methods include Raman spectroscopy, inelastic neutron scattering, inelastic X-ray scattering. These theoretical and experimental methods deepen our understanding of the heat transport in different materials. For eg. PbTe and PbSe have much lower lattice thermal conductivity despite its symmetric cubic structure. This is due to significantly strong coupling between acoustic and optical phonons and soft transverse acoustic phonon modes.

The trend of lattice thermal conductivity is that for a similar crystal structure and similar bonding between atoms, thermal conductivity decreases if we increase the atomic weight [60]. Ionic compounds have much lower lattice thermal conductivity, however their carrier mobility is very low, so they are not useful for thermoelectric applications. The compounds which are worthful for thermoelectric applications are covalent bonded compounds. Lattice thermal conductivity values are smaller when the constituent elements have high mass difference. Formula for lattice thermal conductivity given by Leifried and Schlomann based on variational principle [61],

$$\kappa_l = 3.5(\frac{k_B}{h})^3\frac{MV^{1/3}\theta_D^3}{\gamma^2 T} \tag{1.95}$$

where M is the average atomic mass, V is the unit cell volume, γ is the Gruneisen parameter which measures the effect of change in volume on the frequency spectrum of the phonons.

1.4.2 Anharmonic scattering

Phonons in a solid are scattered by different mechanisms namely anharmonic Umklapp scattering (U-scattering), normal, boundary, defect, alloy scattering etc. We will consider mainly the anharmonic U-scattering which is dominated at reasonable frequencies. Anharmonic scattering is calculated following the three-phonon scattering model. Slack has given the formula for model τ based on the work of Leibfried and Schlomann [61, 62, 63].

$$\tau_U^{-1} = p\omega^2 \frac{T}{\tilde{\theta}_D}e^{-\tilde{\theta}_D/3T} \tag{1.96}$$

where p is an adjustable parameter. Another model for finding thermal conductivity around Debye's temperature is given by Slack [61, 62, 64],

$$\kappa_l(\theta_D) = \frac{0.849 \times 3 \times 4^{1/3}}{20\pi^3(1 - \frac{0.514}{\gamma} + \frac{0.228}{\gamma^2})}(\frac{k_B\theta_D}{\hbar})^2\frac{k_B MV^{1/3}}{\hbar\gamma^2} \tag{1.97}$$

23

On comparing these two models, the value of adjustable parameter is calculated as [65],

$$p = \frac{1 - \frac{0.514}{\sqrt{\bar{\gamma}^2}} + \frac{0.228}{\bar{\gamma}^2}}{0.0948} \frac{\hbar^2 \bar{\gamma}^2}{k_B \tilde{\theta}_D M V^{1/3} s} \tag{1.98}$$

here s is sound speed and θ_D is the Debye's temperature. There are many ways of calculating θ_D, however we will be using the full phonon dispersion to calculate it as defined below,

$$\tilde{\theta}_D = n^{-1/3} \sqrt{\frac{5\hbar^2}{3k_B^2} \frac{\int_0^\infty \omega^2 g(\omega) d\omega}{\int_0^\infty g(\omega) d\omega}} \tag{1.99}$$

here n is the number of atoms per unit cell and $\bar{\gamma}^2$ is mode averaged-squared Grüneisen parameter

$$\bar{\gamma}^2 = \frac{\sum_j \int \frac{d\boldsymbol{q}}{8\pi^3} \gamma_{j\boldsymbol{q}}^2 C_{j\boldsymbol{q}}}{\sum_j \int \frac{d\boldsymbol{q}}{8\pi^3} C_{j\boldsymbol{q}}} \tag{1.100}$$

$$\gamma_{j\boldsymbol{q}} = -\frac{V}{\omega_{j\boldsymbol{q}}} \frac{\partial \omega_{j\boldsymbol{q}}}{\partial V} \tag{1.101}$$

where $\gamma_{j\boldsymbol{q}}$ is the Grüneisen constant for each mode, $\omega_{j\boldsymbol{q}}$ is mode dependent angular frequency. We require the thermal conductivity to be less in thermoelectric materials and will talk about different ways to do the same.

1.4.3 Normal scattering

As suggested by Callaway, although normal processes don't claim to produce thermal resistance, however they can affect the thermal conductivity drastically [57]. The modified Debye-Callaway model is written for both longitudinal and transverse phonons as [63],

$$\kappa_l = \kappa_L + \kappa_T \tag{1.102}$$

where $\kappa_L = \kappa_{L_1} + \kappa_{L_2}$, and similar for the transverse part.

$$\kappa_{L_1} = \frac{1}{3} \frac{k_B^4}{2\pi^2 \hbar^3 v_L} T^3 \int_0^{\theta_L/T} \frac{\tau_C^L(x) x^4 e^x}{(e^x - 1)^2} dx \tag{1.103}$$

$$\kappa_{L_2} = \frac{1}{3} \frac{k_B^4}{2\pi^2 \hbar^3 v_L} T^3 \frac{[\int_0^{\theta_L/T} \frac{\tau_C^L(x) x^4 e^x}{\tau_N^L(x)(e^x-1)^2}]^2 dx}{\int_0^{\theta_L/T} \frac{\tau_C^L(x) x^4 e^x}{\tau_N^L(x)\tau_R^L(x)(e^x-1)^2}}, \quad x = \frac{\hbar\omega}{k_B T} \tag{1.104}$$

where $(\tau_C)^{-1} = (\tau_N)^{-1} + (\tau_R)^{-1}$, where τ_C is the combined relaxation time due to normal and resistive processes. Like U-scattering model as done in the earlier section, there are many forms for N-scattering. The normal scattering rate for one type of crystals is given as,

$$(\tau_N^L(\omega))^{-1} \approx \frac{k_B^3 \gamma_L^2 V}{M\hbar^2 v_L^5} \omega^2 T^3, \quad (\tau_N^T(\omega))^{-1} \approx \frac{k_B^4 \gamma_T^2 V}{M\hbar^3 v_T^5} B_N^T \omega T^4 \tag{1.105}$$

1.4.4 Effect of temperature

Depending upon the melting point and chemical stability, it is not possible to use one material in the full temperature range for thermoelectric applications. For eg., Bi_2Te_3 is used in moderate temperature for cooling purposes. Apart from melting point, when the temperature rises, more electron-hole pairs will be generated which leads to decrease in Seebeck value and simultaneously increasing the thermal conductivity. This is due to bipolar conduction. The ZT increases with T in the absence of bipolar conduction. Optimum Seebeck coefficient remains almost constant with temperature. Carrier concentration varies as $T^{3/2}$ while μ decreases with T and the trend depends upon the scattering process. Electrical conductivity thus becomes temperature independent. Therefore, temperature dependence of ZT arises from thermal conductivity. The κ_e is proportional to T but due to dominance of κ_l, total thermal conductivity decreases as T increases. Therefore, ZT increases as T increases.

1.5 Minimizing lattice thermal conductivity

The spectrum of phonons having large variation of wavelength and mean free path are used in transporting heat through the solid. Mean free path of phonons ranges from few nanometers to micrometers. All these phonons scatter according to their wavelength, so different scattering processes scatter a range of phonons having a particular wavelength. The idea of maximum possible reduction of thermal conductivity was introduced by Slack. Minimum thermal conductivity will be possible when MFP of phonons become equal to their wavelength. Afterwards, Cahill proposed half the thermal conductivity values given by Slack. Cahill based his analysis on random walk theory. Klemens formula based on Debye's theory gave correct trend for large experimental data. However, Debye's model does not take into account the optical modes. These modes are flatter though, even then they have non-zero velocities. Secondly, whole of the acoustic spectrum as taken in Debye theory is not linear. High frequency acoustic phonons have lower velocities. Density of states in a real crystal do not vary as ω^2. Despite these peculiarities, Klemens model based on Debye's theory mimic the experimental trend. This is because of the different set of fitting parameters. The lattice thermal conductivity can be reduced below the minimum value for single crystals (where only phonon-phonon scattering is present) by using defects and boundary scattering. The scattering of phonons is different from scattering of charge carriers. This is due to the difference in the mean free path of the two. Electrons have higher mean free path than phonons, therefore, the electrons will get scattered from large sized grains, whereas phonons are scattered from small sized grains. Both have different scattering windows. Lattice thermal conductivity can be reduced by mainly three ways. The first one is to produce local disorder in the crystal structure and scatter phonons by alloying, interstitial substitution and rattling atoms [66]. Second way is to search for complex crystal structures based on PGEC to enhance ZT. On the third point, the thermal conductivity reduction is done by scattering of phonons at boundaries and interfaces in nanostructures [52, 67].

1.5.1 Phonon scattering by point defects

Thermal conductivity can be reduced to a greater extent by making an alloy from two semiconducting materials having similar crystal structure [8]. The scattering of charge carriers would be negligible due to their long wavelength or long mean free path which matches with the long range order of the alloy. This long range order of alloy is preserved as before. On the other hand, the phonons which transfer the most of the heat were having small wavelength and are now scattered from the short range defects in the crystal [68, 69, 70, 71, 72].

Alloying and phonon rattler have same concept behind their transport behavior. In alloy, there is inclusion of atomic disorder substitutionly and in rattling, disorder is introduced interstitially. Alloying is seen to show reduced thermal conductivity without modifying the electronic transport. In an alloy, the scattering of phonons is due to changes in atomic distribution locally. Rayleigh scattering is used to account for impurity scattering. According to Rayleigh scattering, the scattering rate is proportional to ω^4. In addition to these, other interstitial impurities and partial vacancies add in to the scattering of phonons. In general, the defect scattering rate is given as,

$$\tau_I^{-1}(\omega) = \frac{V}{4\pi v^3} \sum_{i=1}^{N} c_i (1 - \frac{\Delta M_i}{\bar{M}})^2 \omega^4$$

where V is the volume of the unit cell, v is sound speed, c_i is the concentration of the defect or impurity. ΔM_i is the difference in the mass of defect from host atom maas, $\bar{M}$ is the average mass.

The scattering of phonons can be due to local elasticity variation and density variation. Density fluctuation is also known as mass fluctuation. Scattering due to fluctuations in elasticity is difficult to comprehend. The defect atom creates strain in the crystal due to different bonding and inadequate size in the lattice. The comparison of theoretical values with the experimental data shows that strain scattering does exist and therefore experimental values are all lower than calculated ones. Alloying reduces the thermal conductivity of a solid solution to a value less than the average of thermal conductivity of the pure materials. The reduction of alloy thermal conductivity depends upon the mass difference between the pure materials. $Si_{1-x}Ge_x$ alloy has thermal conductivity of 10 $Wm^{-1}K^{-1}$, whereas thermal conductivity of pure Si and Ge is of the order of 150 $Wm^{-1}K^{-1}$ and 60 $Wm^{-1}K^{-1}$ respectively [13, 14, 15]. Abeles introduced a model to study the alloying between different material having same crystal structure. This model was known as the virtual crystal approximation, in which the alloy crystal structure is assumed to be average of the pure materials.

Virtual crystal approximation gives quite satisfying results to match with experimental data. Despite this, the actual alloy properties can not just be a mere average. The actual dispersion and other physical properties might be hidden. During the calculation of scattering times, the application of Rayleigh scattering mechanism is valid only for low frequency phonons, as Rayleigh criterion works when wavelength of phonons is much larger than the scattering site. However, we cannot use this criterion for high frequency

phonons, which make little contribution in the thermal transport [73]. In the model, the atomic mass difference quantity does not take into account the sign of mass difference, as the added impurity is larger or smaller than the pure atom. Due to this, the frequency of the impurity atom is uncertain as it lies above or below the main phonons frequency.

The process of rattling is associated with the loosely bound motion of the guest atom in the open cage structure. This rattling motion creates a local disorder among the periodic crystal which becomes center of the point defect like scattering. In alloying, guest atoms also known as impurity atoms form normal bonds within the crystal lattice. Unlike alloying, guest atoms in rattling motion are loosely bound in an open cage structure of the crystal. These guest atoms locally vibrate in the void and scatter phonons of the host crystal. Skutterudites and clathrates are such examples of guest-host structures proposed by Slack. Both of these structures contain heavy metal atoms or ions in the oversized cages to make the rattling motion possible [18, 74]. Motion of filler atom depends on its relative size in the cage or void. These filler atoms do not share any strong bond with the lattice and give rise to local phonon modes and soft phonon modes due to weaker local interatomic bonding [75].

The reduction of thermal conductivity due to rattler atom is not yet fully understood. There exists many underlying theories and experimental observations. In the independent rattling picture of the guest atoms, many ideas have been proposed. Sales et al. have assumed the localized motion of guest atoms which generates localized modes. These modes in turn are responsible for lower thermal conductivity. These modes are experimentally verified in skutterudites by inelastic neutron scattering. On the other hand, in the resonant scattering of phonons, the phonons with frequencies near the localized frequency get scattered more by these modes. This theory is also verified experimentally by using more than one type of guest atoms in the host cage. In such structures, there exists number of different resonant frequencies. According to this theory, the reduced thermal conductivity is due to resonant interaction between guest and host atoms. In another view, the virtual crystal approximation can also be used with mass fluctuation for more than one type of guest atoms in multi-filled skutterudites. Another observation is due to flattening of phonon modes due to filler atoms, which thus reduce the thermal conductivity. Unlike these views, Koza et al. have studied the different observations of $LaFe_4Sb_{12}$ and $CeFe_4Sb_{12}$, where p-type skutterudites have higher thermal conductivity due to guest atom [76]. This idea thus denies the rattling motion of the guest atom.

Moreover, disorder in a pure material often leads to wave interference phenomenon in the material. It brings about different transport regimes namely ballistic, diffusive and localized. The occurrence of specific regime for transport in the system is based on the characterization length for various phonons [77]. As alloying usually introduces disorder in the system and the amount of disorder is quantified by the energy fluctuations among different sites [78]. Due to alloying, high mass ratio can trigger mass induced Anderson localization of phonons [79, 80, 81, 82, 79]. Anderson localization originates when there is enough disorder in the lattice which can disrupt the band structure of phonons [79]. This broken band structure picture is due to disorder in the bond strength values or masses. This results in scattering or interference of lattice waves due to non-periodicity and confinement

of vibrations to a group of atoms. This scattering of waves leads to reduction of thermal conductivity. Huge mass ratio and inhomogeneity of bonds in Hydrogen-Deuterium alloy has shown evidence of localization [83]. As large amount of disorder is needed for localization effects, the amount of localization is not observable in many systems due to its negligible contribution [79, 77].

1.5.2   Phonon Glass Electron Crystal

Amorphous materials like glass have been known for the lowest thermal conductivity. From this Slack introduced the concept of glass like thermal conductivity in crystals [16]. For glass, in addition to poor thermal conductivity, electrical conductivity is also of the same nature. Therefore amorphous materials are out from the category of good thermoelectric materials due to their unfavorable electronic properties. These crystalline materials have glass like thermal conductivity, even then their electronic properties are like other crystals, are called phonon glass electron crystal materials. Cahill et al. studied such materials and revealed that these materials have loosely bound atoms in their lattice structure. These loosely bound atoms do not usually sit on lattice sites. These rattling atoms are caged in bigger unit cells and thus are responsible for large phonon scattering. The PGEC material having rattling atoms produces damped phonon vibrations. The presence of rattling motion is confirmed by highly enhanced atomic displacement such as in clathrates [84, 85]

Complex unit cell structures also claim to have extremely low lattice thermal conductivity and behave like PGEC. β-Zn_4Sb_3 creates phonon glass due to its disordered Zn-sublattice and electron crystal due to ordered Sb network [86]. Zintl compounds are complex structure containing multiple structural units with different bonding types such as covalent and ionic. $Yb_{14}MnSb_{11}$ is such a structure with multiple units leading to low thermal conductivity of 0.4 $Wm^{-1}K^{-1}$ and $ZT \sim 1.0$ at 900 K [87, 25]. Zintl compounds can be a good candidate for substructure approach. According to this approach, a complex material can have different functioning regions for PGEC to bypass the contradictions in achieving optimum ZT. A complex structure can have electron crystal like properties with high mobility and phonon glass at the different places in the crystal interwoven with each other. Substructure approach can be combined with nanostructuring to achieve high power factor and extremely low lattice thermal conductivity. Thermal conductivity can also be reduced in large unit cells, where phonons have to travel a long distance to transport heat. Thus the mean free path of phonons reduces which decreases the thermal conductivity.

1.5.3   Boundary scattering

Alloy structures scatter very short wavelength phonons. Unlike this, nanostructures are able to scatter long wavelength phonons due to interfaces and boundaries [59]. At low temperatures, boundary scattering is predominant [88]. However, the observation of boundary scattering at room temperature is possible only if the grain size is extremely small. The mean free path of phonons usually fall in range of 10 nm. Boundary scattering

has significant effect in case of an alloy than pure material. It has been said that boundary scattering can occur for grain sizes around 1000 nm also [89]. Free path for a phonon depends upon its frequency. Low frequency phonons contribute to the thermal conductivity as they scatter the least. Therefore, low frequency phonons have large free path lengths. The U-scattering varies as ω^{-2}, whereas defect scattering varies as ω^{-4}. Therefore, point defect scattering will scatter the most high frequency phonons. Rest of the phonons lie in the low frequency range and have large mean free path. These phonons are now not affected by defect and U-scatterings.

MFP of phonons ranges over a wide length scale from nanometer to micrometer. Each material has different type of distribution of phonons as far as their MFP is concerned. This distribution is characteristic of every material. Distribution trend guides us to find the possible nanostructure dimensions of the material to reduce thermal conductivity. For eg., Si-nanostructures of size 100 nm are good at scattering more phonons, whereas for PbTe, the effective dimension is around 10 nm [88, 90].

By the idea of Hicks and Dressulhaus, thermal conductivity of Si-nanowires was studied first of all by Li et al [91]. The two order reduction was understood by phonon-boundary scattering. Many theoretical calculations based on the BTE solutions agree with the experimental results for wire sizes more than 20 nm. When wire's sizes become of the order of 20 nm, many other effects come into picture and theoretical results overestimated the experimental values. The low value of experimental thermal conductivity may be due to the measurement of sleek nanowires which are sensitive to varying diameters and surface roughness. The theoretical model calculations lack in the proper treatment of the phonon-boundary scattering and phonon confinement at lower dimensions. Phonon confinement affects the dispersion spectrum of phonons, and thus calculation of full dispersion spectrum of wires is suggested as one method. The effect of surface roughness on phonon confinement is not fully understood.

As we have already read, the thermal conductivity of superlattices are reduced to values lower than alloys. Therefore, Chen et al. has proposed that the Cahill's model and Slack's model of minimum thermal conductivity might not be valid for low dimensional materials [1]. The basic reason underlying this denial was supposed to be due to anisotropic behavior which generates direction dependent phonon spectrum. Chen found the reason behind this reduction to be diffuse and inelastic interface scattering in case of Si/Ge superlattice. Nanocomposites are alternatives to superlattices because of large density of interfaces.

1.6 Transport in lower dimensions

The increasing demand of microelectronics and nanoelectronics has made size effected transport phenomenon of considerable importance. Theoretical studies of transport in lower dimensions such as nanotubes, nanowires and thin films have been modifying to consider some of the fruitful effects at lower dimensions. These effects comprise of comparable length and time scales with the carrier's mean free path and relaxation time respectively. This leads to quantization of modes in case of phonons having wavelength comparable to the dimensions of the material.

The applicability of Boltzmann transport equation for transport in lower dimensions is justified by considering effective carrier-boundary scattering. The effect on thermal conductivity with the thickness of thin films is examined by using Boltzmann transport equation in Ref.[92, 93, 94]. Dominated boundary scattering at lower dimensions reduces the thermal conductivity and the theoretical values were compared with the experiment [95, 96]. There are other reports of Nath and Chopra [97] considering more rigourous solution of Boltzmann equation considering other scattering effects and obtained results match with the experimental data for thin films. More work on the Boltzmann equation analysis could give the exact view of thin film transport property behavior.

1.7   Potential thermoelectric materials

Since the discovery of thermoelectric materials for waste heat recovery and electric power generation, there has been set up a voyage for exploring superior thermoelectric system. Recently, there has been a great inclination in the investigation of greater ZT materials by various groups in the literature [98, 22, 99, 100, 101] with improved thermoelectric properties either by improving the power factor (P) [99, 100, 102, 103] or by reducing the thermal conductivity κ [103, 104]. New transition metal compounds have been reported with improved thermoelectric performance in the temperature range of 300 K - 1000 K. In one such example, $Cu_{2-x}Se_x$ has shown a high ZT value of 1.4 [100]. Similarly, Sb_2Te_3 and Bi_2Te_3 based nanostructured compounds have shown high values of ZT at room temperature [105]. The thermoelectric power generators based on cubic PbTe (either n-type or p-type) have $ZT \sim 1.0$, and Pb - Ag - Sb - Te alloys have $ZT \sim 2.0$ [106] in the temperature range of 300 K - 700 K. For commercial applications, Pb and Te based compounds are mainly used for waste heat recovery in the temperature range of 300 K - 800 K. However, the use of Pb based thermoelectric devices is restricted due to its toxicity. This motivates for the development of lead free materials for thermoelectric devices.

1.8   Problems addressed in the thesis

Thermoelectric performance of already existing compounds can be extended further by different methods like nanostructuring, doping, rattling atoms, alloying etc. The reduction of thermal conductivity for enhancing efficiency besides the intrinsic properties depends on alloying and nanostructuring. We have incorporated in our work the modification of thermoelectric performance of various materials based on alloying and nanostructuring. There have been reliable and cheaper binary thermoelectric materials (CdSe, PbTe etc) which have shown productive since a long time. However, only a few ternary chalcogenides such as CoSbS, NiSbS, FeSbS have been studied for thermoelectric applications. Thermoelectric performance of ternary pnictide chalcogenide of d^8 transition metal materials PdPS, CoAsS have been investigated in this thesis work. A worth appraised values of ZT have been calculated for these materials. Thermoelectric figure of merit calculated

for PdPS is very significant in the nano regime and due to its layered structure, it will be having many applications in the field of biology, space, computers etc. Another very important application of this research is in the thermoelectric modules in which the provision to use both legs of the module from CoAsS alloy can be possible. A significant reduction in the lattice thermal conductivity of type-I clathrate $Ba_8Cu_6Si_{40}$ by introducing alloy scattering and boundary scattering is observed which can be useful for many Si based technologies.

This thesis deals with finding new thermoelectric materials and the studying the effect of alloying and nanostructuring on thermoelectric materials. In Chapter 2, we present the thermoelectric properties of layered ternary metal chalcogenide Palladium Phosphide Sulphide (PdPS). Due to layered structure, we study its different directional properties and effect of nanostructuring on its lattice transport properties. Orthorhombic PdPS has shown anisotropic transport properties both in electron and phonon due to uneven arrangement of the P and S atoms in the in-plane direction. Through nanostructuring, bulk thermal conductivity and thermal conductivity in layered direction can be made very small in temperature range of 300 K-800 K. This significant reduction is predicted to enhance the thermoelectric power factor ZT.

Chapter 3 studies the effect of alloying on the thermoelectric properties of cobaltite (CoAsS) and paracostibite (CoSbS), both having orthorhombic structure. Both structures having similar atoms show different electronic and lattice properties based on the crystal structure. Using alloying techniques, the thermoelectric performance of cobalt and paracostibite is enhanced for both n-type and p-type in different temperature ranges and concentrations of alloying. The reduction in thermal conductivity is mainly due to reduction of mean free path of phonons on alloying.

In Chapter 4, we study the enhancement of thermoelectric figure of merit under the effect of alloying and nanostructuring on the type-I clathrate $Ba_8Cu_6Si_{40}$. Clathrates are guest-host assemblies, therefore the guest atoms affect the dynamics of transport largely. We have calculated the contribution of various atoms in reducing the lattice thermal conductivity in the clathrate structure using phonon band structure. Alloy scattering has been shown to reduce the lattice thermal conductivity of pure Si-clathrate $Ba_8Cu_6Si_{40}$. Furthermore, the effect of boundary scattering is calculated and there has been seen a reduction of the clathrate lattice thermal conductivity in case of nm-sized $Ba_8Cu_6Si_{17}Ge_{23}$ clathrate alloy nanowire.

Chapter 5 discusses the summary of present thesis work and future applications. We also discuss here the possible ways to steer this work for further enhancement in the thermoelectric performance.

Chapter 2

Thermoelectric properties of layered material PdPS

2.1 Introduction

New materials with superior thermoelectric figures of merit have appeared, thus the possibility of large scale thermoelectric generation for making better use of energy resources has become more obvious. Metal chalcogenides have been seen participating in the thermoelectric performance race from past many years. These compounds contain oxygen, sulphur, selenium, and tellurium in combination with the transition metals in binary, ternary, and quaternary proportions. Transition metals due to their flexibility in oxidation state and coordination number lead to different structures such as pyrite, marcasite, pararammelsbergite. Only few ternary A-B-X class chalcogenides such as CoSbS [107, 108], NiSbS [107], FeSbS [107] have been studied recently for thermoelectric applications, where A is a transition metal, B is an element from group V and X is a chalcogen. Keeping this in mind, the band structure and transport properties of Palladium Phosphide Sulphide (PdPS) have been calculated, which has an orthorhombic crystal structure similar to pararammelsbergite ($NiAs_2$). The PdPS has not been studied for thermoelectric applications so far. The thermopower, anisotropic power factor, and thermal conductivity of PdPS in different crystallographic directions have been calculated.

Thermoelectric applications are limited to binary chalcogenides such as PbTe and Bi_2Te_3 for decades. These traditional materials have chaired the thermoelectric application sector for a long time due to the heavy Te atoms. Heavy atoms contribute in comparatively smaller thermal conductivity in these materials. However, the less abundance, high price and toxic nature of Tellurium has always put metal Tellurides on an edge to be replaced by other similar elements. Sulphur and Selenium being abundant, less costly and nontoxic, can replace the metal Tellurides by metal Sulphides and Selenides. Leading bulk Sulphides and Selenides of copper have ZT values around 2.0 at 1000 K for both Cu_2Se and Cu_2S. High power factor values around 23 $\mu Wcm^{-1}K^{-2}$ have been obtained for SnTe and In_2Te_3 compound [101]. Unlike PbTe, SnSe crystallizes in distorted rock salt structure and is highly anisotropic. Single crystal maximum ZT for SnSe in b-crystallographic

direction is 2.6 at 973 K, whereas polycrystalline sample offers less superior values such as $ZT \sim 1.36$ at 823 K. Thus there are many compounds which can overtake the usage of PbTe in high temperature region. The thermoelectric figure of merit of PbTe is 1.4 around 800 K and Pb-Ag-Sb-Te alloys have $ZT \sim 2.0$ [106] in the temperature range 300 K-700 K. The nanocomposites of Cu_2Se with $CuInSe_2$ gives a maximum ZT of 2.6 at 850 K. Ternary chalcogenides like $CuGaTe_2$ have ZT of 1.4 at 950 K due to superior charge transport properties and strong temperature dependence of thermal conductivity. Similarly, there are quarternary chalcogenides $Cu_{12-x}Co_xSb_4S_{13}$ of copper having ultra low thermal conductivity less than 0.6 $Wm^{-1}K^{-1}$.

For commercial applications, Pb, and Te based compounds are being mainly used for waste heat recovery in 300 K-800 K temperature range, however, due to the toxicity of Pb, the use of the thermoelectric devices based on Pb is restricted. This generates a strong motivation for finding suitable "Pb-free" materials for thermoelectric devices. The ongoing quest for an improved thermoelectric device in the temperature range of 300 K-800 K has been leading many groups, to work in transition metal chalcogenide compounds. Many such compounds have been analyzed to achieve better thermoelectric properties among which there are binary [109, 98] compounds like Bi_2Se_3, PbTe and ternary [110, 111, 108, 112] such as FeSbS, CoSbS, PdPS etc and quaternary [113] such as $Cu_2CdSnSe_4$ etc.

In the present chapter, the thermoelectric properties of PdPS have been calculated using band structure calculations and Boltzmann transport theory. Electronic transport properties have been calculated by using constant time relaxation method for solving Boltzmann equations as embedded in software BoltzTraP. The room temperature Seebeck coefficient is found to be reasonably high for both n-type and p-type PdPS. Similarly, phonon transport properties are calculated based on frozen phonon approach embedded in PHONOPY and homemade code. The calculated thermal conductivity in the layered direction is found to be ultra low than the bulk values. Effect of nanostructuring further reduces the thermal conductivity values which enhances the thermoelectric power factor.

2.2 Electronic structure calculations

2.2.1 Method

PdPS was synthesized experimentally earlier in 1971 [114] and has shown resistivity, $\rho = 3 \times 10^4$ Ωcm, at 425 K [114]. The intrinsic resistivity is quite high due to much lower intrinsic carrier concentration and can be improved by extrinsic doping [114]. An earlier study [115] showed that PdPS is an indirect band gap material with a structure containing puckered net of pentagons. These pentagons act as a building block with the alignment of two nets (PdP_2 and PdS_2) on each other as the distinguishing feature, Fig.2.1. PdPS derives its properties related to both PdP_2 and PdS_2 with bonding in the two nets. It is due to the strong bonding between P atoms of two neighboring nets and an S lone pair with Pd atom of another layer, which gives rise to its double layered type structure [116].
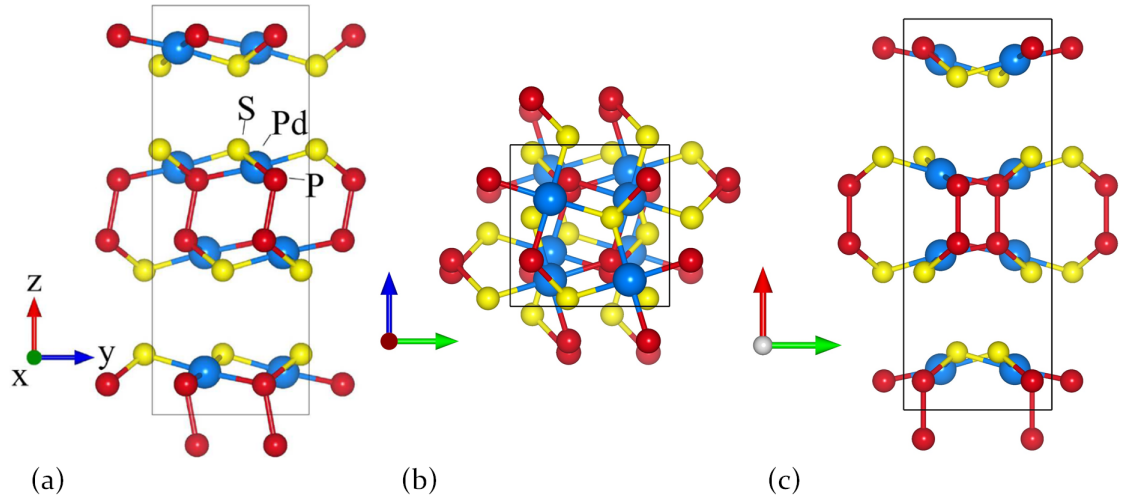
Figure 2.1: Unit cell crystal structure of PdPS, direction x, y and z represents $\Gamma - X$, $\Gamma - Y$ and $\Gamma - Z$ crystallographic directions in the first Brillouin zone (a) Front view (b) Top view (c) Side view.

The raw crystal structure is taken from the earlier published data, and the self consistent calculations are performed using the density functional theory. We used PBE functional [117] and PAW basis set as implemented in VASP [118, 119] with a k-mesh of $2 \times 2 \times 1$ to optimize PdPS structure. The crystal structure unit cell chosen for calculations contains 24 atoms and the energy cut off was chosen to be 350 eV. The k-mesh is obtained after performing a minimum formation energy calculation on the initial structure (Fig.2.2). Orthorhombic PdPS has been obtained with lattice parameters $a = 5.62\text{Å}$, $b = 5.69\text{Å}$, $c = 14.81\text{Å}$.
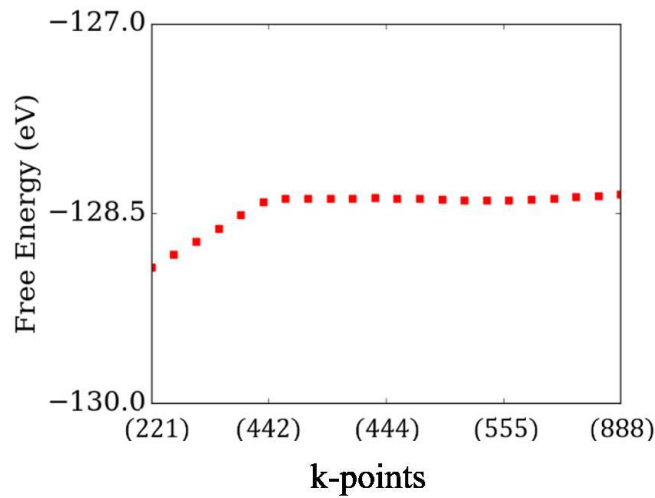

Figure 2.2: Variation of free energy of PdPS vs density of k-point mesh.

35

2.2.2 Electronic band structure

The computed electronic band structure and density of states (DOS) are presented in Fig.2.3. Directions x, y, and z (shown in Fig.2.1) correspond to $\Gamma - X$, $\Gamma - Y$, and $\Gamma - Z$ in the first Brillouin zone. The valence band maximum occurs along the $\Gamma - X$ direction as shown in inset of Fig.2.3, and it is composed of heavy hole band which is favorable for thermoelectric applications as discussed in chapter 1. There is another maximum just below ≈ 5 meV of the Fermi level in the $\Gamma - Y$ direction and it consists of a relatively lighter band. In the conduction band, there are two minima in $\Gamma - X$ and $\Gamma - Y$ directions, and both consist of mixed light and heavy bands. The calculated indirect band gap is 1.24 eV, where experimentally reported band gap is 1.38 eV [114]. Palladium being a transition metal has d - electrons, so that it might show spin-orbit coupling, but for the present time, we have not included spin-orbit calculations.
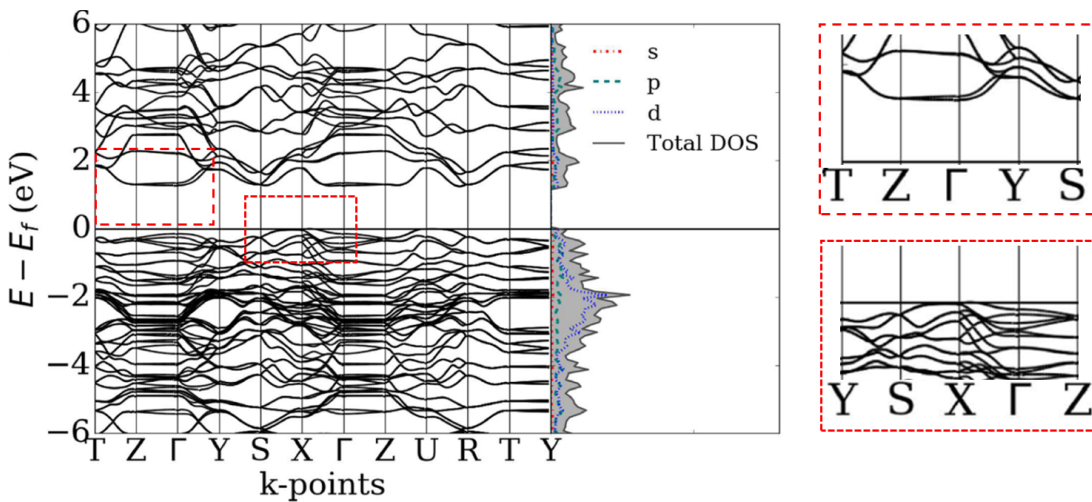

Figure 2.3: Electronic band structure along orthorhombic symmetry k-points (without spin-orbit coupling) on left; on right side, total density of states and projected density of states of PdPS. On the extreme right is the inset for conduction band minimum and valence band maximum.

2.3 Electronic transport properties

2.3.1 Method

The transport of electric charge is due to quasi-free electrons in the solid. In semiconductors and metals, the electrons also carry thermal energy in addition to electrical charge. For the electronic transport properties calculation, we used constant relaxation time approximation as implemented in BoltzTraP [120]. Here large k-point is necessary to obtain the convergence and hence a $19 \times 19 \times 9$ k-mesh for PdPS was used. The calculations of transport coefficients have been carried out as discussed in chapter 1 according to the
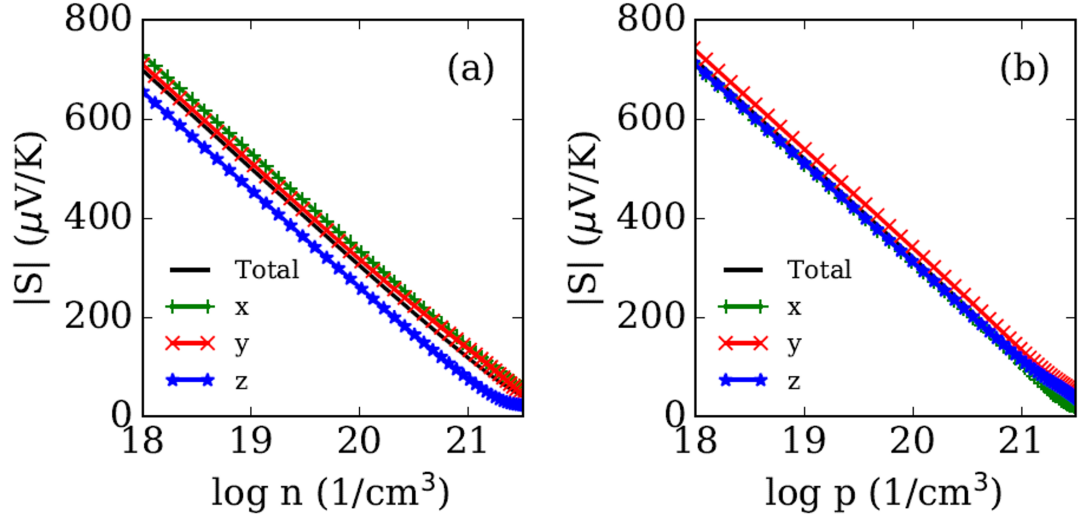
Figure 2.4: Seebeck coefficient of (a) n-type and (b) p-type at 300 K with carrier concentration.

following equations. Each transport coefficient can be calculated from density of states. The electrical conductivity is calculated according to the equation,

$$\sigma = e^2 \int dE (\frac{\partial f_0}{\partial E}) \Sigma(E) \tag{2.1}$$

where Σ is given as,

$$\Sigma = \sum_{\boldsymbol{k}} v_x^2(\boldsymbol{k}) \tau(\boldsymbol{k}) \delta(E - E(\boldsymbol{k})) \tag{2.2}$$

The electrical conductivity seems to depend on the relaxation time, however we have chosen a constant relaxation time as 5×10^{-15} s. On the other hand, the Seebeck coefficient comes out to be independent of the relaxation time and is given as,

$$S = \frac{e}{\sigma T} \int dE (-\frac{\partial f_0}{\partial E}) \Sigma(E)(E - E_F) \tag{2.3}$$

The electronic thermal conductivity is given as,

$$\kappa_e = \frac{1}{T} \int dE (-\frac{\partial f_0}{\partial E}) \Sigma(E)(E - E_F)^2 \tag{2.4}$$

2.3.2 Calculation of Seebeck coefficient

Seebeck coefficient calculation of n-type and p-type PdPS at 300 K in a carrier concentration range of $10^{18} - 10^{21}$ cm^{-3} (which is a suitable carrier concentration range for
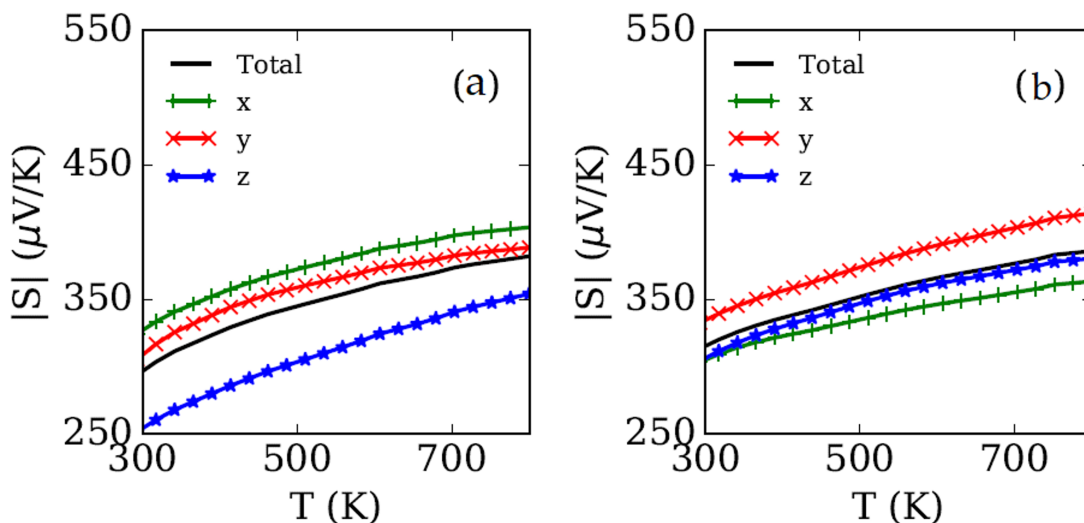
Figure 2.5: Variation of Seebeck coefficient for (a) n-type PdPS and (b) p-type PdPS at carrier concentration, 10^{20} cm^{-3} with temperature.

better ZT) is shown in Fig.2.4 (a, b). The variation of Seebeck coefficient with temperature is shown in Fig.2.5 (a, b) for both the n-type and p-type PdPS. Thermopower of p-type is little superior to n-type, and in n-type, the variation of thermopower with temperature is more anisotropic in different crystallographic directions. At 300 K and carrier concentration of 10^{20} cm^{-3}, thermopower of n-type along x direction is 335 μVK^{-1} and total thermopower is 303 μVK^{-1}, whereas for p-type, thermopower along y direction is 343 μVK^{-1} and total thermopower is 327 μVK^{-1}. At 800 K, these values approach to 400 μVK^{-1} and 380 μVK^{-1} for n-type and 411 μVK^{-1} and 383 μVK^{-1} for p-type at 10^{20} cm^{-3} (see Fig.2.5 (a, b)). This anisotropy in the thermopower values in the two different crystallographic directions might enable to design transverse thermoelectric device [121].

Seebeck coefficient values of PdPS in both the p-type and n-type are quite high as compared to thermoelectric materials reported in the temperature range of 300 K-800 K. These values are more than three times higher of the reported binary chalcogenides [100, 101] and two times greater than those for CoSbS [108]. Calculated n-type thermopower of PdPS in z direction is similar to FeSbS thermopower ($\sim$365 μVK^{-1} along x direction) [107], however for p-type PdPS, we obtain much higher thermopower as compared to FeSbS. High thermopower is crucial to design a stable Pb-free thermoelectric device.

2.3.3   Behavior of electrical conductivity

The behavior of electrical conductivity with carrier concentration is opposite to that of Seebeck coefficient. Electrical conductivity increases with increasing carrier concentration. The Seebeck coefficient in PdPS has mild anisotropy in the three crystallographic directions. However, the electrical conductivity has much higher anisotropy if we consider

isotropic scattering rate in all directions (Fig.2.6) (a, b). Since scattering time, τ or temperature dependence of τ is unknown, the absolute values of σ/τ could not be related to the actual electrical conductivity, $\sigma(T)$. The relative values of σ/τ in different directions are physically very significant and some of the earlier reports [122, 123] of σ/τ show that anisotropy of binary chalcogenides calculated by similar model are highly consistent with experimental values. The conductivity of n-type is much higher than p-type which can
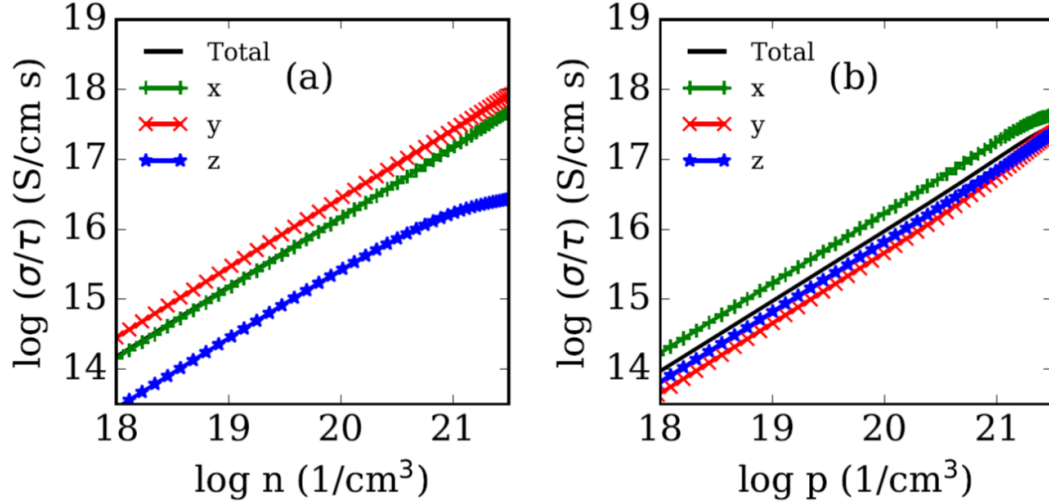

Figure 2.6: Electrical conductivity σ/τ vs carrier concentration for (a) n-type and (b) p-type PdPS at 300 K.

be explained by band structure of the PdPS (Fig.2.3), where valence bands consist mostly of massive holes as compared to lighter electrons in conduction band. Among the three crystallographic directions, x and y directions exhibit strong anisotropy. Unlike the x and y-direction, the n-type PdPS in z-direction may have more electron scattering than other directions as z-direction has both S and σ/τ the lowest of all the directions.

2.3.4 Anisotropic power factor

The performance of a thermoelectric material is assessed by the value of power factor $S^2\sigma$. As power factor combines the behavior of two oppositely varying parameters, it needs to optimize an optimum carrier concentration at which $S^2\sigma$ maximizes. Seebeck usually varies linearly with carrier concentration as discussed in chapter 1, therefore σ dominates due to its exponential behavior at moderate concentration. Large power factor values in PdPS are highly promising for two different type of legs in a thermoelectric module (See Fig.2.7 (a,b)). Electrical conductivity can be improved by external doping or by alloying which can also reduce thermal conductivity. By changing the initial PdPS growth conditions, several phases with minor variation in Pd:P:S can be obtained [114]. A ratio of P:S slightly higher than unity shows very low resistivity $\sim 2 \times 10^{-4}\Omega$cm [114]. Therefore alloying can be highly effective for PdPS based thermoelectrics. High anisotropic
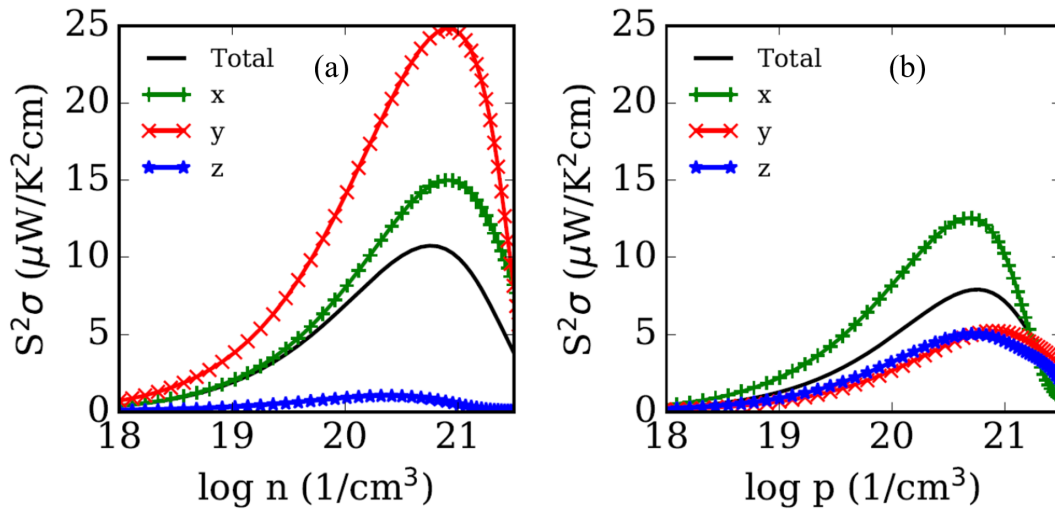
Figure 2.7: Power factor vs carrier concentration for (a) n-type and (b) p-type PdPS at 300 K.

transport properties along different crystallographic directions can also play a major role for nanostructured PdPS thermoelectric power generator (TEG). Nanostructured PdPS or 2D layered doped PdPS in a particular crystallographic direction can be used for TEG. For $\tau \sim 5 \times 10^{-15}s$, power factor reaches 1589 μWm^{-1}K^{-2} and 1015 μWm^{-1}K^{-2} for n-type and p-type PdPS respectively at 400 K and 10^{20} cm^{-3} carrier concentration. These power factor values of PdPS are comparable to those of commercially used p-type ($\sim$ 1670 μWm^{-1}K^{-2}) and n-type ($\sim$ 1200 μWm^{-1}K^{-2}) PbTe [109].

The power factor values are also much anisotropic with n-type values superior to p-type except in the z-direction. The anisotropy in the in-plane transport properties can be related to the periodic fashion in which all the three atoms are aligned in PdPS (as shown in the (Fig.2.8)). It can be seen that the position of Pd atoms is same in x- and y- directions but that of P and S is though periodic in y but not in the x direction. This unevenness in the arrangement of P and S atoms gives anisotropy in the in-plane properties in addition to cross plane layered direction.

2.4 Lattice transport properties

2.4.1 Method

Lattice thermal conductivity depends upon scattering of phonons by other phonons, defects, boundaries, charge carriers etc. As the performance of thermoelectric materials depends on the thermal conductivity, we have calculated phonon transport properties based on a recent ab-initio approach [124]. VASP code is applied to calculate the forces and $2 \times 2 \times 1$ supercell with 96 atoms is used for this force calculation. We have calculated forces on all atoms for symmetry reduced atomic displacement of $0.06\mathring{A}$ and the volume
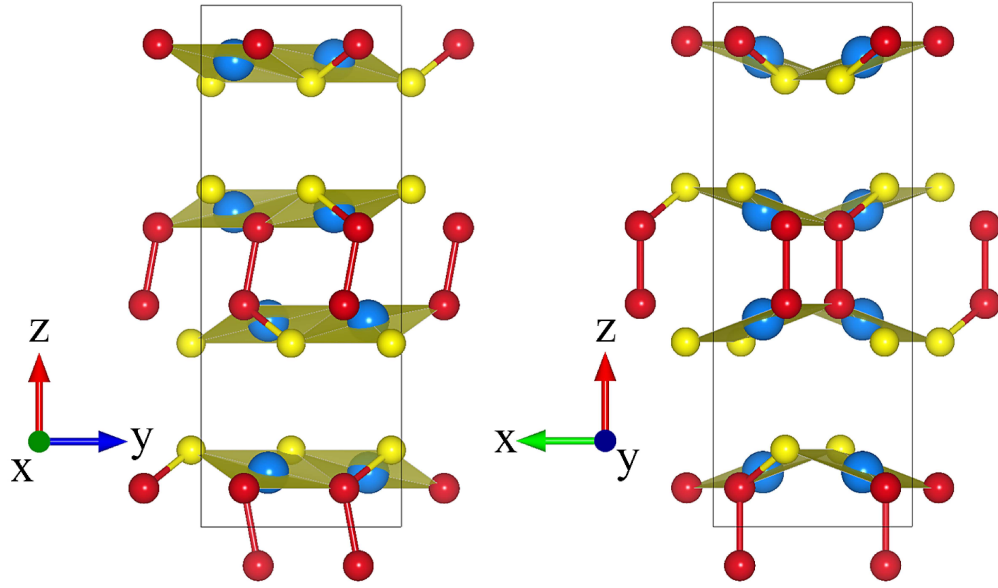
Figure 2.8: Anisotropic arrangement in the in-plane directions (x and y crystallographic directions) in PdPS.

derivative for Grüneisen parameter is calculated using volume range of $\pm 3\%$. The frozen phonon approach is adopted for extracting the force constants as implemented in the program PHONOPY [125]. We have plotted the phonon dispersion for PdPS in Fig.2.9(a) and phonon DOS and phonon velocity distribution in Fig.2.9(b). We have found, phonon dispersion is flat along the $\Gamma - Z$ direction, and phonon velocity distribution is very low in z crystallographic direction. Sound speed is almost 20 times lower in z crystallographic direction of PdPS compared to bulk sound speed. Low phonon velocity in z direction plays a crucial role in reducing thermal conductivity.

The formula for lattice thermal conductivity is generalized as given in Ref.[124],

$$k_l(T) = \frac{1}{3} \sum_j \int \frac{dq}{8\pi^3} v_{jq}^2 \tau_{jq} C_{jq} \tag{2.5}$$

here summation is over all the phonon bands (polarization) from acoustic to optical. The integration is done over all the $\boldsymbol{q}$ points in the first Brillouin zone. Phonons are characterized by band index and $\boldsymbol{q}$ value, each phonon mode has group velocity $v_j\boldsymbol{q}$ and specific heat capacity $C_{j\boldsymbol{q}}$ depending upon frequency and temperature. Phonon relaxation time is calculated considering model for anharmonic scattering as discussed in last chapter. Model relaxation time for anharmonic scattering is taken as,

$$\tau_U^{-1} = p\omega^2 \frac{T}{\tilde{\theta}_D} e^{-\tilde{\theta}_D/3T} \tag{2.6}$$
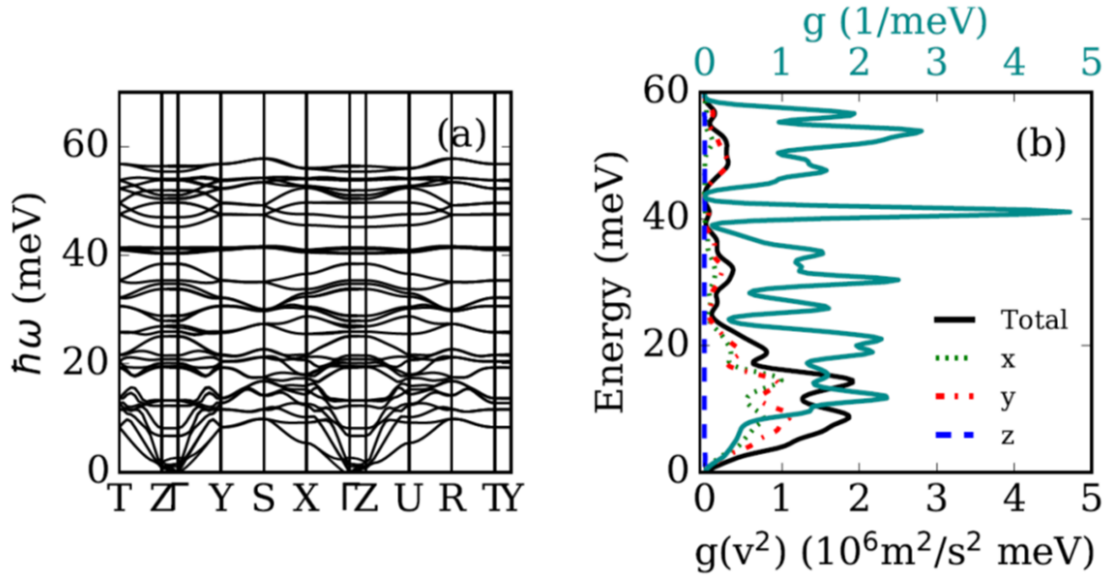
Figure 2.9: (a) Phonon dispersion of PdPS, (b) Phonon DOS and phonon velocity distribution for bulk and different crystallographic direction.

where p is an adjustable parameter whose value is approximated as,

$$p = \frac{1 - \frac{0.514}{\sqrt{\bar{\gamma}^2}} + \frac{0.228}{\bar{\gamma}^2}}{0.0948} \frac{\hbar^2 \bar{\gamma}^2}{k_B \tilde{\theta}_D M V^{1/3} s} \tag{2.7}$$

and s is sound speed and θ_D is the Debye's temperature. There are many ways of calculating θ_D, however we will be using the full phonon dispersion to calculate it as defined below,

$$\tilde{\theta}_D = n^{-1/3} \sqrt{\frac{5\hbar^2}{3k_B^2} \frac{\int_0^\infty \omega^2 g(\omega) d\omega}{\int_0^\infty g(\omega) d\omega}} \tag{2.8}$$

here n is the number of atoms per unit cell and $\bar{\gamma}^2$ is mode averaged-squared Grüneisen parameter taken over all the modes.

$$\bar{\gamma}^2 = \frac{\sum_j \int \frac{d\boldsymbol{q}}{8\pi^3} \gamma_{j\boldsymbol{q}}^2 C_{j\boldsymbol{q}}}{\sum_j \int \frac{d\boldsymbol{q}}{8\pi^3} C_{j\boldsymbol{q}}} \tag{2.9}$$

$$\gamma_{j\boldsymbol{q}} = -\frac{V}{\omega_{j\boldsymbol{q}}} \frac{\partial \omega_{j\boldsymbol{q}}}{\partial V} \tag{2.10}$$

Grüneisen parameter for a single phonon mode may have negative or positive value. The mode value of Grüneisen parameter usually varies from ~ 0.8 to ~ 2.0.

In addition to intrinsic scattering process (U-processes), the effect of nanostructuring is also calculated for PdPS. Apart from intrinsic scattering, phonons get scattered at the

boundaries of the crystal. The trend of thermal conductivity at lower dimensions is governed by the mean free path of phonons and the sample size. A diffusive type scattering rate [126] is used for the boundary scattering,

$$\tau_B^{-1} = v/d \tag{2.11}$$

where v is the phonon velocity and d is the diameter. The overall relaxation time is taken as additive reciprocal relaxation time of boundary scattering and intrinsic phonon scattering. The total value of scattering rate τ_T^{-1} is given as,

$$\tau_T^{-1} = \tau_U^{-1} + \tau_B^{-1} \tag{2.12}$$

where τ_U^{-1} is scattering rate for anharmonic scattering depending upon frequency and temperature and τ_B^{-1} is boundary scattering rate independent of frequency and temperature.

Using above equations, the values of lattice thermal conductivity is calculated for different temperature and sample diameter values. The results of which are shown in next section.

2.4.2 Lattice thermal conductivity calculations

The lattice thermal conductivity for all the crystalline materials has a universal shape depending upon frequency and temperature. As at high temperature, the lattice thermal conductivity decreases with rise in temperature. However, this decrease is much specific to a particular material. PdPS is anisotropic material as far as electronic transport properties were concerned in the first part of this chapter. In Fig.2.10, we plot thermal conductivity of PdPS along different crystallographic directions for temperature range of 300 K-800 K. Lattice thermal conductivity has very large anisotropy in the three crystallographic directions. Along the z crystallographic direction, thermal conductivity is ultra-low and more than ten times lower than the bulk thermal conductivity. In-plane thermal conductivity values are also different similar to charge transport properties. However, the in-plane values of thermal conductivity are quite higher, which can be reduced by alloying.

Fig.2.11 (a) reports the thermal conductivity with reducing size at 300 K. Nanostructuring also has a strong connection with thermal conductivity reduction in z crystallographic direction as compared to other directions and bulk κ. In Fig.2.11 (b), we plot relative κ with phonon mean free path (Λ) for different crystallographic directions. While in x and y direction, Λ below μm size contributes 80% in thermal conductivity, in z direction this contributes only 40%. Therefore, in the z direction, larger wavelength phonon carries most of the heat, which can be easily blocked by nanostructuring. So larger reduction in κ along z direction is obtained as compared to bulk or x and y direction.
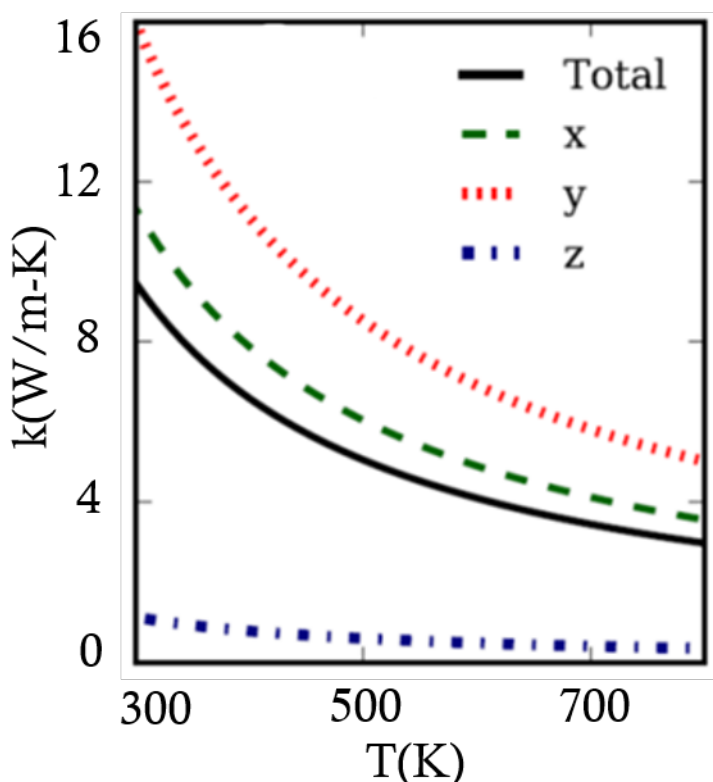
Figure 2.10: Variation of thermal conductivity in different crystallographic directions and in bulk PdPS with temperature.

2.5 Thermoelectric figure of merit

2.5.1 Effect of nanostructuring on figure of merit

The efficiency of a thermoelectric material is calculated by a parameter called figure of merit (ZT), which is a ratio of charge transport to heat transport in a material. Fig.2.12 (a, b) represents ZT for n-type and p-type at 300 K and 800 K. Though, in the z direction, ZT is always higher compared to bulk for p-type, for n-type ZT along z direction starts dominating around 500 nm due to a strong reduction in thermal conductivity. We have obtained $ZT \sim 0.02$ for bulk PdPS and ~ 0.02 along z crystallographic direction of PdPS for n-type and ~ 0.01, ~ 0.09 for p-type at 300 K. These ZT values approach ~ 0.27, ~ 0.20 for n-type and ~ 0.20, ~ 1.17 for p-type at 800 K.

In the realm of 100 nm, ZT values increase to ~ 0.05 and ~ 0.23 for n-type and ~ 0.03 and ~ 0.86 for p-type at 300 K, and $ZT \sim 0.50$ and ~ 0.86 for n-type and ~ 0.34 and ~ 5.15 for p-type at 800 K. Nanostructured p-type PdPS shows a much superior value of ZT in the z crystallographic direction than n-type. All these values are obtained at 10^{20} cm^{-3} carrier concentration and for $\tau = 5 \times 10^{-15}$ s.

Even though bulk thermoelectric properties of PdPS may not be touching the horizon
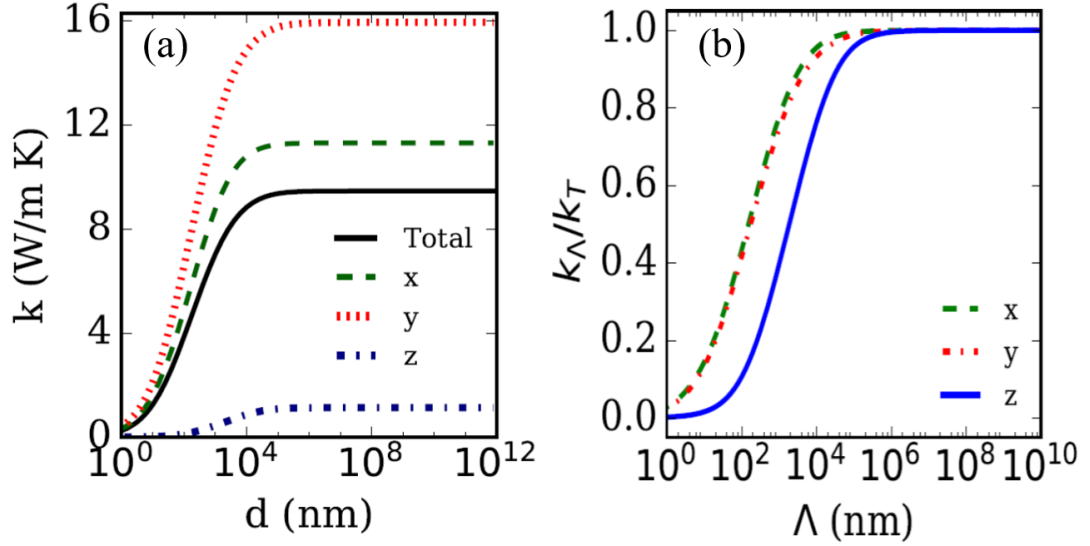
44

Figure 2.11: (a) Thermal conductivity in different crystallographic directions and in bulk PdPS with diameter, (b) Relative contribution in thermal conductivity of phonon mean free path.
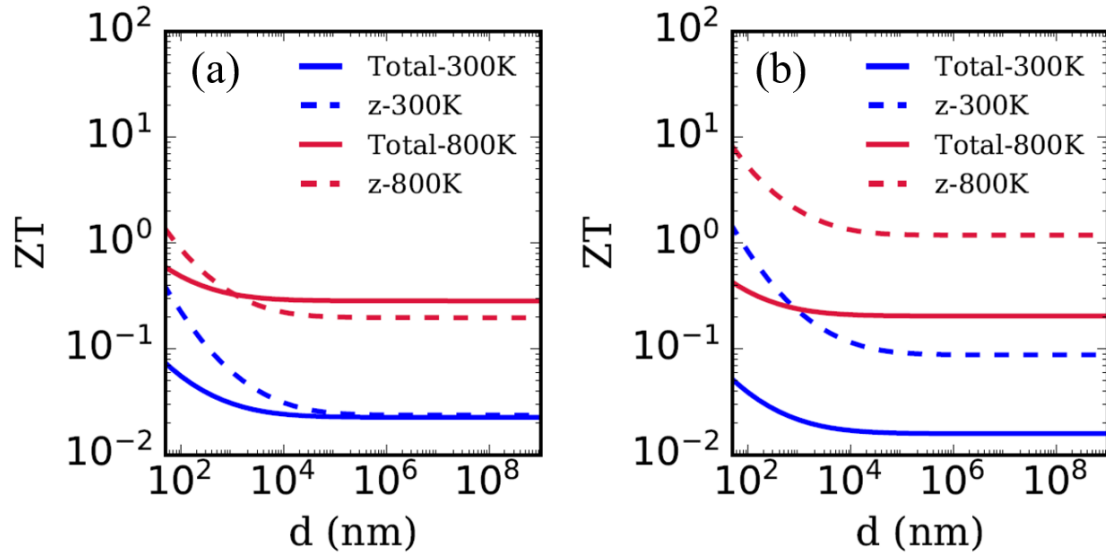
Figure 2.12: (a) ZT with sample diameter for (a) n-type and (b) p-type.

of superior thermoelectric materials, its lower dimensions may prove much useful in thermoelectric applications. Specifically the layered direction has shown ultra superior values of figure of merit theoretically.

Fig.2.13 presents ZT for bulk and nanostructured PdPS at carrier concentration range of $10^{18} - 10^{21}$ cm^{-3} at 800 K. Significant high ZT values have been found by our theo-

Figure 2.13: ZT of bulk and nanostructured PdPS at 800 K.

retical calculation for nanostructured PdPS in both n-type and p-type.

2.6 Conclusions

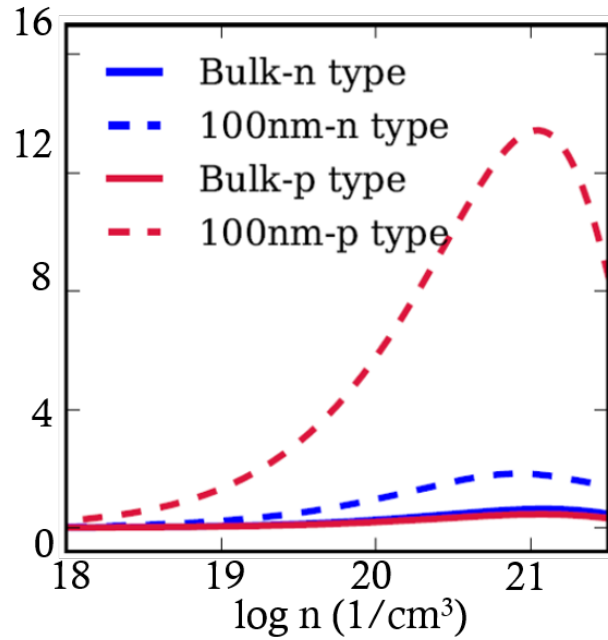In conclusion, we have presented transport properties calculations of a potential candidate for high-performance thermoelectricity, palladium pnictide chalcogenide. Seebeck coefficient found by our calculation is as high as 300 μVK^{-1} at 300 K and reaches to 400 μVK^{-1} at 800 K for both p-type and n-type PdPS and ultra low thermal conductivity of 0.11 Wm^{-1}K^{-1} along z crystallographic direction at 300 K. These high Seebeck coefficient values, large anisotropic power factor, and low thermal conductivity suggest that PdPS can be very useful as a thermoelectric in the medium temperature range (300 K-800 K). To the best of our knowledge, there is no experimental or theoretical report published on PdPS thermoelectric properties so far. These encouraging thermoelectric properties may motivate for further experimental investigations which will also help to optimize the thermoelectric properties of orthorhombic PdPS.

Chapter 3

Effect of alloying on thermoelectric properties of CoAsS and CoSbS

3.1 Introduction

The thermoelectric system is based on an environment-friendly energy conversion technology with the advantages of small size, high reliability, no pollutants and feasibility in a wide temperature range. Many such compounds have been analyzed to achieve better thermoelectric properties among which there are binary compounds like Bi_2Se_3, PbTe [98, 109] and ternary such as FeSbS, CoSbS, PdPS [107, 111, 112] etc and quaternary such as $Cu_2CdSnSe_4$ [113] etc. Transition metal compounds arose with an ample number of structures thus giving rise to a broad spectra of physical properties among them which make them in a constant race for becoming better than the already known compounds. This expedition for exploring better thermoelectric performance among a copious number of compounds is based either on finding a purely new compound or on modifying the thermoelectric properties of existing compounds by specific techniques.

To enhance the thermoelectric performance of already existing compounds, different methods have been devised like nanostructuring, doping with different elements at different sites in a crystal, rattling atoms, alloying with different elements etc. All these methods either target at modifying the existing band structure to fall into the patternized format having larger effective mass but higher mobility too and higher density of states near the Fermi level or on the other hand steering the phonon scatterings to reduce the thermal conductivity. Thus this increases the overall performance based on the strategy of "phonon glass electron crystal" [127, 128]. Among these methods, alloying has remarkable effects on the thermoelectric behavior as it produces defect atoms of different kind on the lattice sites thus changing the volume of the overall crystal structure [127, 128].

3.2 Alloying in pure materials

Alloying is one of the methods of introducing local disorder in the crystal lattice as discussed in chapter 1. Alloying affects a particular range of phonons and scatter them selectively and thus enhances the thermoelectric figure of merit of the alloy. It is substitution of other atoms in the host crystal structure at lattice sites. In literature, the thermal conductivity of binary compound Cu_2X (where X stands for S, Se, Te) is reduced in case of $Cu_2S_{0.52}Te_{0.48}$, $Cu_2S_{0.08}Se_{0.92}$ from 0.8 $Wm^{-1}K^{-1}$ to 0.4 $Wm^{-1}K^{-1}$. The alloy ZT hikes to around 2.2 at 1000 K, whereas the pure material ZT stays around 1.5 [129, 130, 131]. SnTe when alloyed with Mg with composition $Sn_{0.94}Mg_{0.09}Te$ reaches in $ZT \sim 1.2$ at 860 K [132]. $Sn_{1-x}Pb_xSe$ alloy has reduced thermal conductivity from 1.4 $Wm^{-1}K^{-1}$ to 0.85 $Wm^{-1}K^{-1}$ for x=0.12. The intrinsic ZT of polycrystalline SnSe is around 0.85 at 800 K. The value of ZT after alloying enhances due to much reduced thermal conductivity [133, 134]. Half heusler alloy of NbFeSb with Ta has shown a significant increase in ZT. $(Nb_{1-x}Ta_x)_{0.8}Ti_{0.2}FeSb$ (x varies from 0 to 0.4) has a maximum $ZT \sim 1.6$ at 1200 K with much reduced thermal conductivity at $x = 0.4$ [135].

Formation of an alloy is conditioned to the structure of forming components of alloy. The crystal structure of the forming materials should be approximately similar. This is easily achieved by choosing materials with iso-electronic elements which usually tend to make similar kind of structure. Among many chalcogenides of Co, paracostibite CoSbS has orthorhombic structure with space group $Pbca$, it shows semiconducting nature and has been explored for thermoelectric performance. CoAsSe and CoSbSe have also been synthesized long back in 1974 by H. Nahigian and both are shown to have orthorhombic structure [136]. CoAsS, also known as cobaltite possesses similar structure to that of iron pyrite FeS_2, having same number of valence electrons and due to similarity to pyrite, has semiconducting nature. It has been predicted that many such compounds can be obtained by substituting three of its components by other suitable elements [137]. Recently, there has been an experimental research on the Sb alloyed pseudo-ternary compounds $GeTe_{(1-2x)}Se_xS_x$ in which remarkable reduction ($\sim 76\%$) of thermal conductivity has been observed in GeTe on alloying it with Se, S and Sb atoms up to a small concentration [138]. Thus a similar substitution as suggested by Hulliger can surely guide us through making different alloys for this compound in achieving good thermoelectric properties. CoAsS exists in two different forms based on the formation temperature, one is disordered pyrite structure formed at 800 K-850 K and the other one is ordered structure formed at lower temperatures [139]. Among these two forms, we are using the ordered orthorhombic form having space group $Pca2_1$ which is synthesized in the laboratories[139].

3.3 Electronic structure calculations

3.3.1 Method

DFT calculation is performed on CoAsS and CoSbS for our present calculations, among which there has been already considerable theoretical and experimental published

data on thermoelectric performance of paracostibite CoSbS [107, 111, 108], however the cobaltite CoAsS has not yet been investigated thoroughly apart from some preliminary electrical properties studies [136]. Both the cobaltite and paracostibite are orthorhombic in nature. DFT calculation is done using PBE functional [117] and PAW basis set as embedded in VASP [118, 119].
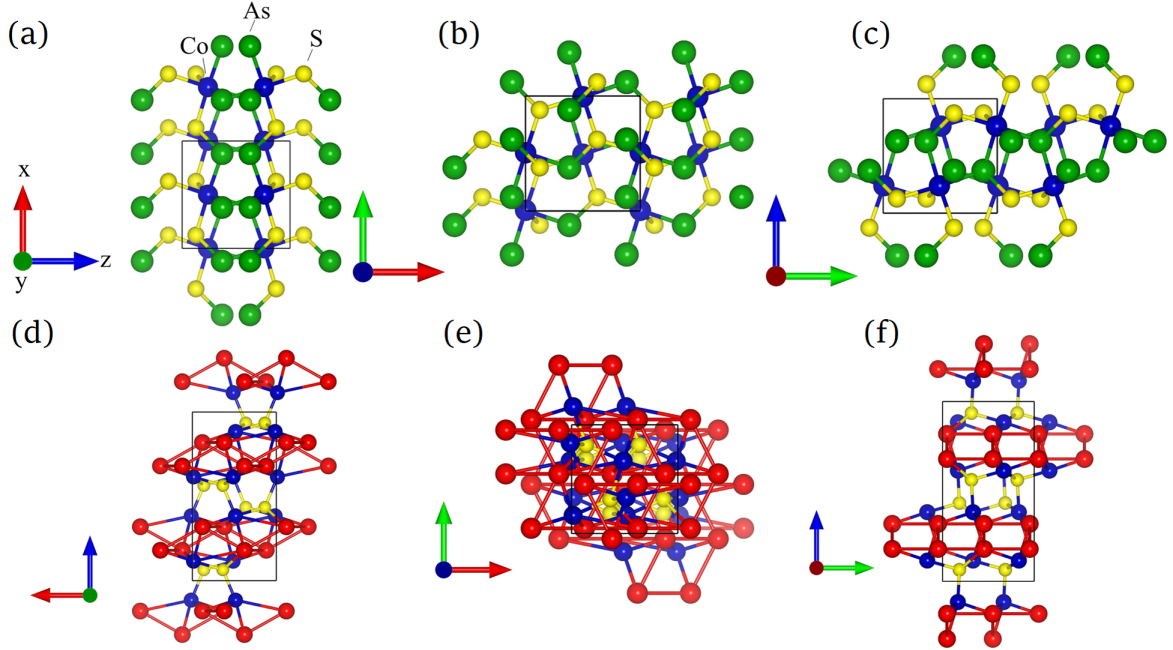

Figure 3.1: Crystal Structure of CoAsS (a) Front view (b) Side view (c) Top view and CoSbS (a) Front view (b) Top view (c) Side view, direction x, y and z represents $\Gamma - X$, $\Gamma - Y$ and $\Gamma - Z$ crystallographic directions in the first Brillouin zone in CoAsS and CoSbS.

The lattice sides a, b, and c of CoAsS are obtained as 5.576 Å, 5.578 Å, and 5.582 Å respectively after performing the self-consistent calculations using VASP on unit cell containing 12 atoms. Similarly for CoSbS relax structure, the lattice parameters are 5.833 Å, 5.966 Å, and 11.691 Å choosing unit cell of 24 atoms, where the experimentally reported lattice constant is 5.576 Å for CoAsS [136] and 5.834 Å, 5.953 Å, and 11.664 Å for CoSbS [136]. The k-points for structure optimization in case of CoAsS and CoSbS are taken (4×4×4) and (2×2×1) with energy cut off values around 350 eV. In the ordered structure, the anions occupy the lattice sites in the same pairing as 4 As-ions will be lying in the lower part of the cube and the 4 S-ions lie in the upper half of the cube and vice-versa Fig.3.1 (a). Earlier electrical measurements on the compound CoAsS were carried out showing the electrical resistivity of 1.49×10^{-1} Ωcm which is lesser than that of CoSbS (1.12 Ωcm) and by substitution of S by heavier Se, a much lower resistivity of 4.57×10^{-4} Ωcm has been reported [136].

3.3.2 Electronic band structure

The electronic band structure calculations are carried out for both the compounds and Fig. 3.2 (a) represents CoAsS electronic band structure and density of states (DOS) plot. The theoretically calculated band gap for CoAsS is 0.75 eV, and 0.33 eV for CoSbS, where the experimentally measured values in Ref.[136] are 0.05 eV and 0.11 eV respectively. The density of states for p-type CoAsS is very high near Fermi level, which is good for electronic transport properties as temperature rises. In recent publications of electronic band structure and electronic properties of CoSbS by using the linearized augmented plane wave (LAPW) code WIEN2K and experimental date have reported much higher band gap of 0.5 eV and 0.37 eV respectively and the reported electrical conductivity in Ref. [111, 108] is much higher as compared to values given in Ref. [136] values. Our electronic structure calculations based on VASP agrees with these recent calculations in Ref. [111, 108]. We have further calculated the electronic transport properties of both the compounds. We have compared our theoretical calculations with the experimental data reported on CoSbS [111]. In the Fig.3.2 (b), there are many small pockets in the band structure in the valence band which is favorable for the p-doping and good thermoelectric properties optimization. The conduction band has much flat regions at $\Gamma-$point, which are directly responsible for the higher Seebeck coefficient, S of the compound. In comparison, the valence band has replicate maxima at $\Gamma - X$, $\Gamma - Y$ and $\Gamma - Z$ direction which are sharper giving lesser Seebeck coefficient. However, for the higher temperature, as there are more number of smaller pockets in the valence band than conduction band, the electrical conductivity of p-type will rise sharply. Also the conduction band second minima are lesser flat so rise in Seebeck coefficient with temperature will be slower in n-type as compared to the p-type which has a more flat second maxima. And apart from that, the p-type has a high density of states near the Fermi level which is also good for enhancing the thermoelectric properties, thus making CoAsS a very prominent candidate to be a good p-type TE material.

3.4 Electronic transport properties

3.4.1 Method

The electronic transport properties have been calculated using Boltzmann transport equation with constant value of relaxation time embedded into the BoltzTraP software [120]. The equations used to calculate transport coefficients are same as discussed in chapter 1. The electrical conductivity data of CoAsS has been calculated by using constant relaxation time by fitting the experimental data of CoSbS with the current calculations. Relaxation time, τ will depend on different scattering mechanisms involved in the materials, depending on the scattering mechanism, τ has different temperature dependence. Here we consider an isotropic τ as $1.8 \times 10^{-18}\, T^{-1.2}$ s for CoSbS at concentration of 4×10^{20} cm^{-3}, and the same has been taken for CoAsS transport calculations. Since As atom is lighter than Sb, thus apart from structural differences, there can be a slight higher
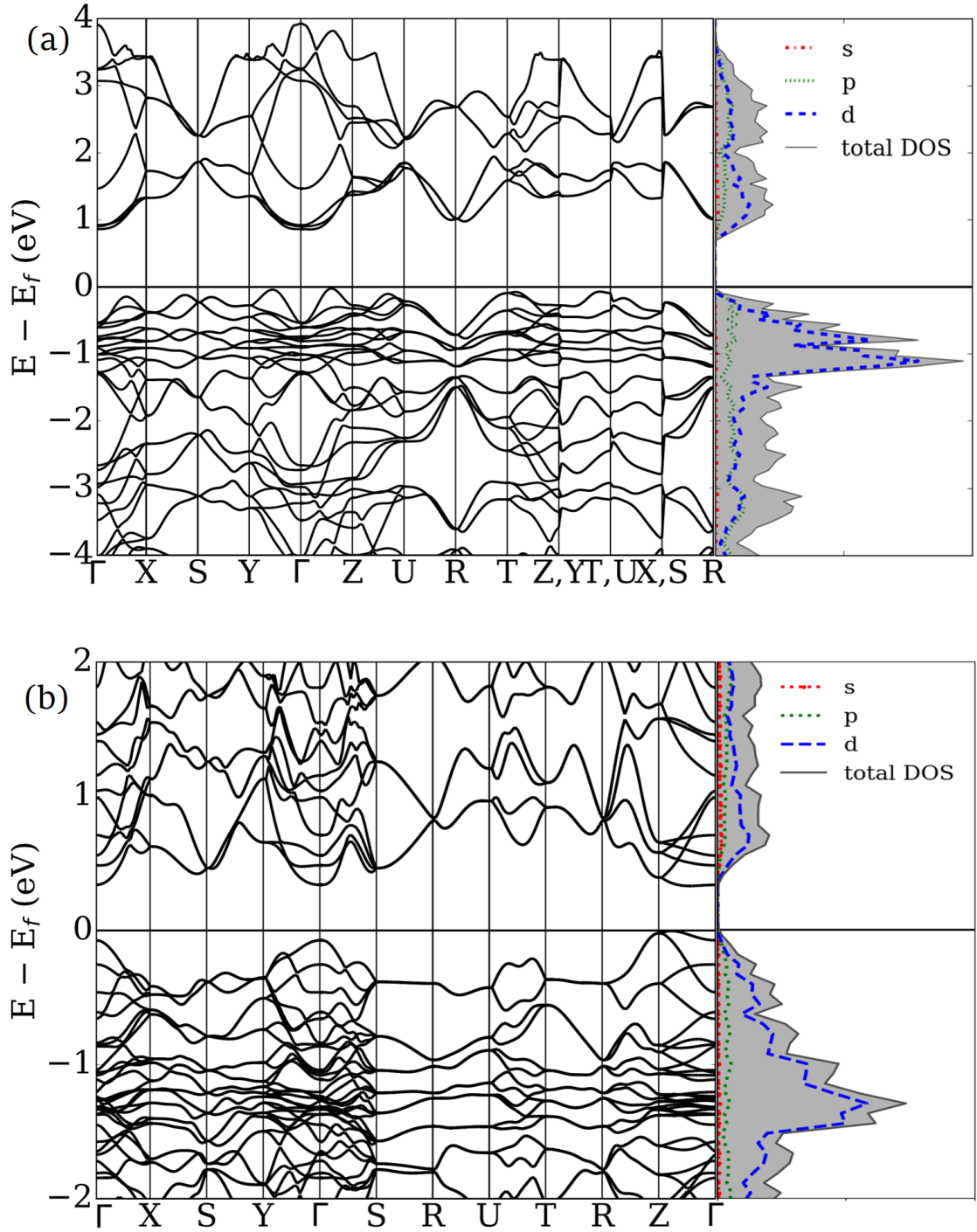
Figure 3.2: Electronic band structure of (without spin-orbit coupling) (a) CoAsS and (b) CoSbS.

value of relaxation time for the CoAsS based on the mass difference which will further increase the electrical conductivity, thus enhancing the power factor values calculated.
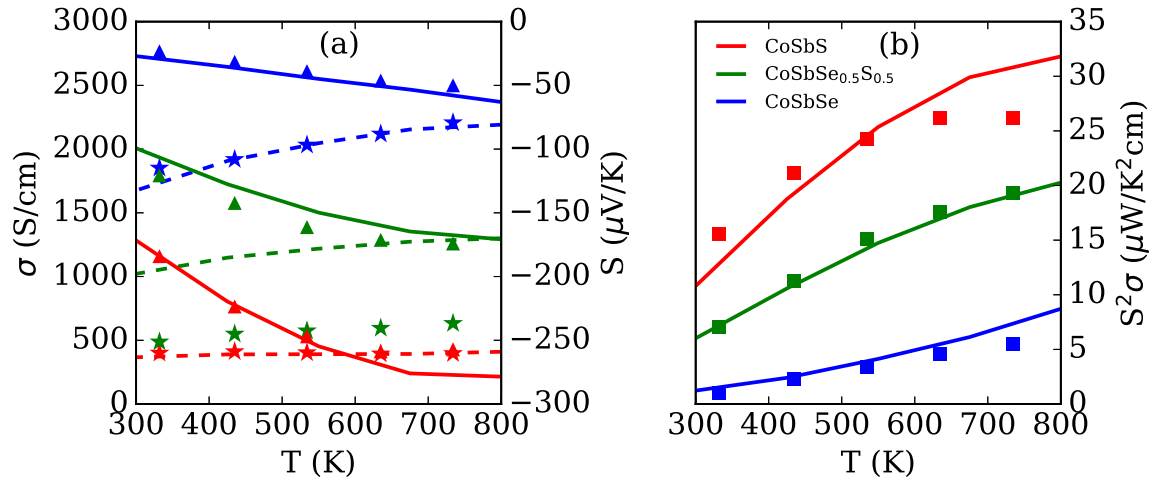
Figure 3.3: (a) Electrical conductivity, σ vs temperature, T and Seebeck coefficient, S vs
T for CoSbS, CoSbSe, and CoSbS$_{0.5}$Se$_{0.5}$ alloy. The scatterer represents the experimental
values (Ref. [140]), and solid lines are theoretical values for S and dashed lines are for σ.
(b) Power factor vs T.

An alloy is supposed to be an average of its component structures. The electronic
properties of alloy can be calculated by considering the virtual crystal approximation (as
discussed in chapter 1). We have calculated the power factor of the recently reported
CoSbSe$_x$S$_{1-x}$ alloy by using the virtual crystal approximation (Fig.3.3). We have found
very good agreement of theoretical calculations of experimental measurement of Seebeck
coefficient for pure and alloy materials. Theoretical and experimental power factor also
match with the virtual crystal approximation. We have calculated the power factor of alloy
considering the virtual crystal approximation as,

$$S^2\sigma T = x(S_A^2\sigma_A T) + (1-x)(S_B^2\sigma_B T) \tag{3.1}$$

where the ($S_A^2\sigma_A$) and ($S_B^2\sigma_B$) are the power factors of two components A and B of the
alloy.

3.4.2 Seebeck coefficient and electrical conductivity

3.4.2.1 Calculations for CoAsS and CoSbS

The calculated transport properties have been compared in the case of CoSbS with the
Ref.[111] at 300 K and as found from the Fig.3.4, there is a maximum agreement ($\sim 93\%$)
between the theoretical CoSbS and experimental data at concentration of $\sim 10^{21}$ cm^{-3}
and the maximum mismatch of $\sim 13\%$ is observed between experimental and theoretical
values of Seebeck coefficient at concentration of 10^{20} cm^{-3}. The calculated values of
Seebeck coefficient for n-type CoAsS is ~ 193 μVK^{-1} and for p-type, ~ 154 μVK^{-1} and
~ 155 μVK^{-1}, ~ 145 μVK^{-1} for CoSbS respectively at 300 K temperature and 4×10^{20}
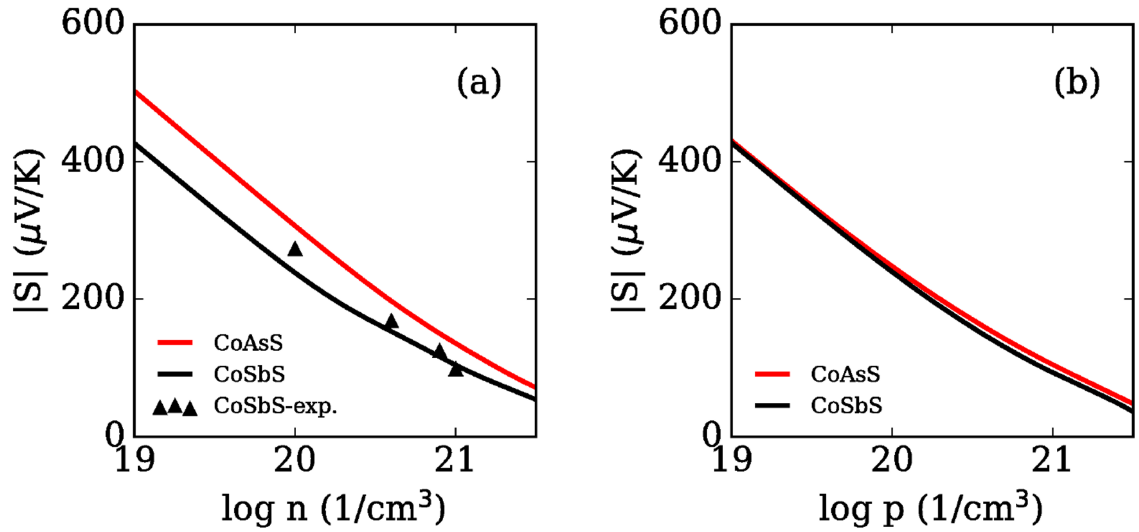cm^{-3} carrier concentration. It has been observed that Seebeck coefficient for CoAsS is

Figure 3.4: Seebeck coefficient, S of both CoAsS and CoSbS (a) n-type and (b) p-type at temperature 300 K with carrier concentration along with the experimental data of the Ref.[111] for n-type CoSbS.

higher than that of CoSbS for the same charge carrier concentration of 4×10^{20} cm^{-3} for both n and p-type at 300 K (Fig.3.4). The Seebeck coefficient data has been calculated for the temperature range of 300 K-800 K. As the temperature is increased up to 800 K, the Seebeck coefficient keeps on rising for CoAsS as shown in Fig.3.5 whereas in the case of CoSbS, it starts saturating around 650 K, but this bend in the Seebeck curve smooths out as we increase the concentration.

The electrical conductivity values for p-type CoAsS are more enhanced as shown in Fig.3.6, which is clear from the band structure as there are several maxima lying just below the Fermi level. Due to substantially higher conductivity values ~ 304 Ω^{-1}cm^{-1} of the p-type than n-type ~ 98 Ω^{-1}cm^{-1}, the power factor values for the p-type CoAsS are more enhanced than n-type and are even more superior to n-type CoSbS by a factor of two. The power factor values are calculated for the same relaxation time τ and concentration of 4×10^{20} cm^{-3} and data has been compared with the CoSbS experimental data [111] turning up with a good agreement in all temperature range.

3.4.2.2 Calculations for alloy

We have studied the method and validity of virtual crystal approximation to study the properties of alloy in Sec.3.4.1. It can be seen that this average approximation works good for Seebeck coefficient as it does not depend upon the relaxation time, however electrical conductivity for alloy case differs from virtual crystal approximation values. Apart from this, the power factor values quite match in the theoretical and experimental case. Similar method has been used to calculate the alloy properties of CoAsS and CoSbS. The power factor values are always average of the two participating materials, and resultant values
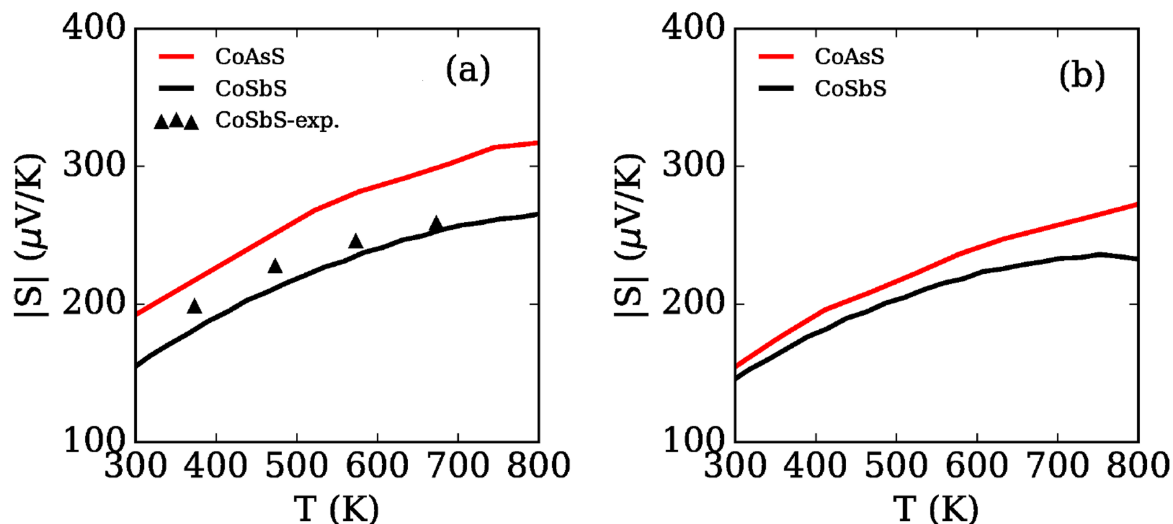
Figure 3.5: Variation of Seebeck coefficient, S for CoAsS and CoSbS (a) n-type and (b) p-type at carrier concentration, 4×10^{20} cm^{-3} with temperature, T along with the experimental data of the Ref.[111] for n-type CoSbS.

bend towards the major component used in the alloy as shown in Fig.3.7 (a,b). The power factor of CoAsS is superior to CoSbS for both n-type and p-type data.

3.5 Lattice transport properties

3.5.1 Method

Another major component of TE properties is the thermal conductivity, κ. For calculating it, the phonon band structure has been calculated using the PHONOPY code [125]. Phonon band structure for both the CoAsS and CoSbS has been presented in Fig.3.8 (a,b). The speed of sound as seen from the acoustic modes is higher in case of CoAsS ~ 5136 ms^{-1} than CoSbS ~ 4292 ms^{-1}, so as the thermal conductivity of CoAsS is also higher than CoSbS which has lower sound speed. As the thermal conductivity is highlighted mainly due to the lattice part in semiconductor material, we have calculated the lattice thermal conductivity using the recent ab-initio approach [124, 112]. The force constant calculations are carried out via making a CoAsS supercell of $2 \times 2 \times 2$ using VASP code with 96 atoms using the frozen phonon approach as implemented in the program PHONOPY [125]. Similarly, the force constant calculations for CoSbS are carried out by constructing a supercell of $2 \times 2 \times 1$ constituting 96 atoms. We have calculated forces on all the atoms in both the compounds for symmetry reduced atomic displacement of 0.06 Å and the volume derivative for Grüneisen parameter is calculated using volume range of $\pm 1\%$. The thermal conductivity is calculated from the generalized formula as given in the previous chapter by considering the anharmonic scattering. We have incorporated alloy
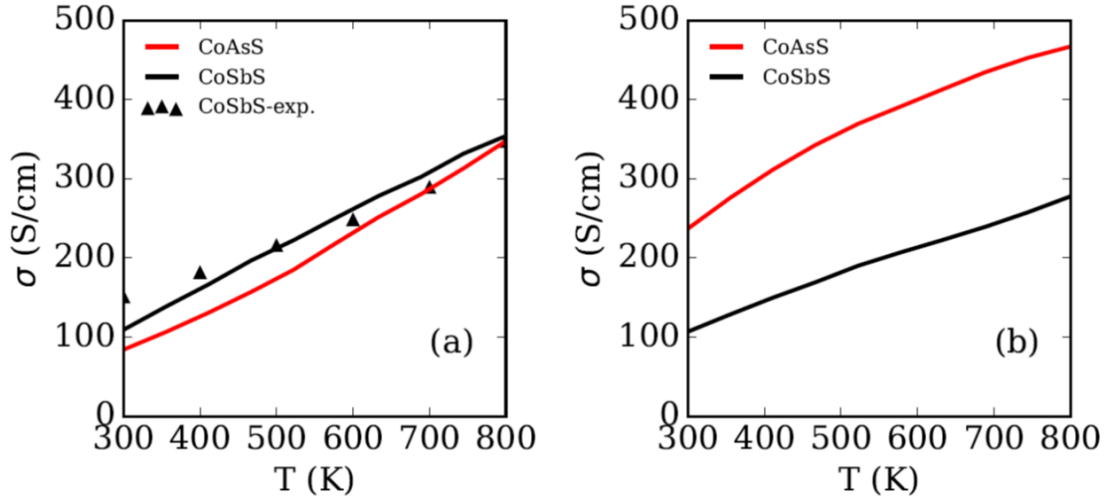
Figure 3.6: Electrical conductivity σ in temperature range of 300 K-800 K for CoAsS and CoSbS (a) n-type and (b) p-type at concentration of 4×10^{20} cm^{-3} along with the experimental data of n-type CoSbS [111].

scattering into the scattering of phonon transport via following equations. The inverse relaxation time corresponding to alloy scattering [141, 142]

$$\tau_A^{-1} = \frac{\omega^4 \delta^3 \Gamma}{4\pi v^3} \tag{3.2}$$

where ω is the angular frequency of the alloy, v is the speed of sound in the alloy, δ^3 is the atomic volume of the alloy given as

$$\delta^3 = x(V_A) + (1-x)(V_B) \tag{3.3}$$

where the V_A and V_B are the atomic volumes of the component A and B and Γ is the scattering cross section of the impurity atom and given as

$$\Gamma = x(1-x)(\frac{\Delta M}{M})^2 \tag{3.4}$$

where ΔM is given as,

$$\Delta M = M_A - M_B \tag{3.5}$$

$$M = xM_A + (1-x)M_B \tag{3.6}$$

where M_A and M_B are the masses of the components A and B in the alloy and x is the fractional concentration of A in the alloy.

3.5.2 Effect of alloying on thermal conductivity

The thermal conductivity data is plotted for both CoAsS and CoSbS along with the un-doped (pure) and doped experimental data of CoSbS [111]. The calculated thermal conductivity of CoAsS is quite higher ~ 12 Wm^{-1}K^{-1} at temperature of 300 K (Fig.3.9 (a,b))
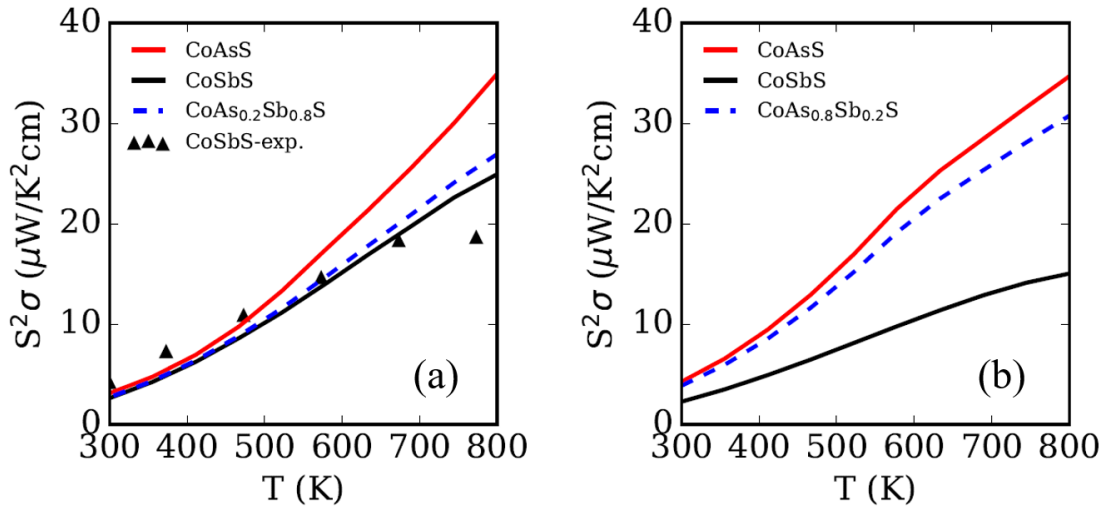
Figure 3.7: Power factor vs T for CoAsS and CoSbS in temperature range of 300 K-800 K (a) n-type and (b) p-type at concentration of 4×10^{20} cm^{-3} along with the experimental data of n-type CoSbS [111].
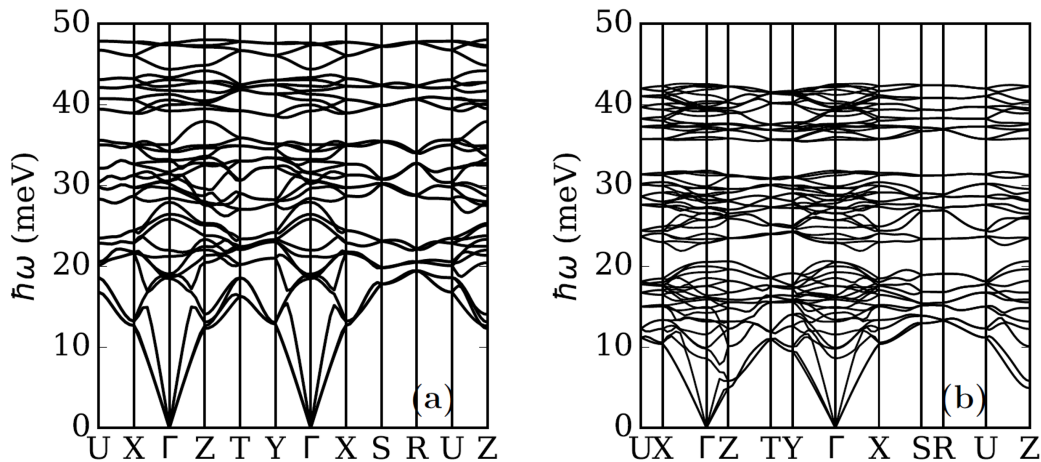

Figure 3.8: Phonon band structure of (a) CoAsS and (b) CoSbS.

than other thermoelectric materials like PbTe, Bi$_2$Se$_3$ or even CoSbS. As the power factor of CoAsS is having superior values, a small reduction in thermal conductivity can provide very efficient ZT. As concluded by Hulliger [137], the cobaltite CoAsS can have many substitutions in its atomic positions which can be used for finding a fine alloy of the compound.

The effect of alloying has been calculated for the CoAs$_x$Sb$_{1-x}$S, CoAsS$_x$Se$_{1-x}$, and CoSbSe$_x$S$_{1-x}$ (Fig.3.10) and it is observed that the reduction of thermal conductivity from 13 Wm^{-1}K^{-1} to 5.37 Wm^{-1}K^{-1} is maximum when the concentration of Sb in the CoAs$_x$Sb$_{1-x}$S alloy is 80%, as the reduction is around 2 times thus increasing the figure of

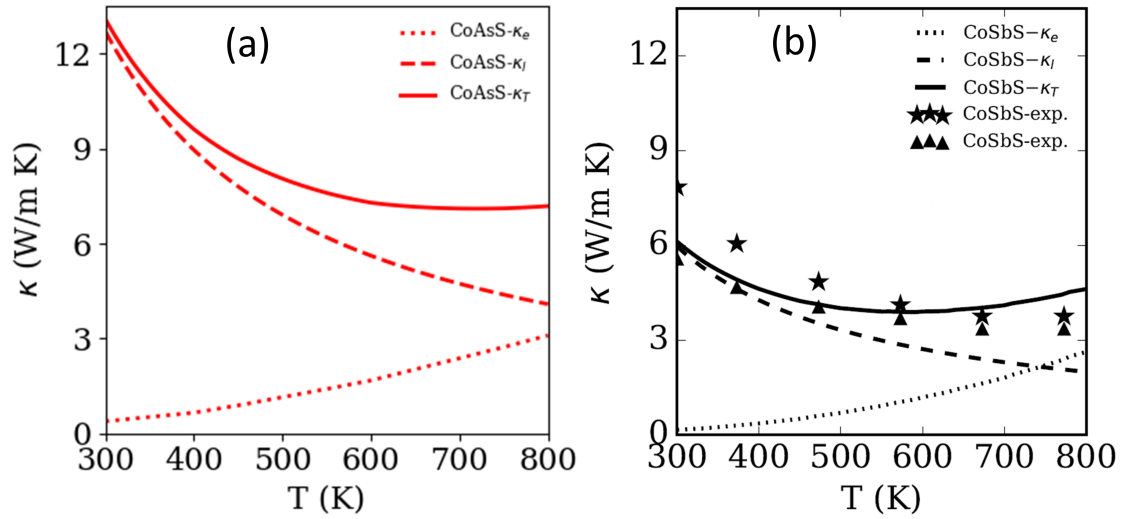Figure 3.9: Thermal conductivity κ vs temperature T of alloying for (a) CoAsS, (b) CoSbS along with the pure and doped experimental data of CoSbS Ref.[140].

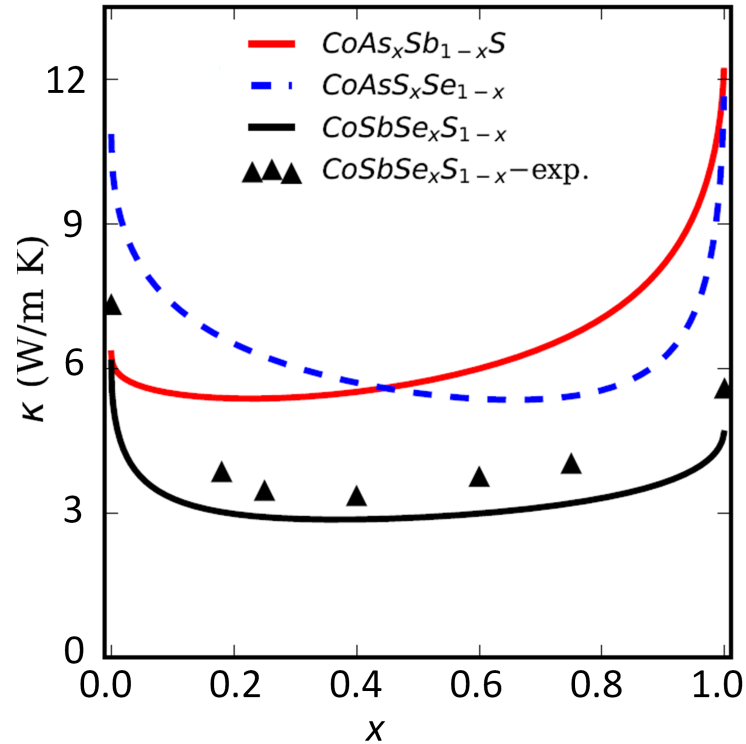

Figure 3.10: Thermal conductivity κ vs fractional concentration x of alloying for three alloys CoAs$_x$Sb$_{1-x}$S, CoAsS$_x$Se$_{1-x}$, and CoSbSe$_x$S$_{1-x}$ at 300 K along with the experimental data of CoSbSe$_x$S$_{1-x}$ Ref.[140].
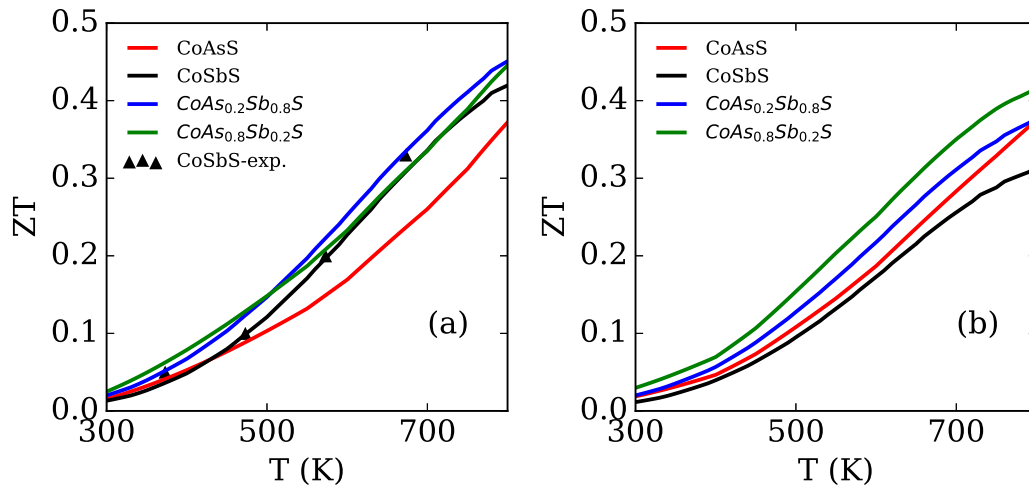
Figure 3.11: Figure of merit ZT vs temperature T for pure CoAsS, CoSbS and alloyed
CoAs$_x$Sb$_{1-x}$S (a) n-type (b) p-type at carrier concentration 4×10^{20} cm^{-3} along with the
experimental data of n-type CoSbS.

merit with the similar scale. A 44% reduction in thermal conductivity is also observed for
20% of Sb in CoAs$_x$Sb$_{1-x}$S alloy. It will play a significant role to further optimize p-type
TE materials based on CoAs$_x$Sb$_{1-x}$S alloy. There is further reduction of thermal conduc-
tivity when CoAsS is alloyed with Se in place of S giving the reduced value of thermal
conductivity of 5.36 Wm^{-1}K^{-1} in the Se concentration of 0.4. Such reduced values of
thermal conductivity on alloying will increase the ZT to higher values.

3.6 Thermoelectric figure of merit

3.6.1 Effect of alloying

The figure of merit calculations are carried out in the carrier concentration of 4×10^{20}
cm^{-3} (Fig.3.11). The figure of merit calculations for the alloy case has been done using
the formula

$$ZT = \frac{x(S_A^2 \sigma_A T) + (1-x)(S_B^2 \sigma_B T)}{\kappa_{alloy}} \qquad (3.7)$$

where the $(S_A^2 \sigma_A)$ and $(S_B^2 \sigma_B)$ are the power factors of the two components A and B of
the alloy and the κ_{alloy} is the value of thermal conductivity of alloy as calculated above.

The figure of merit of p-type CoAsS is higher than that of n-type in between the tem-
perature range of 300 K-800 K. As we reach the higher temperature range, n-type CoAsS
starts dominating in this concentration range and becomes ~ 0.37 for both n-type and p-
type at temperature of 800 K. As the fraction of alloying is incorporated, the n-type will
start overcoming the p-type values and will reach 0.45, a bit higher than p-type value of
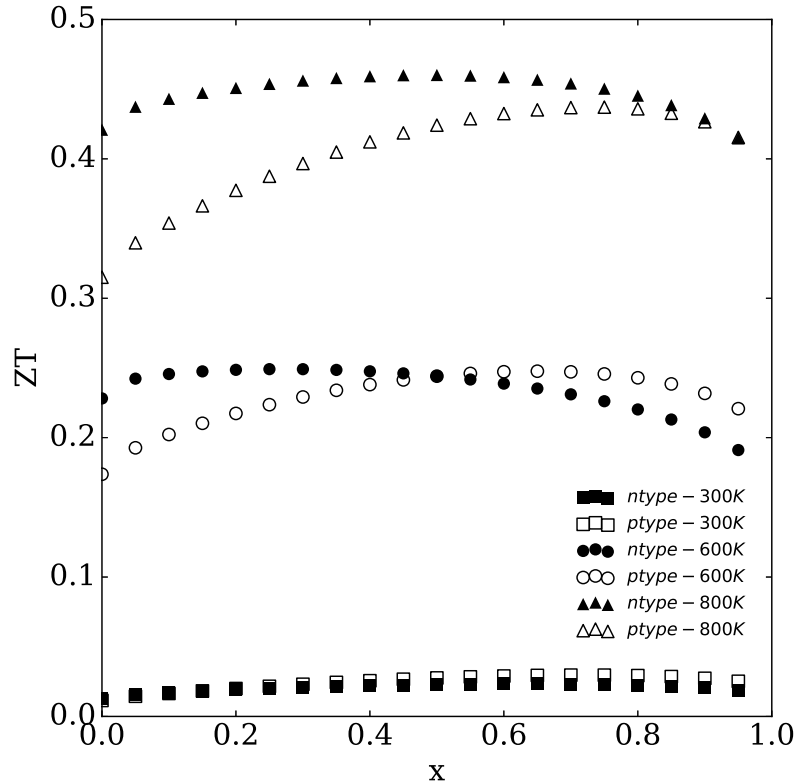
Figure 3.12: Variation of figure of merit ZT with fractional concentration of alloying x in $CoAs_xSb_{(1-x)}S$ at different temperatures such as 300 K, 600 K and 800 K. The filled scatter are for n-type and empty scatter are for p-type at different temperature.

0.41. As alloying is increased, the ZT values start becoming superior than the pure CoAsS and both n-type and p-type CoAsS show raised ZT values. With increasing the alloying concentration, the n-type starts dominating in the temperature regime 300 K-800 K and reaches much higher values of ZT 0.45 for n-type at temperature 800 K.

The behavior of ZT is different for the two charge carriers. As it can be seen in the Fig.3.12, the ZT values show up the maximum for n-type and p-type at different fractional values of alloying. When $x = 0$, the n-type dominates as it is purely CoSbS and as x increases, the p-type starts dominating. We have found maximum ZT for n-type in $CoAs_{0.2}Sb_{0.8}S$ alloy and for p-type, the maximum ZT is obtained for $CoAs_{0.8}Sb_{0.2}S$ alloy at temperature of 800 K. At 300 K, ZT values for n-type and p-type in these alloys are 0.019 and 0.029, and these values approach 0.45 and 0.41 respectively at 800 K.

Almost similar ZT for both n-type and p-type can be achieved by varying As percentage in $CoAs_xSb_{(1-x)}S$ alloy. For a TE device, same ZT values are important for both n-type and p-type, and alloying can play a crucial role to achieve this. Although many other properties, such as thermal expansion coefficient, thermal and mechanical stability and doping by n-type and p-type element control the possibility of designing a TE device, the almost similar ZT values for both p-type and n-type in the temperature range of 300 K-800 K for $CoAs_xSb_{(1-x)}S$ alloy can lead to a TE device based on abundant and cheap

59

metal chalcogenide.

3.7 Conclusions

The ordered cobaltite CoAsS is concluded to show good thermoelectric behavior in both
n-type and p-type based on the different conditions of doping and alloying. The power
factor value for the p-type CoAsS is much superior to n-type. The thermal conductivity
values are higher ~ 13 Wm^{-1}K^{-1}, so on reducing this value by alloying, the figure of
merit ZT values rise for both n-type and p-type. The substantial superiority of charge
carriers depend upon the alloy concentration and temperature leading to maximum value
of n-type $ZT \sim 0.45$ and that of p-type ~ 0.41. Thus, alloyed cobaltite and paracostibite
is shown to have enhanced thermoelectric properties which can be utilized as both n-type
and p-type in different temperature ranges and concentration. This work provides insight
into rational design of alloy for TE device, and the high ZT values of CoAs$_x$Sb$_{1-x}$S alloy
is good enough to encourage further investigation of this alloy.

Chapter 4

Thermoelectric figure of merit and thermal conductivity of type-I clathrate alloy nanowires

4.1 Introduction

Understanding of thermal transport properties in complex nanomaterials can lead to the design of many modern devices such as thermoelectric [10, 143], optoelectronic [144, 145], photovoltaics [145, 146] and storage devices [147]. The ability to optimize the thermoelectric performance of materials by minimizing its lattice thermal conductivity opens for the fabrication of a much larger category of efficient thermoelectric materials. There is a close relation between the complexity of the crystal structure and the thermal conductivity. Thermal conductivity is directly related to the phonon velocities in the system, which in turn can be strongly anisotropic depending on the crystal structure [112]. The anharmonic scattering rates also depend intricately on the crystal structure and constituent atoms [65]. Besides the intrinsic properties, alloying, substitution and nano-structuring have been found to be very effective in controlling the thermal conductivity of large range of materials. For thermoelectric applications, a semi-conducting material with low (lattice) thermal conductivity and high electrical conductivity is a long-standing quest. Clathrates are one type of compounds which show such behavior and have been reported as potential efficient thermoelectric materials due to their very low thermal conductivity [22, 148, 149, 150].

4.2 Crystal structure of clathrate

Clathrates are made up of a guest-host assembly with a complex crystal structure, Fig.4.1, and the anharmonicity of the atoms depends on the chemical bonding between the different atoms. The vibrations of the guest atoms depend on their position in the clathrate cage [151] as off-center and on-center vibrations of the guest atoms will be very different.
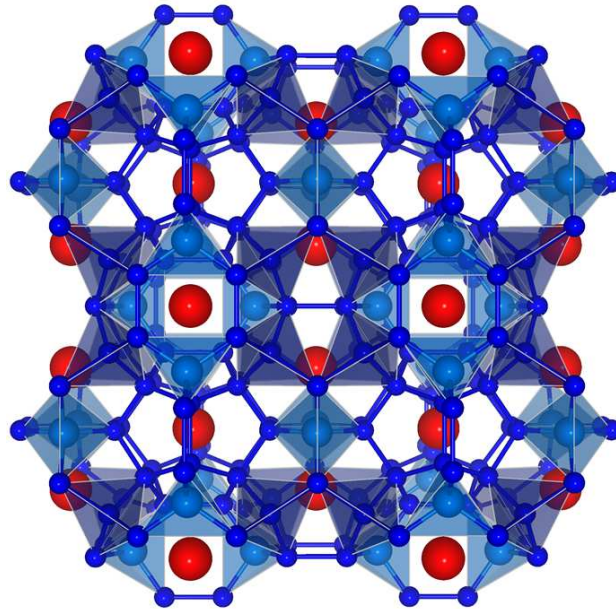
Figure 4.1: $Ba_8Cu_6Si_{40}$ clathrate where red atoms are Ba, dark blue atoms are Si and light blue atoms are Cu.

Type-I and II clathrate structures with the general formulas A_8E_{46} and A_xE_{136} ($0 < x < 24$) (where "A belongs to alkali or alkaline earth metals and "E belongs to group 14 of the periodic table), both have tetrahedral bonded networks as host structures. Type-II clathrates have partially filled cages in contrast to the completely filled type-I clathrates. Type-I and II clathrates exhibit a comparable lattice thermal conductivity. However, most of the type-II fully filled clathrate structures are metallic and have a low Seebeck coefficient. On the other hand, type-I clathrate compounds are generally narrow band gap semiconductors. Due to this, they have desirable electronic properties to fall in the category of potential thermoelectric materials [152, 153, 154].

Clathrates have a complex structure where a cage-like structure hosts looser bound atoms which are usually heavier in mass and have very low energy optical modes, also known as rattler modes. These low energy localized modes can give rise to acoustic phonon scattering, thus reducing the thermal conductivity. In Ref.[124], it has been observed that the complex crystal structure and rattler atom both contribute to reducing the lattice thermal conductivity by increasing anharmonicity by a factor of six and reducing sound speed by a factor of two as compared to diamond-Si structure. Recently, it has been reported that the guest atom significantly increases the anharmonic scattering and very high scattering rate in the type-I Ba_8Si_{46} structure compared to Si_{46} [155]. The inclusion of Ba and Cu also modifies the electronic transport, as the Ba guest atoms provide valence electrons and fill the bands of the covalent network, whereas the inclusion of Cu atoms also helps in tuning the cage electronic structure [152].

We have studied the thermal properties of clathrate alloys with special focus on type-I Silicon containing clathrates which are potentially useful for application in Silicon-based

62

technology. Furthermore, the effect of nano-structuring on this complex structure has been investigated for further optimization of thermoelectric efficiency. The lattice thermal conductivity is calculated based on a model approach to the relaxation time approximation (RTA) for phonon transport. We have included anharmonic scattering, alloy scattering and boundary scattering for the relaxation time calculation as discussed in previous chapters.

4.3 Electronic transport properties

Clathrates of type-I have cubic structure with space group $Pm\bar{3}n$. The relaxed structure of cubic clathrates $Ba_8Cu_6Si_{40}$ and $Ba_8Cu_6Ge_{40}$ are obtained using VASP [119] with PBE correlation functional [118]. Energy cut off was set to 300.0 eV and k-mesh was converged with k-points $4\times4\times4$. The lattice constant of the cubic clathrates comes out to be 10.38 $\dot{A}$.

The electronic transport coefficients were calculated using the Boltzmann transport equation coded in BoltzTraP software [120]. The data was fitted with the concentration of experimental alloy [156]. The concentration of $Ba_8Cu_6Si_{40}$ and $Ba_8Cu_6Ge_{40}$ was chosen to fit the data was 1.12×10^{21} cm^{-3} and 1.57×10^{21} cm^{-3} respectively. The relaxation time fitted with the experimental data [156] was 1.8×10^{-15} s.

Figure 4.2: (a) Seebeck coefficient and (b) Electrical conductivity for $Ba_8Cu_6Si_{40}$, $Ba_8Cu_6Ge_{40}$ and $Ba_8Cu_6Si_{17}Ge_{23}$.

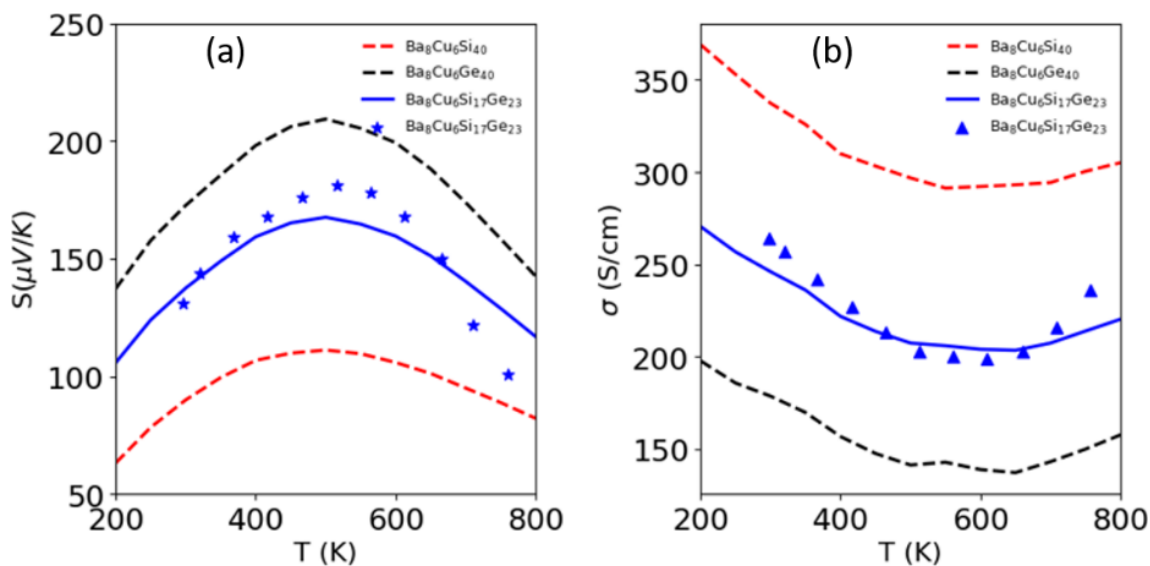The calculation of Seebeck coefficient and electrical conductivity for $Ba_8Cu_6Si_{40}$, $Ba_8Cu_6Ge_{40}$ and $Ba_8Cu_6Si_{17}Ge_{23}$ is shown in Fig.4.2. The data is sufficiently matching with the experimental data for alloy. The calculation of Seebeck coefficient and electrical conductivity for alloy is done using virtual crystal approximation as discussed in last chapter.

4.4   Lattice transport properties

4.4.1   Method

The phonon dispersion of the type-I clathrates $Ba_8Cu_6Si_{40}$, $Ba_8Cu_6Ge_{40}$ and diamond-Si structures have been calculated using the frozen phonon approach as implemented in PHONOPY [125]. The forces are calculated on the atoms using 54-atoms unit cells using VASP [119]. The forces on all atoms are calculated using the PBE-GGA functional and a 300 eV cut-off energy. The forces on all the atoms in both $Ba_8Cu_6Si_{40}$ and $Ba_8Cu_6Ge_{40}$ clathrates are calculated with symmetry reduced atomic displacement of 0.03 $\dot{A}$ and the volume derivatives for the Grüneisen parameter are calculated using a volume range of $\pm 1\%$. A k-grid of size ($4 \times 4 \times 4$) is used for calculating the forces. The dynamical matrix calculations are carried out on denser k-point mesh ($20 \times 20 \times 20$). Similarly, for the diamond-Si structure, the Gruneisen parameter and thermal properties are calculated and compared with the clathrate structure.
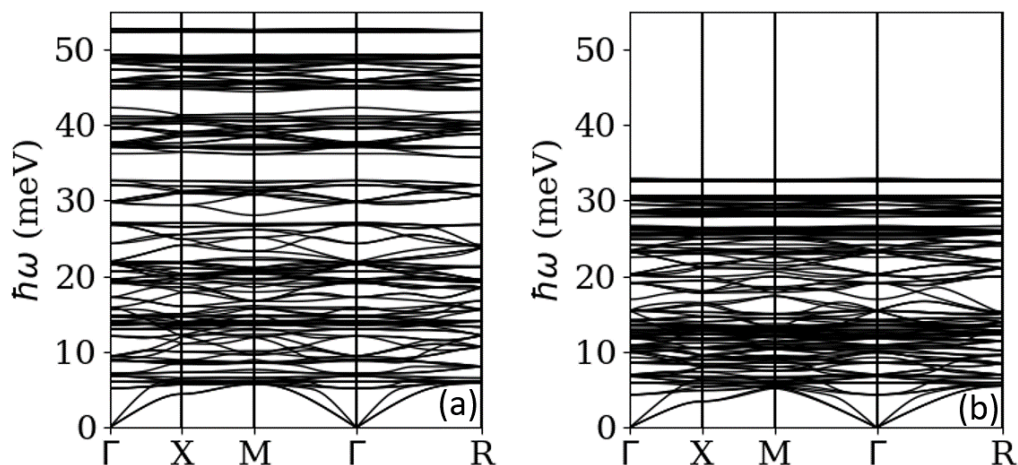
Figure 4.3: Phonon band structure along high symmetry direction for (a) $Ba_8Cu_6Si_{40}$ and (b) $Ba_8Cu_6Ge_{40}$.

Lattice thermal conductivity of a material is related to how the energy is being transferred across the whole lattice by each phonon mode. The phonon band structures of $Ba_8Cu_6Si_{40}$ and $Ba_8Cu_6Ge_{40}$ are shown in Fig.4.3. The acoustic modes of both $Ba_8Cu_6Si_{40}$ and $Ba_8Cu_6Ge_{40}$ clathrates have similar slopes. However, the $Ba_8Cu_6Ge_{40}$ has much lower energy optical phonon modes and the bands are flatter compared to $Ba_8Cu_6Si_{40}$.

4.4.2   Atom-wise calculation of anharmonicity

From the calculation of atomistic contribution of the Gruneisen coefficient of diamond-Si (Fig.4.4(a)), $Ba_8Cu_6Si_{40}$ clathrate (Fig.4.4 (b)), and $Ba_8Cu_6Ge_{40}$ clathrate (Fig.4.4 (c)) by its constituent atoms, it is found that in $Ba_8Cu_6Si_{40}$ and $Ba_8Cu_6Ge_{40}$, the Ba atoms have
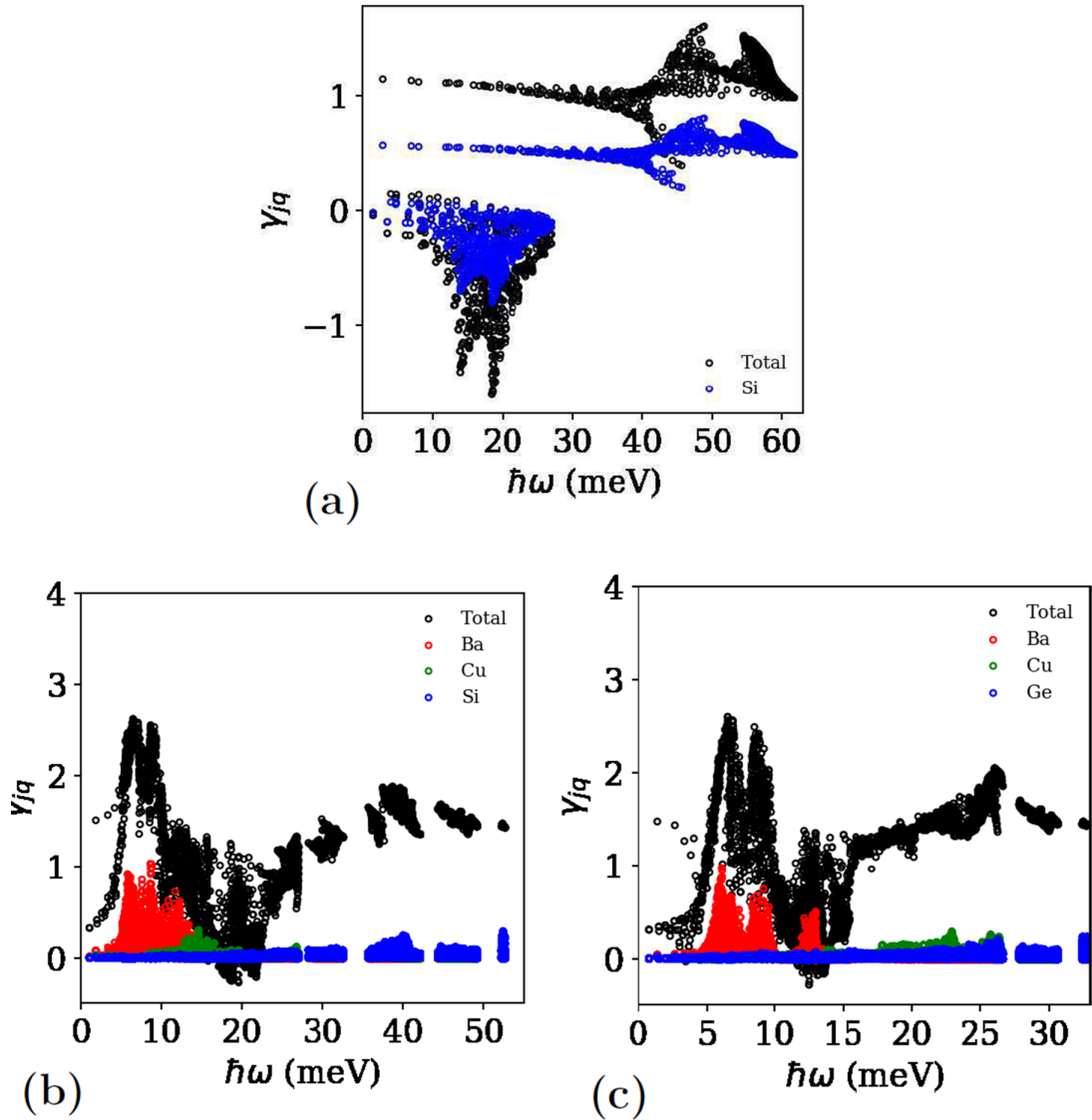
Figure 4.4: Atomistic contribution of Gruneisen parameter in (a) Diamond-Si, (b) $Ba_8Cu_6Si_{40}$ and (c) $Ba_8Cu_6Ge_{40}$.

the largest contribution to Grüneisen parameter in lower energy phonon modes. The Ba atoms contribution are ~ 10 times higher as compared to Si atoms and ~ 3 times higher as compared to the Cu atoms in both the clathrate structures. Contributions from the framework atoms to the Grüneisen coefficient in both $Ba_8Cu_6Si_{40}$ and $Ba_8Cu_6Ge_{40}$ are very similar (see Fig.4.4). The thermal conductivity due to phonons is calculated from the RTA as discussed in chapter 2. Overall scattering includes anharmonic, alloy and boundary scattering mechanisms. The calculated value of Debye temperature for $Ba_8Cu_6Si_{40}$ is 128 K and for $Ba_8Cu_6Ge_{40}$ is 83 K respectively. The mode squared Grüneisen parameter for the $Ba_8Cu_6Si_{40}$ and $Ba_8Cu_6Ge_{40}$ are 1.92 and 1.89 respectively. The transport mode distri-
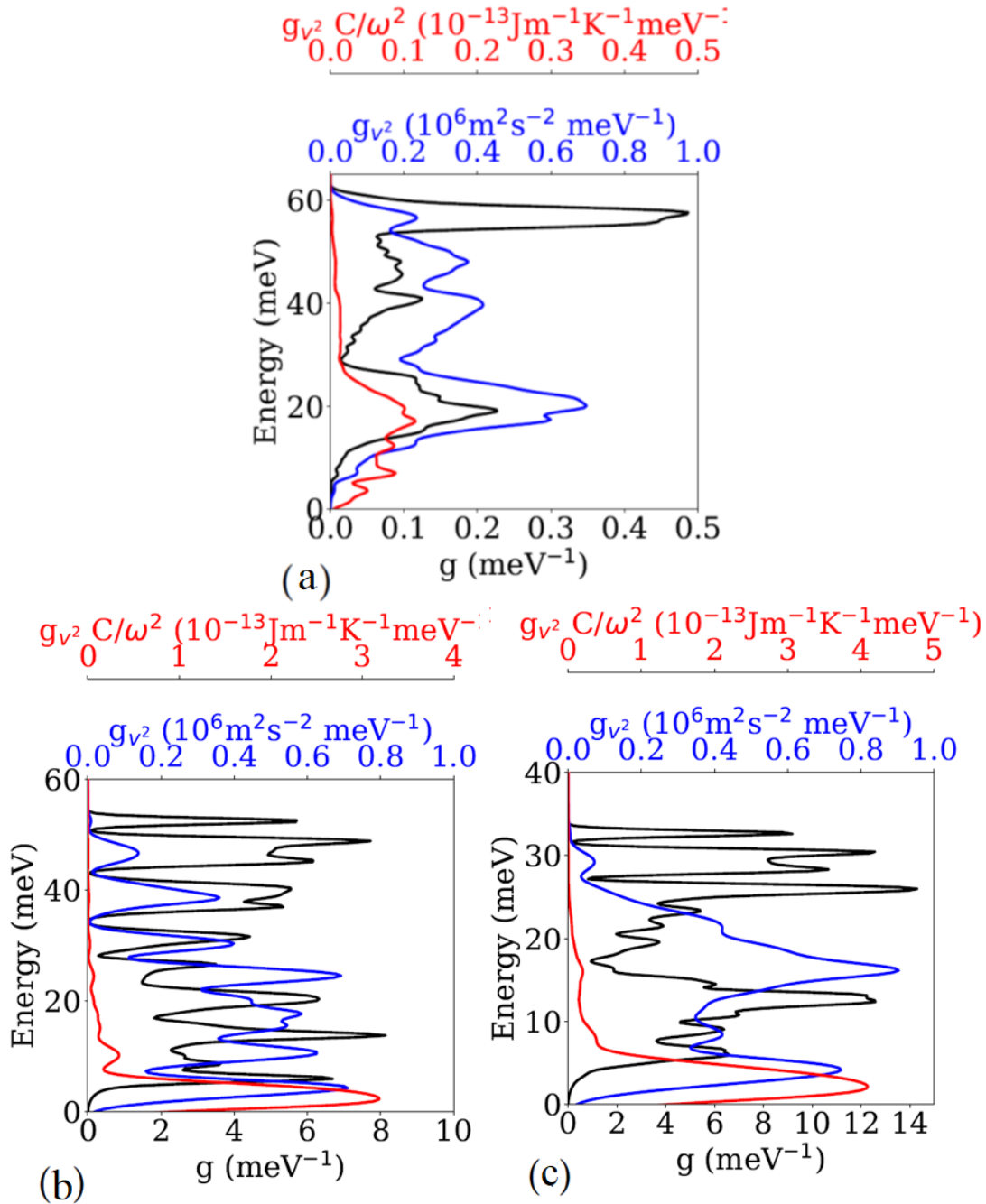
Figure 4.5: Phonon DOS (black line), velocity density distribution (blue line) and transport distribution (red line) in (a) diamond-Si, (b) $Ba_8Cu_6Si_{40}$ and (c) $Ba_8Cu_6Ge_{40}$.

bution, $(g_{v^2}C/\omega^2)$, and velocity distribution in $Ba_8Cu_6Si_{40}$, $Ba_8Cu_6Ge_{40}$ and diamond-Si, Fig4.5 (a, b, c), are calculated following Ref. [65]. Due to the strong anharmonicity at low energy due to the guest Ba atom, $Ba_8Cu_6Si_{40}$ has a sharp decrease in transport mode distribution. In diamond-Si, a broad energy mode contributes in thermal transport, these

modes sharply decrease in the clathrates due to anharmonicity of Ba atoms.

4.4.3 Effect of alloying on total thermal conductivity

Alloy scattering is incorporated in phonon transport by atomistic mass difference in the alloy as given in chapter 3. The scattering rate due to alloy scattering is calculated as given in Ref.[157, 158]. The calculated speed of sound is 2872 ms^{-1} for the Ba$_8$Cu$_6$Si$_{17}$Ge$_{23}$ clathrate alloy, whereas the speed of sound in the pure compounds Ba$_8$Cu$_6$Si$_{40}$ and Ba$_8$Cu$_6$Ge$_{40}$ is calculated as 3297 ms^{-1} and 2559 ms^{-1} respectively.

The total thermal conductivity (κ_T) due to phonons and electrons is plotted for Ba$_8$Cu$_6$Si$_{40}$, Ba$_8$Cu$_6$Ge$_{40}$ and Ba$_8$Cu$_6$Si$_{17}$Ge$_{23}$ in the Fig.4.6 with the experimental data from Ref.[156, 159]. The experimental data includes both lattice and electronic transport. The electrical conductivity is fitted with the experimental data and the fitted value of electronic relaxation time is $\sim 1.8 \times 10^{-15}$s. The electronic thermal conductivity of Ba$_8$Cu$_6$Si$_{17}$Ge$_{23}$ clathrate alloy is calculated as,

$$\kappa_{el} = x(\kappa_{elA}) + (1 - x)(\kappa_{elB}) \tag{4.1}$$

where κ_{elA} and κ_{elB} are the electronic thermal conductivities of two compounds A, B. The total thermal conductivity for pure and alloy compounds is calculated as $\kappa_T = \kappa_{ph} + \kappa_{el}$, where κ_{ph} and κ_{el} are phonon and electronic thermal conductivities respectively of pure compounds Ba$_8$Cu$_6$Si$_{40}$, Ba$_8$Cu$_6$Ge$_{40}$ and Ba$_8$Cu$_6$Si$_{17}$Ge$_{23}$ clathrate alloy. The plotted data is sufficiently capturing the transport of heat in the pure clathrate Ba$_8$Cu$_6$Si$_{40}$ and Ba$_8$Cu$_6$Si$_{17}$Ge$_{23}$ clathrate alloy.

The total thermal conductivity of the Ba$_8$Cu$_6$Si$_{40(1-x)}$Ge$_{40x}$ clathrate is calculated by tuning alloying and nano-structuring. The total thermal conductivity of Ba$_8$Cu$_6$Si$_{40(1-x)}$Ge$_{40x}$ is plotted for varying alloy concentration at temperature of 400 K in Fig.4.6 and it is observed that the value of the pure Si-clathrate Ba$_8$Cu$_6$Si$_{40}$ is reduced by 40% when the alloying concentration is $\sim 50\%$. This reduction is mainly due to a 50% reduction of the phonon lattice thermal conductivity from 1.64 Wm^{-1}K^{-1} to 0.80 Wm^{-1}K^{-1}. The theoretical values for the total lattice thermal conductivity is in good agreement with the experimental values for pure Si-clathrate Ba$_8$Cu$_6$Si$_{40}$ and Ba$_8$Cu$_6$Si$_{17}$Ge$_{23}$ clathrate alloy [156, 159].

4.4.4 Effect of nanostructuring on total thermal conductivity

The clathrate lattice thermal conductivity can be further reduced by around $\sim 90\%$ by nano-structuring compared to the pure Ba$_8$Cu$_6$Si$_{40}$ clathrate (Fig.4.7 (a)). Boundary scattering is incorporated using a diffusive model as discussed in chapter 2. Such a model has been shown to predict the thermal conductivity of Si nanowires [160] and Si$_{1-x}$Ge$_x$ alloy nanostructure [126, 161] accurately for nanostructure with sizes larger than 20 nm [162]. The phonon lattice thermal conductivity (κ_{ph}) of Ba$_8$Cu$_6$Si$_{17}$Ge$_{23}$ clathrate alloy nanowire with a diameter of 30 nm is found to be 0.15 Wm^{-1}K^{-1}. The total thermal conductivity, κ_T for the Ba$_8$Cu$_6$Si$_{17}$Ge$_{23}$ clathrate alloy nanowire is ~ 0.50 Wm^{-1}K^{-1}. In Fig.4.7 (b), as we decrease the nanostructure of the alloy, more phonons get scattered.
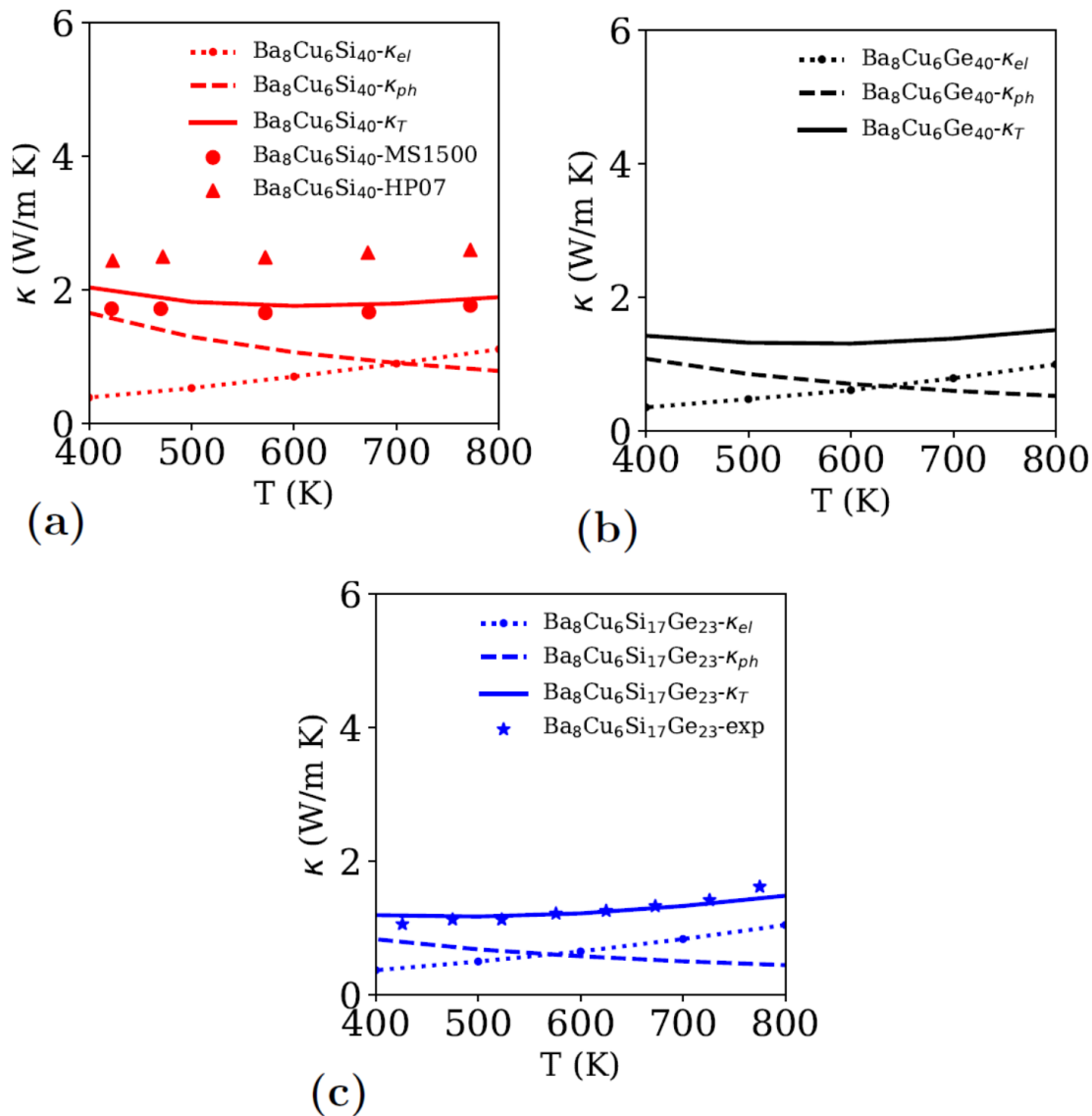
Figure 4.6: Thermal conductivity of (a) $Ba_8Cu_6Si_{40}$, (b) $Ba_8Cu_6Ge_{40}$ and (c) $Ba_8Cu_6Si_{17}Ge_{23}$ alloy due to phonons (dashed line) and electrons (dotted line) with temperature along with experimental data from Ref.[156] and [159]. Solid lines are for total thermal transport due to both phonons and electrons transport.

The cumulative thermal conductivity is plotted for the mean free path (MFP) range in different compounds Fig.4.7(b). It has been seen that as the wavelength of the heat carrying phonons decreases, the cumulative contribution sharply decreases for both pure diamond-Si and type-I $Ba_8Cu_6Si_{40}$. The behavior of $Ba_8Cu_6Si_{17}Ge_{23}$ clathrate alloy and $Si_{0.5}Ge_{0.5}$ alloy is similar. Alloy scattering due to atomistic mass difference strongly reduces the heat transport by short wavelength phonon. Therefore, thermal conductivity in both the simple $Si_{1-x}Ge_x$ alloy and $Ba_8Cu_6Si_{40(1-x)}Ge_{40x}$ clathrate alloy is reduced as compared to the

pure materials. A large reduction in thermal conductivity is also possible in the complex structure like clathrates by increasing the atomistic mass difference. The thermal conductivity profile of diamond-Si and Si-clathrate $Ba_8Cu_6Si_{40}$ is quite similar at large phonon wavelength but as the wavelength of phonon decreases, the effect of the clathrate structure starts impinging. As the phonon wavelength for Si-clathrate $Ba_8Cu_6Si_{40}$ decreases, the heat conduction also reduces which is indicative of the complex structure. Nano-structuring has different effect for pure diamond-Si and $Ba_8Cu_6Si_{40}$ clathrate. We can see here that the alloying decreases the phonon lattice thermal conductivity by 50% and nano-structuring reduces the same by $\sim$90% with ultra-low values near 0.15 $Wm^{-1}K^{-1}$ (Fig.4.7(a)). The scattering rates of the nanostructure are determined by its dimensions. For clathrates, more than 90% of heat is carried by the phonons having wavelength more than 10 nm (See Fig.4.7(b)). Nano-structuring can block these heat carrying phonons very effectively. Hence, we observed a large reduction in thermal conductivity in nanostructure clathrates alloy and found an ultra-low thermal conductivity in semiconducting materials.
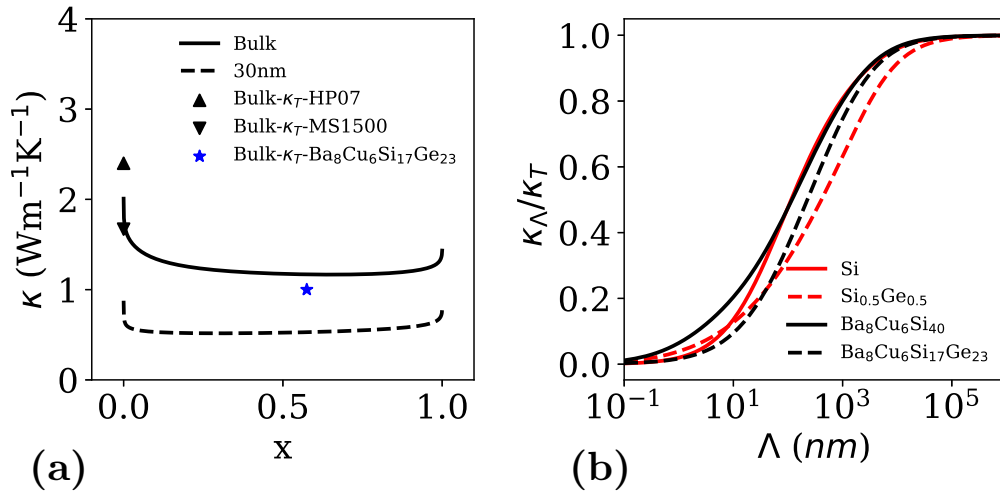
Figure 4.7: (a) Total thermal conductivity of $Ba_8Cu_6Si_{(1-x)40}Ge_{40x}$ clathrate alloy (bulk) and clathrate alloy nanowire at 400 K along with the experimental data (Ref.[156, 159]) and (b) cumulative contribution of phonon lattice thermal conductivity by phonon mean free path.

4.5 Thermoelectric figure of merit

Experimentally, the thermoelectric figure of merit, ZT, of type-I $Ba_8Cu_6Si_{40}$ clathrate is reported to be 0.07 with a total thermal conductivity of 2.40 $Wm^{-1}K^{-1}$ at 400 K [159]. The reported ZT of Si clathrate is low compared to other Si based materials. The figure of merit for the alloy is calculated according to the formula,

$$ZT = (x(S_A^2\sigma_A T) + (1-x)(S_B^2\sigma_B T))/\kappa_{alloy} \tag{4.2}$$

where x is the fractional concentration of the pure compound A and rest is of the other pure
compound B. In the numerator, the $S_A^2\sigma_A$ and $S_B^2\sigma_B$ are power factors for compounds A
and B respectively. The denominator κ_{alloy} is total thermal conductivity of clathrate alloy
comprising of phonon and electron part as $\kappa_{alloy} = \kappa_{ph} + \kappa_{el}$. The value of figure of merit
for bulk and nanometer size is shown in the Fig.4.8. The value of figure of merit for bulk
clathrate alloy is around 0.17 at temperature $\sim$ 400 K with total thermal conductivity of
1.18 Wm^{-1}K^{-1}. The ZT values can be further optimized to $\sim$ 0.39 for Ba$_8$Cu$_6$Si$_{17}$Ge$_{23}$
clathrate alloy nanowire (diameter 30 nm) with the calculated total thermal conductivity
0.50 Wm^{-1}K^{-1} and considering electronic properties (electrical conductivity (σ) (0.022$\times$
10^6 Sm^{-1}), Seebeck coefficient (S) (159 μVK^{-1})). For the electronic properties, there are
minimal effects of alloying [163] and nano-structuring and the predicted ZT for clathrate
alloy nanowire is encouraging for further experimental investigation of this system.
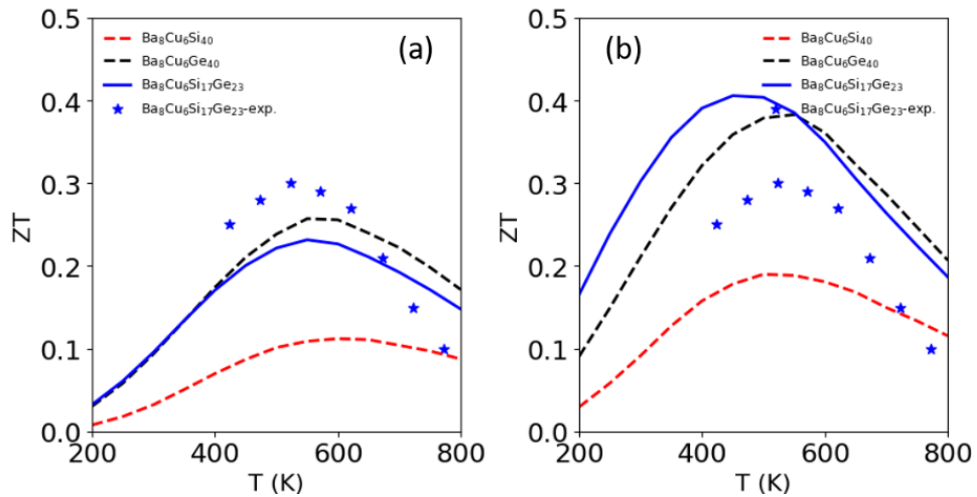
Figure 4.8: (a) Figure of merit (ZT) with temperature for Ba$_8$Cu$_6$Si$_{40}$, Ba$_8$Cu$_6$Ge$_{40}$ and
Ba$_8$Cu$_6$Si$_{17}$Ge$_{23}$ for (a) Bulk and (b) 30 nm.

4.6 Conclusions

In conclusion, we have found a significant reduction in the lattice thermal conductiv-
ity of type-I Si-clathrate Ba$_8$Cu$_6$Si$_{40}$ by introducing alloy and boundary scattering. Alloy
scattering has been shown to reduce the lattice thermal conductivity of pure Si-clathrate
Ba$_8$Cu$_6$Si$_{40}$ from 1.64 Wm^{-1}K^{-1} to 0.80 W/m-K in Ba$_8$Cu$_6$Si$_{17}$Ge$_{23}$ clathrate alloy at 400
K. Furthermore, the effect of boundary scattering is calculated and there has been seen
a reduction of the clathrate lattice thermal conductivity to 0.15 W/m-K in case of 30 nm
sized Ba$_8$Cu$_6$Si$_{17}$Ge$_{23}$ clathrate alloy nanowire. Such reduced values of the nanostructured
clathrate alloy can direct to make good performing Si based thermoelectrics. Si$_{1-x}$Ge$_x$ al-
loy has very low $ZT \sim 0.1$ at room temperature. A nanowire of Ba$_8$Cu$_6$Si$_{17}$Ge$_{23}$ clathrate

alloy with $ZT \sim 0.40$ around room temperature can be useful for micro refrigeration in Si-chips. It can also be very useful for heat barrier application in nanoelectronics.

Chapter 5

Summary and future perspectives

Looking towards the conclusive remarks, we have assessed the effect of two techniques alloying and nanostructuring on the performance of various thermoelectric systems. A worth appraised values of figures of merit of transition metal compounds have been seen in this thesis. As thermoelectric systems urge the unison of contradictory properties, there is a vast field of research for finding materials with such properties. Apart from finding new materials, there is a grand room for screwing the existing materials for better performance.

In the first instance, as there are binary chalcogenides which have shown good thermoelectric properties, we have selected the ternary materials in metal chalcogenides. We have chosen the orthorhombic material Palladium Phosphide Sulphide, which is quite stable up to high temperature. Apart from chemical and physical stability, PdPS exists in double layer structure, which makes it interesting for many lower dimension applications. Anisotropic thermoelectric figure of merit calculated for PdPS is very significant in the nano regime and due to its layered structure, it will be having many applications in the field of biology, space, computers etc. The calculated values will get even enhanced on steering the lattice thermal conductivity values. Alloying can also play a specific role in reducing the thermal values.

On the similar line of ternary material, we selected the chalcogenides of Co family viz., cobaltite (CoAsS) and paracostibite (CoSbS). The thermal conductivity of both the materials is not extremely low, howsoever it is reduced to quite lower values by alloying. This results in superior ZT values for both the n-type and p-type compounds. Therefore, another very important application of this research is in the thermoelectric modules in which there will be a provision to use both legs of the module from a single material CoAsS as it is having high ZT values for both n-type and p-type.

As enhanced thermoelectric performance is easily achievable by reducing lattice thermal conductivity, we chose to select materials with already known low thermal conductivity. We steered the values of final ZT by reducing the lattice thermal conductivity by alloying and nanostructuring in clathrate structure $Ba_8Cu_6Si_{40}$ and $Ba_8Cu_6Ge_{40}$. These alloy nanowires can be a potential alternative to Si-nanowires.This research will definitely lead to greatly improved efficiencies if it lives up to its theoretical promise.

The future prospects for extension of the present work in this thesis can be stated

below: Alloying can be an efficient tool for enhancing the thermoelectric properties of materials having low values of thermal conductivity and large room for substitution of different atoms. There are many bulk complex crystal structures which can be alloyed to have even reduced values of thermal conductivity. Another direction can be the study of possible doping for present materials to achieve the required level of carrier concentration. Among 370 combinations of ternary chalcogenide material from groups VIII, VA, VIA, only 23 have been reported, further study can be done among these numerous combination for finding thermoelectric properties.

Reference

[1] G. Chen. Nanoscale energy transport and conversion: A parallel treatment of electrons, molecules, phonons, and photons. *Oxford University Press, New York*, 2005.

[2] H. J. Goldsmid. Electronic refrigeration. *Pion, London*, page 7, 1986.

[3] A. F. Ioffe. Semiconductor thermoelements and thermoelectric cooling. *Infosearch, London*, page 36, 1957.

[4] T. Zhiting, L. Sangyeop, and C. Gang. Comprehensive review of heat transfer in thermoelectric materials and devices. pages 425–484, 2014.

[5] W. Liu, J. Hu, S. Zhang, M. Deng, C.-G. Han, and Y. Liu. New trends, strategies and opportunities in thermoelectric materials: A perspective. *Materials Today Physics*, 1:50 – 60, 2017.

[6] M. C. Steele and F. D. Rosi. Thermal conductivity and thermoelectric power of germanium-silicon alloys. *Journal of Applied Physics*, 29:1517–1520, 1958.

[7] H. J. Goldsmid and R. W. Douglas. The use of semiconductors in thermoelectric refrigeration. *British Journal of Applied Physics*, 5:386–390, 1954.

[8] A. F. Ioffe, S. V. Airepetyants, A. V. Ioffe, N. V. Kolomoets, and L. S. Stil'bans. *Dokl. Akad. Nauk. SSSR*, 106:981, 1956.

[9] C. Wood. Materials for thermoelectric energy conversion. *Reports on Progress in Physics*, 51:459539, 1988.

[10] G. J. Snyder and E. S. Toberer. *Complex Thermoelectric Materials*, pages 101–110. 2008.

[11] K. Biswas, J. He, I. D. Blum, C.-I. Wu, T. P. Hogan, D. N. Seidman, V. P. Dravid, and M. G. Kanatzidis. High-performance bulk thermoelectrics with all-scale hierarchical architectures. *Nature*, 489:414–418, 2012.

[12] J. R. Sootsman, D. Y. Chung, and M. G. Kanatzidis. New and old concepts in thermoelectric materials. *Angewandte Chemie International Edition*, 48:8616–8639, 2009.

[13] C. B. Vining, W. Laskow, J. O. Hanson, R. R. Vanderbeck, and P. D. Gorsuch. Thermoelectric properties of pressure-sintered Si0.8Ge0.2 thermoelectric alloys. *Journal of Applied Physics*, 69:4333–4340, 1991.

[14] X. W. Wang, H. Lee, Y. C. Lan, G. H. Zhu, G. Joshi, D. Z. Wang, J. Yang, A. J. Muto, M. Y. Tang, J. Klatsky, S. Song, M. S. Dresselhaus, G. Chen, and Z. F. Ren. Enhanced thermoelectric figure of merit in nanostructured n-type silicon germanium bulk alloy. *Applied Physics Letters*, 93:193121, 2008.

[15] G. Joshi, H. Lee, Y. C. Lan, X. W. Wang, G. H. Zhu, D. Z. Wang, R.W. Gould, D. C. Cuff, M. Y. Tang, M. S. Dresselhaus, G. Chen, and Z. F. Ren. Enhanced thermoelectric figure of merit in nanostructured p-type silicon germanium bulk alloys. *Nano Letters*, 8:4670–4674, 2008.

[16] G. A. Slack. *CRC Handbook of thermoelectrics, ed. by M.Rowe*, page 407, 1995.

[17] M. Rull-Bravo, A. Moure, J. F. Fernndez, and M. Martn-Gonzlez. Skutterudites as thermoelectric materials: revisited. *RSC Advances*, 5:41653–41667, 2015.

[18] C. Uher. Chapter 5 skutterudites: Prospective novel thermoelectrics. In T. M. Tritt, editor, *Recent Trends in Thermoelectric Materials Research I*, volume 69 of *Semiconductors and Semimetals*, pages 139 – 253. Elsevier, 2001.

[19] G. S. Nolas, G. A. Slack, D. T. Morelli, T. M. Tritt, and A. C. Ehrlich. The effect of rare-earth filling on the lattice thermal conductivity of skutterudites. *Journal of Applied Physics*, 79:4002–4008, 1996.

[20] B. C. Sales, D. Mandrus, and R. K. Williams. Filled skutterudite antimonides: A new class of thermoelectric materials. *Science*, 272:1325–1328, 1996.

[21] D. T. Morelli, G. P. Meisner, B. X. Chen, S. Q. Hu, and C. Uher. Cerium filling and doping of cobalt triantimonide. *Physical Review B*, 56:7376–7383, 1997.

[22] A. Saramat, G. Svensson, A. E. C. Palmqvist, C. Stiewe, E. Mueller, D. Platzek, S. G. K. Williams, D. M. Rowe, J. D. Bryan, and G. D. Stucky. Large thermoelectric figure of merit at high temperature in Czochralski-grown clathrate Ba8Ga16Ge30. *Journal of Applied Physics*, 99:023708, 2006.

[23] S. K. Deng, X. F. Tang, P. Li, and Q. J. Zhang. High temperature thermoelectric transport properties of p-type Ba(8)Ga(16)Al(x)Ge(30-x) type-I clathrates with high performance. *Journal of Applied Physics*, 103:073503, 2008.

[24] T. Caillat, J. P. Fleurial, and A. Borshchevsky. Preparation and thermoelectric properties of semiconducting Zn4Sb3. *Journal of Physics and Chemistry of Solids*, 58: 1119–1125, 1997.

[25] S. R. Brown, S. M. Kauzlarich, F. Gascoin, and G. J. Snyder. Yb14MnSb11 new high efficiency thermoelectric material for power generation. *Chemistry of Materials*, 18:1873–1877, 2006.

[26] X. A. Yan, G. Joshi, W. S. Liu, Y. C. Lan, H. Wang, S. Lee, J. W. Simonson, S. J. Poon, T. M. Tritt, G. Chen, and Z. F. Ren. Enhanced thermoelectric figure of merit of p-type half-heuslers. *Nano Letters*, 11:556–560, 2011.

[27] I. Terasaki, Y. Sasago, and K. Uchinokura. Large thermoelectric power in NaCo2O4 single crystals. *Physical Review B*, 56:12685–12687, 1997.

[28] R. Funahashi, I. Matsubara, H. Ikuta, T. Takeuchi, U. Mizutani, and S. Sodeoka. An oxide single crystal with high thermoelectric performance in air. *Japanese Journal of Applied Physics Part 2-Letters*, 39:L1127–L1129, 2000.

[29] S. Ohta, T. Nomura, H. Ohta, and K. Koumoto. High-temperature carrier transport and thermoelectric properties of heavily La- or Nb-doped SrTiO3 single crystals. *Journal of Applied Physics*, 97:034106, 2005.

[30] D. Flahaut, T. Mihara, R. Funahashi, N. Nabeshima, K. Lee, H. Ohta, and K. Koumoto. Thermoelectrical properties of A-site substituted Ca1-xRexMnO3. *Journal of Applied Physics*, 100:084911, 2006.

[31] M. S. Dresselhaus, G. Chen, M. Y. Tang, R. G. Yang, H. Lee, D. Z. Wang, Z. F. Ren, J. P. Fleurial, and P. Gogna. New directions for low-dimensional thermoelectric materials. *Advanced Materials*, 19:1043–1053, 2007.

[32] L. D. Hicks and M. S. Dresselhaus. Effect of quantum-well structures on the thermoelectric figure of merit. *Physical Review B*, 47:12727–12731, 1993.

[33] L. D. Hicks and M. S. Dresselhaus. Thermoelectric figure of merit of a one-dimensional conductor. *Physical Review B*, 47:16631–16634, 1993.

[34] R. Venkatasubramanian, E. Siivola, T. Colpitts, and B. OQuinn. Thin-film thermoelectric devices with high room-temperature figures of merit. *Nature*, 413:597–602, 2001.

[35] M. N. Touzelbaev, P. Zhou, R. Venkatasubramanian, and K. E. Goodson. Thermal characterization of Bi2Te3/Sb2Te3 superlattices. *Journal of Applied Physics*, 90: 763767, 2001.

[36] J. C. Caylor, K. Coonley, J. Stuart, T. Colpitts, and R. Venkatasubramanian. Enhanced thermoelectric performance in PbTe-based superlattice structures from reduction of lattice thermal conductivity. *Applied Physics Letters*, 87:23105, 2005.

[37] H Beyer, J Nurnus, H Böttner, A Lambrecht, E Wagner, and G Bauer. High thermoelectric figure of merit ZT in PbTe and Bi2Te3-based superlattices by a reduction

of the thermal conductivity. *Physica E: Low-dimensional Systems and Nanostructures*, 13:965968, 2002.

[38] A. I. Boukai, Y. Bunimovich, J. Tahir-Kheli, J. K. Yu, W. A. Goddard, and J. R. Heath. Silicon nanowires as efficient thermoelectric materials. *Nature*, 451:168–171, 2008.

[39] C. Chiritescu, D. G. Cahill, N. Nguyen, D. Johnson, A. Bodapati, P. Keblinski, and P. Zschack. Ultralow thermal conductivity in disordered, layered WSe2 crystals. *Science*, 315:351353, 2007.

[40] D. M. Rowe, V. S. Shukla, and N. Savvides. honon-scattering at grain-boundaries in heavily doped fine-grained silicon-germanium alloys. *Nature*, 290:765766, 1981.

[41] J. M. Ziman. *Electrons and phonons: the theory of transport phenomena in solids*. Oxford university press, 2001.

[42] H. J. Goldsmid. *Introduction to thermoelectricity*, volume 121. Springer, 2010.

[43] J. M. Ziman. The general variational principle of transport theory. *Canadian Journal of Physics*, 34:1256–1273, 1956.

[44] J.-P. M Péraud, C. D. Landon, and N. G. Hadjiconstantinou. Monte carlo methods for solving the boltzmann transport equation. *Annual Review of Heat Transfer*, 17, 2014.

[45] C. Jacoboni, P. Poli, and L. Rota. A new monte carlo technique for the solution of the boltzmann transport equation. In J. Shah and G. J. Iafrate, editors, *Hot Carriers in Semiconductors*, pages 523 – 526. Pergamon, Amsterdam, 1988. ISBN 978-0-08-036237-3.

[46] A. Sommerfeld. *Z., Phys.*, 47:43, 1928.

[47] G. Kumar, G. S.and Prasad and R. O. Pohl. Experimental determinations of the lorenz number. *Journal of Materials Science*, 28:4261, 1993.

[48] G. D. Mahan and J. O. Sofo. The best thermoelectric. *Proc. Natl. Acad. Sci. U. S. A.*, 93:7436–7439, 1996.

[49] P. J. Price. Cxxxv. ambipolar thermodiffusion of electrons and holes in semiconductors. *The London, Edinburgh, and Dublin Philosophical Magazine and Journal of Science*, 46:1252, 1955.

[50] E Muller, W. Heiliger, P. Reinshaus, and H. Sussmann. Proceedings of the 15th international conference on thermoelectrics. *pasadena,IEEE*, page 412, 1996.

[51] H. J. Goldsmid and J. W. Sharp. Estimation of the thermal band gap of a semiconductor from seebeck measurements. *Journal of Electronic Materials*, 28:869, 1999.

[52] D. M. Bhandari, C. M. Rowe. CRC handbook of thermoelectrics (ed. Rowe, D. M.). (Ch. 5):43–53, 1995.

[53] K. Koumoto, I. Terasaki, and R. Funahashi. Complex oxide materials for potential thermoelectric applications. *Mrs Bulletin*, 31:206–210, 2006.

[54] G. J. Snyder, T. Caillat, and J. P. Fleurial. Thermoelectric transport and magnetic properties of the polaron semiconductor FexCr3-xSe4. *Physical Review B*, 62:10185, 2000.

[55] P. Debye. *vortrage uber die kinetische theorie*, 1914.

[56] R. E. Peierls. *Ann. Phys.*, 3:1055, 1929.

[57] J. Callaway. Model for lattice thermal conductivity at low temperatures. *Physical Review*, 113(4):1046, 1959.

[58] W. J. de Haas and T. Biermasz. The dependence of thickness of the thermal resistance of crystals at low temperatures. *Physica*, 5:619–624, 1938.

[59] H. B. G. Casimir. *Physica*, 5:495, 1938.

[60] A. V. Ioffe and A. F. Ioffe. *Dokl. Akad. Nauk SSSR*, 97:821, 1954.

[61] G. Leibfried and E. Schlomann. *Nachr. Akad. Wiss. Gottingen*, 2:71, 1954.

[62] G. A. Slack. The thermal conductivity of nonmetallic crystals. *Solid State Physics*, 34:1–71, 1979.

[63] D. T. Morelli, J. P. Heremans, and G. A. Slack. Estimation of the isotope effect on the lattice thermal conductivity of group IV and group III-V semiconductors. *Physical Review B*, 66:195304, 2002.

[64] C. L. Julian. Theory of heat conduction in rare-gas crystals. *Physical Review*, 137: A128–A137, Jan 1965.

[65] L. Bjerg, B. B. Iversen, and G. K. H. Madsen. Modeling the thermal conductivities of the zinc antimonides ZnSb and Zn4Sb3. *Physical Review B*, 89:024304, 2014.

[66] C. M. Bhandari. CRC handbook of thermoelectrics (ed. Rowe, D. M.). *CRC, Boca Raton, 1995*, pages 55–65, 1995.

[67] M. S. Dresselhaus. New directions for low-dimensional thermoelectric materials. *Advanced Materials*, 19:1043–1053, 2007.

[68] D. A. Wright. Thermoelectric properties of bismuth telluride and its alloys. *Nature*, 181:834, 1958.

[69] D. Kusano and Y. Hori. Thermoelectric properties of p-type (Bi2Te3)(0.2) (Sb2Te3)(0.8) thermoelectric material doped with PbTe. *Journal of the Japan Institute of Metals*, 66:1063–1065, 2002.

[70] P. Zhu, Y. Imai, Y. Isoda, Y. Shinohara, X. Jia, and G. Zou. Enhanced thermoelectric properties of PbTe alloyed with Sb2Te3. *Journal of Physics: Condensed Matter*, 17(46):7319, 2005.

[71] P. FP Poudeu, J. D'Angelo, H. Kong, A. Downey, J. L. Short, R. Pcionek, T. P. Hogan, C. Uher, and M. G. Kanatzidis. Nanostructures versus solid solutions: Low lattice thermal conductivity and enhanced thermoelectric figure of merit in Pb9.6Sb0.2Te10-xSex bulk materials. *Journal of the American Chemical Society*, 128(44):14347–14355, 2006.

[72] Pierre FP Poudeu, Jonathan D'Angelo, Adam D Downey, Jarrod L Short, Timothy P Hogan, and Mercouri G Kanatzidis. High thermoelectric figure of merit and nanostructuring in bulk p-type Na1- xPbmSbyTem+ 2. *Angewandte Chemie International Edition*, 45(23):3835–3839, 2006.

[73] P. G. Klemens. Effect of crystal lattice defects on thermal conductivity. *Physical Review*, 119:507, 1960.

[74] G. S. Nolas, J. Poon, and M. Kanatzidis. Recent developments in bulk thermoelectric materials. *MRS bulletin*, 31:199205, 2006.

[75] B. C. Sales. Electron crystals and phonon glasses: a new path to improved thermoelectric materials. *MRS bulletin*, 23:1521, 1998.

[76] M. M. Koza, M. R. Johnson, R. Viennois, H. Mutka, L. Girard, and D. Ravot. Breakdown of phonon glass paradigm in La-and Ce-filled Fe4Sb12 skutterudites. *Nature Materials*, 7(10):805, 2008.

[77] I. Savić, N. Mingo, and D. A. Stewart. Phonon transport in isotope-disordered carbon and boron-nitride nanotubes: Is localization observable? *Physical Review Letters*, 101:165502, Oct 2008.

[78] E. Abrahams, P. W. Anderson, D. C. Licciardello, and T. V. Ramakrishnan. Scaling theory of localization: Absence of quantum diffusion in two dimensions. *Physical Review Letters*, 42:673–676, Mar 1979.

[79] C. Monthus and T. Garel. Anderson localization of phonons in dimension $d = 1, 2, 3$: Finite-size properties of the inverse participation ratios of eigenstates. *Physical Review B*, 81:224208, Jun 2010.

[80] P. W. Anderson. Absence of diffusion in certain random lattices. *Physical Review*, 109:1492–1505, Mar 1958.

[81] A. Lagendijk, B. van Tiggelen, and D. S. Wiersma. Fifty years of anderson localization. *Physics Today*, 62(8):24–29, 2009.

[82] F. Evers and A. D. Mirlin. Anderson transitions. *Reviews of Modern Physics*, 80: 1355–1417, Oct 2008.

[83] R. T. Howie, I. B. Magdău, A. F. Goncharov, G. J. Ackland, and E. Gregoryanz. Phonon localization by mass disorder in dense hydrogen-deuterium binary alloy. *Physical Review Letters*, 113:175501, Oct 2014.

[84] B. C. Sales, B. C. Chakoumakos, D. Mandrus, and J. W. Sharp. Atomic displacement parameters and the lattice thermal conductivity of clathrate-like thermoelectric compounds. *Journal of Solid State Chemistry*, 146:528, 1999.

[85] J. Donga, O. F. Sankey, G. K. Ramachandran, and P. F. McMillan. Chemical trends of the rattling phonon modes in alloyed germanium clathrates. *Journal of Applied Physics*, 87:7726, 2000.

[86] E. S. Toberer, K. A. Sasaki, C. R. I. Chisholm, S. M. Haile, and G. J. Snyder. Local structure of interstitial Zn in β-Zn4Sb3. *Physica Status Solidi*, 1:253255, 2007.

[87] S. M. Kauzlarich, S. R. Brown, and G. J. Snyder. Zintl phases for thermoelectric devices. *Dalton Transactions*, page 20992107, 2007.

[88] A. J. Minnich, J. A. Johnson, A. J. Schmidt, K. Esfarjani, M. S. Dresselhaus, K. A. Nelson, and G. Chen. Thermal conductivity spectroscopy technique to measure phonon mean free paths. *Physical Review Letters*, 107(9):095901, 2011.

[89] H.J. Goldsmid and A.W. Penn. Boundary scattering of phonons in solid solutions. *Physics Letters A*, 27(8):523 – 524, 1968.

[90] D. Aketo, T. Shiga, and J. Shiomi. Scaling laws of cumulative thermal conductivity for short and long phonon mean free paths. *Applied Physics Letters*, 105(13): 131901, 2014.

[91] D. Li, Y. Wu, P. Kim, L. Shi, P. Yang, and A. Majumdar. Thermal conductivity of individual silicon nanowires. *Applied Physics Letters*, 83(14):2934–2936, 2003.

[92] S. Kumar and G. C. Vradis. Thermal conduction by electrons along thin films. effects of thickness according to boltzmann transport theory. In *Micromechanical Sensors, Actuators, and Systems*, volume 32, pages 89–101. Publ by ASME, 1991. ISBN 0791808637.

[93] W. Li, J. Carrete, and N. Mingo. Thermal conductivity and phonon linewidths of monolayer MoS2 from first principles. *Applied Physics Letters*, 103(25):253103, 2013.

[94] L. Lindsay, W. Li, J. Carrete, N. Mingo, D. A. Broido, and T. L. Reinecke. Phonon thermal transport in strained and unstrained graphene from first principles. *Physical Review B*, 89:155426, Apr 2014.

[95] T. Pandey, C. A. Polanco, V. R. Cooper, D. S. Parker, and L. Lindsay. Symmetry-driven phonon chirality and transport in one-dimensional and bulk Ba_3N-derived materials. *Physical Review B*, 98:241405, Dec 2018.

[96] S.-Y. Yue, T. Ouyang, and M. Hu. Diameter dependence of lattice thermal conductivity of single-walled carbon nanotubes: Study from ab initio. *Scientific Reports*, 5:2045–2322, Oct 2015.

[97] P. Nath and K.L. Chopra. Thermal conductivity of copper films. *Thin Solid Films*, 20(1):53 – 62, 1974.

[98] H. Beyer. High thermoelectric figure of merit ZT in PbTe and Bi2Te3-based super-lattices by a reduction of the thermal conductivity. *Physica E*, 13:965–968, 2002.

[99] Y. Pei, X. Shi, A. LaLonde, H. Wang, L. Chen, and G. J. Snyder. Convergence of electronic bands for high performance bulk thermoelectrics. *Nature*, 473(7345): 66–69, 2011.

[100] H. Liu, X. Shi, F. Xu, L. Zhang, W. Zhang, L. Chen, Q. Li, C. Uher, T. Day, and G. J. Snyder. Copper ion liquid-like thermoelectrics. *Nature Materials*, 11(5):422–425, May 2012.

[101] G. Tan, W. G. Zeier, F. Shi, P. Wang, G. J. Snyder, V. P. Dravid, and M. G. Kanatzidis. High thermoelectric performance SnTeIn2Te3 solid solutions enabled by resonant levels and strong vacancy phonon scattering. *Chemistry of Materials*, 27(22):7801–7811, November 2015.

[102] L. D. Hicks, T. C. Harman, and M. S. Dresselhaus. Use of quantum-well superlat-tices to obtain a high figure of merit from nonconventional thermoelectric materials. *Applied Physics Letters*, 63(23):3230, 1993.

[103] J. Heremans, C. M. Thrush, Yu-Ming Lin, S. Cronin, Z. Zhang, M. S. Dresselhaus, and J. F. Mansfield. Bismuth nanowire arrays: Synthesis and galvanomagnetic properties. *Physical Review B*, 61(4):2921–2930, January 2000.

[104] J. L. Feldman, D. J. Singh, I. I. Mazin, D. Mandrus, and B. C. Sales. Lattice dynamics and reduced thermal conductivity of filled skutterudites. *Physical Review B*, 61:R9209–R9212, 2000.

[105] W. Liu, X. Yan, G. Chen, and Z. Ren. Recent advances in thermoelectric nanocom-posites. *Nano Energy*, 1:42–56, January 2012.

[106] N. Chen, F. Gascoin, G. J. Snyder, E. Mller, G. Karpinski, and C. Stiewe. Macroscopic thermoelectric inhomogeneities in (AgSbTe2)x(PbTe)1x. *Applied Physics Letters*, 87(17):171903, October 2005.

[107] D. Parker, A. F. May, H. Wang, M. A. McGuire, B. C. Sales, and D. J. Singh. Electronic and thermoelectric properties of CoSbS and FeSbS. *Physical Review B*, 87(4):045205, January 2013.

[108] R. Chmielowski, S. Bhattacharya, W. Xie, D. Pere, S. Jacob, R. Stern, K. Moriya, A. Weidenkaff, G. K. H. Madsen, and G. Dennler. High thermoelectric performance of tellurium doped paracostibite. *Journal of Materials Chemistry C*, 4:3094–3100, 2016.

[109] X. Hu, P. Jood, M. Ohta, M. Kunii, K. Nagase, H. Nishiate, M. G. Kanatzidis, and A. Yamamoto. Power generation from nanostructured PbTe-based thermoelectrics: comprehensive development from materials to modules. *Energy & Environmental Science*, 9(2):517–529, February 2016.

[110] D. Parker, A. F. May, H. Wang, M. A. McGuire, B. C. Sales, and D. J. Singh. Electronic and thermoelectric properties of CoSbS and FeSbS. *Physical Review B*, 87:045205, 2013.

[111] Z. Liu, H. Geng, J. Shuai, Z. Wang, J. Mao, D. Wang, Q. Jie, W. Cai, J. Sui, and Z. Ren. The effect of nickel doping on electron and phonon transport in n-type nanostructured thermoelectric material CoSbS. *Journal of Material Chemistry C*, 3:10442–10450, 2015.

[112] P. Kaur, S. Chakraverty, A. K. Ganguli, and C. Bera. High anisotropic thermoelectric effect in palladium phosphide sulphide. *Physica Status Solidi B*, pages 1–5, 2017.

[113] M. Ibanez, D. Cadavid, R. Zamani, N. Garca-Castello, V. Izquierdo-Roca, W. Li, A. Fairbrother, J. D. Prades, A. Shavel, J. Arbiol, A. Perez-Rodrguez, J. R. Morante, and A. Cabot. Composition control and thermoelectric properties of quaternary chalcogenide nanocrystals: The case of stannite Cu2CdSnSe4. *Chemistry of materials*, 24:562570, 2012.

[114] T. A. Bither, P. C. Donohue, and H. S. Young. Palladium and platinum phosphochalcogenidesSynthesis and properties. *Journal of Solid State Chemistry*, 3(2):300–307, May 1971.

[115] A. Hamidani and B. Bennecer. Electronic and optical properties of the orthorhombic compounds PdPX (X = S and Se). *Computational Materials Science*, 48(1): 115–123, March 2010.

[116] W. Jeitschko. The structure of PdPS and the crystal chemistry of late transition-metal dipnictides and dichalcogenides. *Acta Crystallographica Section B Structural Crystallography and Crystal Chemistry*, 30(11):2565–2572, November 1974.

[117] J. P. Perdew, K. Burke, and M. Ernzerhof. Generalized Gradient Approximation Made Simple. *Physical Review Letters*, 77(18):3865–3868, October 1996.

[118] P. E. Blchl. Projector augmented-wave method. *Physical Review B*, 50(24):17953–17979, 1994.

[119] G. Kresse and D. Joubert. From ultrasoft pseudopotentials to the projector augmented-wave method. *Physical Review B*, 59(3):1758–1775, January 1999.

[120] G. K. H. Madsen and D. J. Singh. BoltzTraP. A code for calculating band-structure dependent quantities. *Computer Physics Communications*, 175(1):67–71, 2006.

[121] C. Zhou, S. Birner, Y. Tang, K. Heinselman, and M. Grayson. Driving perpendicular heat flow:(pxn)- type transverse thermoelectrics for microscale and cryogenic peltier cooling. *Physical Review Letters*, 110:227701–1, 2013.

[122] C. Bera, S. Jacob, I. Opahle, N. S. H. Gunda, R. Chmielowski, G. Dennler, and G. K. H. Madsen. Integrated computational materials discovery of silver doped tin sulfide as a thermoelectric material. *Physical Chemistry Chemical Physics*, 16(37): 19894–19899, August 2014.

[123] D. Parker and D. J. Singh. First principles investigations of the thermoelectric behavior of tin sulfide. *Journal of Applied Physics*, 108(8):083712, October 2010.

[124] G. K. H. Madsen, A. Katre, and C. Bera. Calculating the thermal conductivity of the silicon clathrates using the quasi-harmonic approximation. *Physica Status Solidi (a)*, 213(3):802–807, March 2016.

[125] A. Togo, F. Oba, and I. Tanaka. First-principles calculations of the ferroelastic transition between rutile-type and CaCl2 -type SiO2 at high pressures. *Physical Review B*, 78(13):134106, October 2008.

[126] C. Bera, M. Soulier, C. Navone, G. Roux, J. Simon, S. Volz, and N. Mingo. Thermoelectric properties of nanostructured Si1-xGex and potential for further improvement. *Journal of Applied Physics*, 108(12):124306, 2010.

[127] E. J. Skoug, J. D. Cain, and D. T. Morelli. Improved thermoelectric performance in Cu-based ternary chalcogenides using S for Se substitution. *Journal of Electronic Materials*, 41(6):1232–1236, 2012.

[128] X. Lu, D. T. Morelli, Y. Wang, W. Lai, Y. Xia, and V. Ozolins. Phase stability, crystal structure, and thermoelectric properties of Cu12Sb4S13-xSex solid solutions. *Chemistry of Materials*, 28:1781–1786, 2016.

[129] K. Zhao, A.B. Blichfeld, H. Chen, Q. Song, T. Zhang, C. Zhu, D. Ren, R. Hanus, P. Qiu, B.B. Iversen, F. Xu, G.J. Snyder, X. Shi, and L. Chen. Enhanced thermoelectric performance through tuning bonding energy in Cu2Se1-xSx liquid-like materials. *Chemistry of Materials*, 29:6367–6377, 2017.

[130] K. Zhao, A.B. Blichfeld, E. Eikeland, P. Qiu, D. Ren, B.B. Iversen, X. Shi, and L. Chen. Extremely low thermal conductivity and high thermoelectric performance in liquid-like Cu2Se1-xSx polymorphic materials. *Journal of Materials Chemistry A*, 5:18148–18156, 2017.

[131] Y. He, P. Lu, X. Shi, F. Xu, T. Zhang, G.J. Snyder, C. Uher, and L. Chen. Ultrahigh thermoelectric performance in mosaic crystals. *Advanced Materials*, 27:3639, 2015.

[132] A. Banik, U. S. Shenoy, S. Anand, U. V. Waghmare, and K. Biswas. Mg alloying in snte facilitates valence band convergence and optimizes thermoelectric properties. *Chemistry of Materials*, 27(2):581–587, 2015.

[133] T.-R. Wei, G. Tan, C.-F. Wu, C. Chang, L.-D. Zhao, J.-F. Li, G. J. Snyder, and M. G. Kanatzidis. Thermoelectric transport properties of polycrystalline SnSe alloyed with PbSe. *Applied Physics Letters*, 110(5):053901, 2017.

[134] C. Chang, Q. Tan, Y. Pei, Y. Xiao, X. Zhang, Y.-X. Chen, L. Zheng, S. Gong, J.-F. Li, J. He, and L.-D. Zhao. Raising thermoelectric performance of n-type SnSe via Br doping and Pb alloying. *RSC Advances*, 6:98216–98220, 2016.

[135] J. Yu, C. Fu, Y. Liu, K. Xia, U. Aydemir, T. C. Chasapis, G. J. Snyder, X. Zhao, and T. Zhu. Unique role of refractory Ta alloying in enhancing the figure of merit of NbFeSb thermoelectric materials. *Advanced Energy Materials*, 8(1):1701313, 2018.

[136] H. Nahigian, J. Steger, H. L. Mckinzie, R. J. Arnott, and A. Wold. Preparation and characterisation of some CoXY compounds where X=P,As,Sb and Y=S,Se. *Inorganic Chemistry*, 13:1498–1503, 1974.

[137] F. Hulliger. New compounds with cobaltite structure. *Nature*, 198:382–383, 1963.

[138] M. Samanta and K. Biswas. Low thermal conductivity and high thermoelectric performance in (GeTe)1-2x(GeSe)x(GeS)x: Competition between solid solution and phase separation. *Journal of the American Chemical Society*, 139(27):9382–9391, 2017.

[139] R. F. Giese Jr. and P. F. Kerr. the crystal structures of ordered and disordered cobaltite. *The American Mineralogist*, 50:1002–1014, 1965.

[140] R. Chmielowski, S. Bhattacharya, A. Jacob, K. Moriya, G. K. H. Madsen, and G. Dennler. Strong reduction of thermal conductivity and enhanced thermoelectric properties in CoSbS1-xSex paracostibite. *Scientific Reports*, 7:46630, 2017.

[141] P. G. Klemens. The scattering of low frequency lattice waves by static imperfections. *Proceedings of the Physical Society*, A68:1113–1128, 1955.

[142] B. Abeles. Lattice thermal conductivity of disordered semiconductor alloys at high temperature. *Physical Review*, 131(5):1906–1911, 1963.

[143] N. Mingo, D. Hauser, N. P. Kobayashi, M. Plissonnier, and A. Shakouri. Nanoparticle-in-alloy approach to efficient thermoelectrics: Silicides in SiGe. *Nano Letters*, 9:711–715, 2009.

[144] D. G. Cahill, W. K. Ford, K. E. Goodson, G. D. Mahan, A. Majumdar, H. J. Maris, R. Merlin, and S. R. Phillpot. Nanoscale thermal transport. *Journal of Applied Physics*, 93:793, 2003.

[145] S. Witanachchi, R. Hyde, M. Beekman, D. Mukherjee, P. Mukherjee, and G. S. Nolas. Synthesis and characterization of bulk and thin film clathrates for solid state power conversion applications. *25th International Conference on Thermoelectrics*, page 44, 2006.

[146] A. Goetzberger and C. Hebling. Photovoltaic materials, past, present, future. *Solar Energy Materials and Solar Cells*, 62:1–19, 2000.

[147] B. Zalba, J. M. Marn, L. F. Cabeza, and H. Mehling. Review on thermal energy storage with phase change: materials, heat transfer analysis and applications. *Applied Thermal Engineering*, 23:251–283, 2003.

[148] M. Beekman and A. VanderGraaff. High-temperature thermal conductivity of thermoelectric clathrates. *Journal of Applied Physics*, 121:205105, 2017.

[149] J. L. Cohn, G. S. Nolas, V. Fessatidis, T. H. Metcalf, and G. A. Slack. Glasslike heat conduction in high-mobility crystalline semiconductors. *Physical Review Letters*, 82:779–782, 1999.

[150] J.-Y. Yang, L. Cheng, and M. Hu. Unravelling the progressive role of rattlers in thermoelectric clathrate and strategies for performance improvement: Concurrently enhancing electronic transport and blocking phononic transport. *Applied Physics Letters*, 111:242101, 2017.

[151] S. Christensen, M. S. Schmkel, K. A. Borup, G. K. H. Madsen, G. J. McIntyre, S. C. Capelli, M. Christensen, and B. B. Iversen. glass-like thermal conductivity gradually induced in thermoelectric Sr8Ga16Ge30 clathrate by off-centered guest atoms. *Journal of Applied Physics*, 119:185102, 2016.

[152] T. Takabatake, K. Suekuni, T. Nakayama, and E. Kaneshita. Phonon-glass electron-crystal thermoelectric clathrates: Experiments and theory. *Reviews of Modern Physics*, 86:669–716, 2014.

[153] H. Borrmann M. Baitinger Y. Grin M. Beekman, W. Schnelle and G. S. Nolas. Intrinsic electrical and thermal properties from single crystals of Na24Si136. *Physical Review Letters*, 104:018301, 2010.

[154] A. P. Wilkinson G. S. Nolas, D. G. Vanderveer and J. L. Cohn. Temperature dependent structural and transport properties of the type II clathrates A8Na16E136 (A=Cs or Rb and E=Ge or Si). *Journal of Applied Physics*, 91:8970–8973, 2002.

[155] H. Euchner, S. Pailh'es, V. M. Giordano, and M. de Boissieu. Understanding lattice thermal conductivity in thermoelectric clathrates: A density functional theory study on binary Si-based type-I clathrates. *Physical Review B*, 97:014304, 2018.

[156] X. Yan, M. Falmbigl, S. Laumann, A. Grytsiv, E. Bauer, P. Rogl, and S. Paschen. Structural and thermoelectric properties of Ba8CuxSi23-xGe23. *Journal of Electronic Materials*, 41:1159–1164, 2012.

[157] P. G. Klemens. The scattering of low frequency lattice waves by static imperfections. *Proceedings of the Physical Society A68*, pages 1113–1128, 1955.

[158] B. Abeles. Lattice thermal conductivity of disordered semiconductor alloys at high temperature. *Physical Review*, 131:1906–1911, 1963.

[159] S. Laumann E. Bauer P. Rogl R. Podloucky X. Yan, M. X. Chen and S. Paschen. Thermoelectric properties of Ba-Cu-Si clathrates. *Physical Review B*, 85:165127, 2012.

[160] R. Chen, A. I. Hochbaum, P. Murphy, J. Moore, P. Yang, and A. Majumdar. Thermal conductance of thin silicon nanowires. *Physical Review Letters*, 101:105501, 2008.

[161] A. J. Minnich, H. Lee, X. W. Wang, G. Joshi, M. S. Dresselhaus, Z. F. Ren, G. Chen, and D. Vashaee. Modeling study of thermoelectric sige nanocomposites. *Physical Review B*, 80:155327, 2009.

[162] N. Mingo. Calculation of si nanowire thermal conductivity using complete phonon dispersion relations. *Physical Review B*, 68:113308, 2003.

[163] P. Kaur and C. Bera. Effect of alloying on thermal conductivity and thermoelectric properties of CoAsS and CoSbS. *Physical Chemistry Chemical Physics*, 19:24928–24933, 2017.